JOURNAL OF GEOPHYSICAL RESEARCH, VOL. 96, NO. B3, PAGES 4187–4227, MARCH 10, 1991

Crustal Structure of Accreted Terranes in Southern Alaska, Chugach Mountains and Copper River Basin, From Seismic Refraction Results

GARY S. FUIS, ELIZABETH L. AMBOS,[1] AND WALTER D. MOONEY

U.S. Geological Survey, Menlo Park, California

NIKOLAS I. CHRISTENSEN

Department of Earth and Atmospheric Sciences, Purdue University, West Lafayette, Indiana

ERIC GEIST

U.S. Geological Survey, Menlo Park, California

Seismic refraction data were collected along a 320-km-long "Transect" line in southern Alaska, crossing the Prince William, Chugach, Peninsular, and Wrangellia terranes, and along several shorter lines within individual terranes. Velocity structure in the upper crust (less than 9-km depth) differs among the four terranes. In contrast, layers in the middle crust (9- to 25-km depth) in some cases extend across projected terrane boundaries. The following observations can be made: (1) An intermediate-velocity layer (6.4 km/s) at 9-km depth extends across the deep projection of the suture between the Chugach and Peninsular terranes, suggesting that the northern Chugach and southern Peninsular terranes are detached and rest on a deeper terrane of unknown origin. (2) The top of a gently north dipping sequence of low- and high-velocity layers (5.7–7.8 km/s), more than 10 km thick, extends from near the surface in the southern Chugach terrane to more than 20-km depth beneath the southern Peninsular terrane. This sequence, truncated by the suture between the Prince William and Chugach terranes, is interpreted to be an underplated "terrane" made up of fragments of the Kula plate and its sedimentary overburden that were accreted during subduction in the late Mesozoic and/or early Tertiary, during or between times of accretion of the Prince William and Chugach terranes. (3) A thick crustal "root", with a laminated sequence at its top, extends from a depth of 19 km to as much as 57 km beneath the northern Peninsular and Wrangellia terranes. This root extends across the deep projection of the suture between the Peninsular and Wrangellia terranes, although resolution of this apparent crosscutting relationship is relatively poor. This root may represent tectonically or, possibly, magmatically emplaced rocks. The lower crust beneath the Prince William, Chugach, and southern Peninsular terranes includes a north dipping, 3- to 8-km-thick section of subducting oceanic crust.

INTRODUCTION

Southern Alaska, like much of western North America, is believed to be a composite of crustal fragments, or terranes, of various rock compositions, ages, and origins [*Jones et al.*, 1977, 1982, 1984; *Coney et al.*, 1980; *Csejtey et al.*, 1982; *Nokleberg et al.*, 1985; *Plafker*, 1987; *Plafker et al.*, 1989]. Although the terrane concept has proved useful in elucidating the tectonic history of western North America, there are many unanswered questions concerning the process of accretion that require knowledge of the subsurface. These include the following: (1) How deep do terranes extend? (2) Are terranes accreted by underplating as well as by overthrusting and strike-slip faulting? (3) Do different types of crust (oceanic, island arc, continental, accretionary prism) accrete in characteristic ways? (4) What percentage of accreted rock is constituted by the several different types of crust listed above? (5) What happens to terranes after accretion? (6) What is the role of the Moho in terrane accretion? Alaska is an important place in which to attempt to answer these questions because terrane accretion is occurring at present [*Bruns*, 1985; *Plafker*, 1987], and numerous, diverse terranes which were accreted in the late Mesozoic and Cenozoic have boundaries that have not been obscured by intrusion or metamorphism. We address a number of these questions in this paper and in the sequel to this paper [*Fuis and Plafker*, this issue].

Until recently, the deep structure of accreted terranes has been poorly known. A goal of the Trans-Alaska Crustal Transect (TACT) program is to elucidate the process of terrane accretion in Alaska by coordinated geological and geophysical studies. A major component of the TACT program is the collection and analysis of seismic refraction/wide-angle reflection profiles. In 1984 and 1985, we collected a number of such profiles to examine in three dimensions many of the terranes of southern Alaska (Figure 1 and Table 1). In this paper we report the analyses of four 130-km-long profiles that examine the crustal structure of the Prince William, Chugach, Peninsular, and Wrangellia terranes. Three of these profiles compose a north-south transect across these terranes from near the Pacific coast to the Alaska Range; these lines are referred to collectively as the

[1]Now at Department of Geological Sciences, California State University, Long Beach.

Paper number 90JB02316.
0148-0227/91/90JB-02316$05.00.

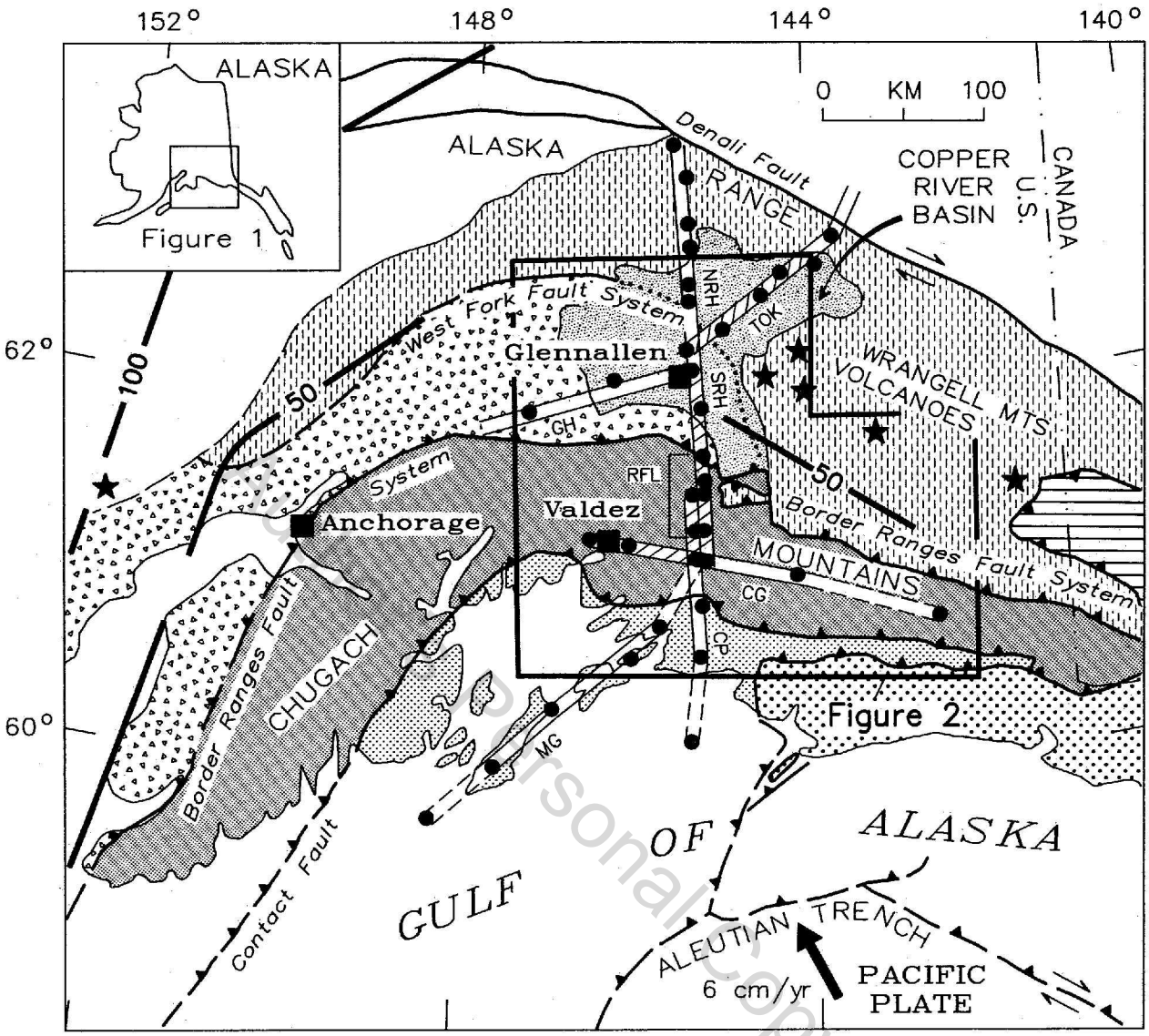

EXPLANATION

- Unconsolidated sediments
- Wrangellia terrane
- Alexander terrane
- Peninsular terrane
- Chugach terrane
- Prince William terrane
- Yakutat terrane
- Fault: dashed where uncertain; dotted where buried; teeth on upper plate of thrust or reverse fault
- —50— Isopleth on top of Wrangell and Aleutian Wadati–Benioff zones; depth in km
- ★ Active volcano

Fig. 1. Map of south-central Alaska showing tectonostratigraphic terranes [*Jones et al.*, 1984], suture zones, volcanoes, depth contours on tops of Aleutian and Wrangell Wadati-Benioff zones [*Stephens et al.*, 1984; *Page et al.*, 1989], and TACT seismic refraction lines (double lines). Refraction lines are labeled CG, Chugach; CP, Cordova Peak; GH, Glenn Highway; MG, Montague; NRH, North Richardson Highway; SRH, South Richardson Highway; and TOK, Tok Highway. Lines CP, SRH, and NRH are referred to collectively in this report as the Transect line. Large dots are shot points. Offset shots are linked by double-dashed lines. The diagonally lined segments of refraction lines are panels in the fence diagram of Figure 20. TACT reflection data shown in this report (RFL) are indicated by a bracket.

TABLE 1. Seismic Refraction and Seismic Reflection Lines in Southern Alaska in 1984, 1985, and 1986, Terranes Examined, and References to Data and Data Analysis

Terrane	Parallel Profile	Perpendicular Profile
Wrangellia	...	NRH (2, 7, 17) and TOK (3, 15)
Peninsular	GH (1, 4, 16)	SRH (2, 5, 9, 10, 17), NRH(2, 7, 17), and RFL (13)
Chugach	CG (1, 4, 5, 9, 10, 11, 14, 17)	SRH (2, 5, 9, 19, 17), CP (3, 6, 17), and RFL (12, 13)
Prince William	MG (3, 8)	CP (3, 6, 17)

Lines approximately parallel and perpendicular to structural grain are distinguished (Figure 1). Abbreviations for line names are CG, Chugach; CP, Cordova Peak; GH, Glenn Highway; MG, Montague; NRH, North Richardson Highway; SRH, South Richardson Highway; and TOK, Tok Highway. The Transect line referred to in this paper includes lines CP, SRH, and NRH. RFL refers to reflection data collected along the South Richardson Highway line. References for data are (1) *Daley et al.* [1985], (2) *Meador et al.* [1986], (3) *Wilson et al.* [1987], and (4) *Wilson* [1987]; and for data analysis are (5) *Page et al.* [1986], (6) *Fuis and Ambos* [1986], (7) *Colburn and Fuis* [1986], (8) *Taber et al.* [1986], (9) *Fuis et al.* [1987], (10) *McMechan and Fuis* [1987], (11) *Wolf and Levander* [1989], (12) *Fisher et al.* [1989], (13) *Brocher et al.* [1989*a*], (14) *Flueh et al.* [1989], (15) *Goodwin et al.* [1989], (16) E. L. Ambos et al. (submitted manuscript, 1988), and (17) this paper.

Transect line. A fourth line, referred to as the Chugach line, extends eastward from near Valdez along the axis of the coastal Chugach Mountains and examines the Chugach terrane parallel to its structural grain (Figures 1 and 2). For three-dimensional control on the crustal structure of the Prince William, Peninsular, and Wrangellia terranes, we rely on the analyses by *Taber et al.* [1986], E. L. Ambos et al. (Seismic refraction measurements within the Peninsular terrane, south central Alaska, submitted to *Journal of Geophysical Research*, 1988), and *Goodwin et al.* [1989], respectively (Figure 1 and Table 1).

The data and models discussed in this report are the most complex and unusual of any in our experience. The data include not only complex refractions, with lateral variations in traveltime and amplitude, but also numerous clear secondary arrivals, some of which are primary reflections and some of which are peg-leg or free-surface multiples. Fortunately, the data are of good quality; most arrivals are clearly separated from each other; and the complexity can be modeled. The models include strong lateral and vertical velocity changes, including pronounced low-velocity zones and anomalously high-velocity, mantle-like refractors at relatively shallow levels in the crust. In addition, there is abundant complementary data to aid in constraining the models, including detailed surface geologic mapping, vertical incidence reflection data, laboratory rock velocity measurements, and gravity, aeromagnetic, and magnetotelluric data. The reader must be aware, however, that our models are far from unique, particularly for the middle and lower crust, given the complexity of both data and models. We have produced several alternate models for deep features in an attempt to quantify uncertainties.

GEOLOGIC SETTING

Terranes in southern Alaska generally form arcuate belts of rock of differing composition, age, and origin (Figure 1) [*Jones et al.*, 1984]. Most are deformed around the Alaska orocline [*Carey*, 1958]. Present arc volcanism and Wadati-Benioff zone seismicity trends change near the axis of this orocline, just west of TACT corridor [*Stephens et al.*, 1984; *Page et al.*, 1989]. Seismicity defines a shallowly dipping Aleutian Wadati-Benioff zone to the west of the axis and a moderately dipping Wrangell Wadati-Benioff zone to the east (Figure 1).

In this section we present brief descriptions of the geology of the Prince William, Chugach, Peninsular, and Wrangellia terranes. More details are given by *Winkler and Plafker* [1981], *Winkler et al.* [1981], *Plafker et al.* [1985, 1989], and *Nokleberg et al.* [1985, 1986, 1989].

The Prince William terrane is composed of the Orca Group, an accreted deep-sea fan complex interbedded with oceanic volcanic rocks (tholeiitic basalt) and minor pelagic deposits [*Winkler and Plafker*, 1981; *Plafker et al.*, 1986]. Its age is Paleocene and early through middle Eocene. It is complexly folded and faulted and lightly metamorphosed in most places (zeolite), although near 50 Ma granitic plutons it is locally highly metamorphosed (amphibolite facies) [*Hudson and Plafker*, 1982; *Sisson et al.*, 1989]. The suture between the Prince William and Chugach terranes is the moderately to steeply north dipping Contact fault, which, near our transect, experienced only reverse movement [*Nokleberg et al.*, 1989] and which is intruded by 50 Ma granitic plutons (Figure 2).

The Chugach terrane is an accretionary prism consisting of three fault-bounded, highly deformed sequences of marine sedimentary and volcanic rocks that range in metamorphic facies from zeolite to greenschist and blueschist along our transect (Figure 2) [*Plafker et al.*, 1977, 1989]. The sequences range in age from Late Cretaceous in the south to Early Jurassic or older in the north. The southern sequence is foliated flysch and greenstone (Valdez Group) that is isoclinally folded (south vergence) and locally refolded (north vergence) [*Nokleberg et al.*, 1989]. Greenstone (mafic metatuff and metabasalt) predominates in the structurally lowest part of the Valdez Group. Metamorphic grade increases from west to east in the Valdez Group: lower greenschist facies at shot point 17 (Figure 2), upper greenschist facies (garnet to cordierite zone) at shot point 20, and amphibolite facies at shot point 21 [*Hudson and Plafker*, 1982; *Sisson et al.*, 1989]. The northern two sequences of the Chugach terrane are melange (McHugh Complex) and minor glaucophanitic greenschist-blueschist (schists of Liberty Creek and Iceberg Lake). The Chugach terrane is separated from the Peninsular and Wrangellia terranes to the north by

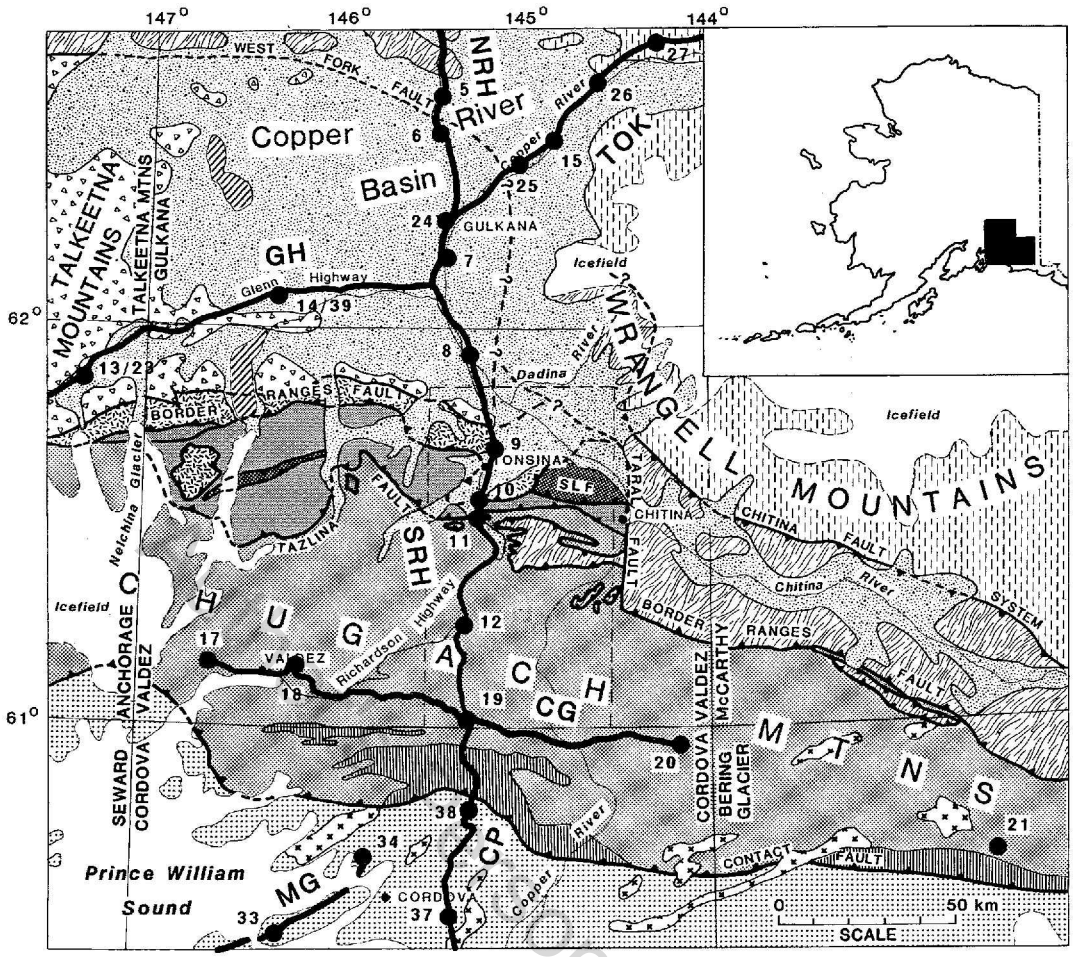

EXPLANATION

- Unconsolidated sediments
- Northern Wrangellia terrane (volcanic and sedimentary rocks)
- Southern Wrangellia terrane (igneous and metamorphic rocks)
- Talkeetna Formation (volcanic and sedimentary rocks) and granitic rocks, undivided
- Peninsular terrane middle and lower crust (BRUMA--ultramafic rocks and gabbro-- plus granitic and metamorphic rocks)

WRANGELLIA TERRANE

PENINSULAR TERRANE

- Schists of Liberty Creek and Iceberg Lake, undivided (greenschist-blueschist)
- McHugh Complex (melange)
- Valdez Group (metaflysch and metabasalt; metabasalt indicated by vertical lines)
- Orca Group (sedimentary and volcanic rocks)

CHUGACH TERRANE

PRINCE WILLIAM TERRANE

- Eocene granitic rocks
- Lithologic Contact
- Fault; short dashed where buried; teeth on upper plate of reverse or thrust fault; SLF, Second Lake fault
- Lake

Fig. 2. Simplified geologic map of the Chugach Mountains and Copper River basin, southern Alaska, showing the seismic refraction lines discussed in this paper (abbreviations same as in Figure 1; shot point numbers are given). The geologic base map is taken from *Plafker et al.* [1989].

the Border Ranges fault system, which had a history of movement from the Jurassic to the early Tertiary. This fault system and the northern Chugach terrane are intruded by 50 Ma granitic dikes.

The Peninsular terrane is part of a Mesozoic island arc that was built on a basement of metasedimentary and metavolcanic rocks (now scantily exposed) [*Burns*, 1985; *Plafker et al.*, 1989]. From south to north, the Peninsular terrane consists of the Tonsina ultramafic-mafic suite (Early or Middle Jurassic) [*Winkler et al.*, 1981; *DeBari and Coleman*,

1989], the Nelchina River Gabbronorite (Early or Middle Jurassic) [*Burns*, 1982, 1985; *Plafker et al.*, 1989], and the Talkeetna Formation (Lower Jurassic), consisting of andesitic and lesser basaltic volcaniclastic and marine sedimentary rocks [*Winkler et al.*, 1981; *Plafker et al.*, 1989]. The Tonsina ultramafic-mafic suite and the Nelchina River Gabbronorite are part of a belt of ultramafic and mafic rocks extending westward along the south margin of the Peninsular terrane referred to as the Border Ranges ultramafic-mafic assemblage (BRUMA) [see *Plafker et al.*, 1989]. The ultramafic rocks crystallized at high pressures (as much as 1100 MPa [*DeBari and Coleman*, 1989]), suggesting that they have been exhumed from deep crustal levels (as much as 35 km). The Tonsina suite and the lower-pressure Nelchina River Gabbronorite, which crystallized at 400?–700 MPa (S. DeBari, oral communication, 1988), have closer affinities to island arc rocks than to mid-ocean ridge rocks. In other parts of the BRUMA, nearly coeval intermediate plutonic rocks make up 40% of the outcrops [*Burns*, 1985]. Intermediate plutonic rocks also intrude the Talkeetna Formation, and it is extensively faulted and folded. Mesozoic and Cenozoic sedimentary rocks overlie the Talkeetna Formation in the Copper River basin.

The Wrangellia terrane was formed primarily in an island arc setting in the Late Paleozoic and Mesozoic, although an episode of rifting is recorded in the Late Triassic [*Jones et al.*, 1977; *Nokleberg et al.*, 1985]. The terrane is divided by the Chitina fault system into a southern area and a northern, or "type", area (Figure 2) [*Nokleberg et al.*, 1986; *Plafker et al.*, 1989]. The southern area comprises chiefly metavolcanic and metasedimentary rocks of lower greenschist to lower amphibolite facies intruded by intermediate to felsic granitic rocks of Middle Pennsylvanian and Late Jurassic age. The "type" Wrangellia terrane consists of Pennsylvanian and Permian volcanic and sedimentary rocks, the Triassic Nikolai Greenstone, and Mesozoic sedimentary rocks. Paleomagnetic studies of the Nikolai Greenstone indicate at least 29° of northward movement since the Triassic [*Hillhouse and Gromme*, 1984]. The suture between the Peninsular and Wrangellia terranes is the West Fork fault system [*Nokleberg et al.*, 1986].

The composite Peninsular-Wrangellia terrane collided with North America in the mid-Cretaceous based on (1) age of thrusting of the composite terrane over mid- and older Cretaceous flysch deposits in a region northwest of our study area [*Csejtey et al.*, 1982] and (2) metamorphism and deformation in the Wrangellia terrane in the study area [*MacKevett*, 1978; *Silberman et al.*, 1981].

PREVIOUS GEOPHYSICAL WORK

Few controlled-source seismic studies have been carried out in southern and central Alaska. *Hales and Asada* [1966] determined a crustal thickness of 46–53 km and an average crustal velocity of 6.8 km/s in southern Alaska, using data collected by *Tatel and Tuve* [1956] from a shot in College Fiord, 75 km west of Valdez (Figure 1). *Hanson et al.* [1968] suggested a south dipping Moho in the region of central Alaska between Fairbanks and the Alaska Range, using a series of unreversed quarry shots in the Alaska Range. Estimated Moho depths ranged from 32 km at Fairbanks to 47 km in the Alaska Range. Shallow structure has been addressed by the oil industry; seismic reflection data (4-s total two-way travel time) and sonic logging in exploratory oil wells have characterized the upper few kilometers of sedimentary rocks in the Copper River basin [*Alaska Geological Society*, 1970; R. Shafer, written communication, 1985; E. L. Ambos et al., submitted manuscript, 1988]. For studies of seismic refraction and seismic reflection data collected in southern Alaska in the period 1984–1986 under the TACT program, the reader is referred to Table 1.

Gravity and aeromagnetic data have heretofore provided the clearest definition of structural features in southern Alaska. *Woollard et al.* [1960], using their own gravity data and the seismic data of *Tatel and Tuve* [1956], interpreted the crust north of Prince William Sound to have a relatively high density and a thickness of 49–53 km. Aeromagnetic maps of the Copper River basin [*Andreason et al.*, 1958] and Chugach Mountains [*U.S. Geological Survey*, 1979] indicate strong east-west trending magnetic anomalies corresponding to (1) metavolcanic rocks in the structurally lowest part of the Chugach terrane, (2) the BRUMA, and (3) the West Fork fault system. A detailed gravity map of Alaska [*Barnes*, 1977] indicates gravity anomalies for these same features. Potential field data have been used to model these three features [*Burns*, 1982; *Campbell and Barnes*, 1985; *Campbell*, 1987], and some of these results are used in this study.

Seismicity studies in southern Alaska delineate the Wrangell Wadati-Benioff zone (Figure 1) [*Stephens et al.*, 1984; *Page et al.*, 1989] and provide the best estimate of the depth of the current plate interface in the region.

DATA COLLECTION AND ANALYSIS

The four lines described in this paper include the Cordova Peak, South Richardson Highway, North Richardson Highway, and Chugach lines (Figure 1 and Table 1). The first three compose what is referred to as the Transect line. The Chugach line and the part of the Transect line south of about shot point (SP) 12 (Figure 2) were deployed by helicopter across rugged terrain ranging in elevation from 2 to 1800 m. Average station spacing for the Transect and Chugach lines was 1.1 km, and average shot point spacing ranged from 22 km for the Transect line to 45 km for the Chugach line. Offset shots on the Transect line were arranged to provide reversed coverage of the deep crust and mantle from the southern Chugach Mountains to the Copper River basin. For logistical reasons, the Chugach line recorded only one offset shot (SP21, Figure 2), providing unreversed coverage of deep crust and mantle under the east end of the recording interval. Shots ranged in size from 450 to 2730 kg of explosive and were detonated in drill holes (0.2 m in diameter and 40–55 m deep), lakes (15 m deep), and, in one instance, the Gulf of Alaska.

The seismographs are portable cassette tape recorders with three independent amplifiers (low, medium, and high gain) and programmable turn-on and turn-off; the sensor is a vertical, 2-Hz seismometer [*Blank et al.*, 1979; *Healy et al.*, 1982]. Data on the cassette tapes were digitized at a 5-ms sampling interval and are displayed in a number of reports (Table 1). Normal timing errors for a given trace on a record section are estimated to be on the order of 0.02 s, with rare instances of errors as large as 0.1 s. Seismograph location errors are estimated to be of the order of 50 m, with the worst errors being approximately 100 m.

Current methods of analyzing seismic refraction data are described by *Meissner* [1986] and by *Mooney* [1989]. Our

data analysis proceeded along the following lines. First, a two dimensional starting model, obtained chiefly from one-dimensional models for each shot point, was iteratively modified using an interactive two-dimensional ray-tracing program [*Luetgert*, 1988], based on geometrical ray theory described by *Červený et al.* [1977], until agreement within 0.05 s between predicted and observed travel time branches was achieved. Some mismatches of as much as 0.15 s still persist, however. We attempted to match branch terminations and cusps to within 5-km range, but mismatches of 10–15 km are still seen. Second, synthetic record sections were calculated using the ray-density method of *McMechan and Mooney* [1980], and model velocity gradients were further refined, if necessary, to achieve closer agreement with the observed amplitude distributions. Finally, major features in the models were perturbed, one after another, in order to obtain estimates of uncertainty (in depth and velocity) for each feature. These estimates are crudely 80% confidence limits. In this process, three alternate models were created that fit the data nearly as well as the preferred models. These models are presented in this report in an attempt to quantify uncertainties.

The Transect line was initially modeled in several overlapping segments. Models for each of these segments involved as many as 50 iterations. The model for the Transect line as a whole required nearly 200 additional iterations, including perturbations and the creation of alternate models (as discussed above). The model for the Chugach line required over 100 iterations.

Except as noted in the figure captions and appendices, we have routinely calculated all possible refractions, postcritical reflections, and distal precritical reflections that can be generated by our model from each shot point. In addition, we have calculated free-surface multiples from the few shot points where these arrivals are predicted (in regions of high near-surface velocity gradient), and we have also calculated postcritical peg-leg multiples for three strong low-velocity zones. Amplitudes for peg-leg multiples may not be well predicted, however, using ray theory. For clarity in our diagrams below, we have not routinely calculated reflections from negative velocity steps, because amplitudes for these reflections are considerably lower than postcritical reflections from positive steps, and they are generally masked by such postcritical reflections.

Analysis of the Chugach line included calculation of synthetic record sections using the reflectivity method [*Fuchs and Mueller*, 1971]. This method, designed for one-dimensional media, could be used for the middle and upper crust of the eastern Chugach line, which is relatively free of two-dimensional complexity (see below). The results of reflectivity modeling are used in this paper but are discussed by *Flueh et al.* [1989].

None of the models discussed below are unique. The presence of lateral velocity changes and low-velocity zones (LVZs) leads to trade-offs between velocity and boundary depth. Additional uncertainties arise from the identification and correlation of observed phases in the record sections. We estimate from the numerous models attempted that velocities are accurate to 2 or 3% except within LVZs, where they are more poorly known. Depths to boundaries are estimated to be accurate to 5–10%. Below LVZs, boundary depths are somewhat less certain. Choosing the type of velocity boundary to be used in a given location (for example, a step in velocity versus a high velocity gradient) accounts for much of the variability possible in this type of forward modeling. We have chosen the types of boundaries that seem to provide the best matches to secondary arrivals in our record sections, but in some cases, alternate models are equally plausible. Because of these uncertainties in modeling, we describe in some detail in Appendices A and B our reasons for modeling each major feature as we do. Model uncertainties for each feature are also estimated in the appendices. In spite of the inherent uncertainties in this type of forward modeling, the method is robust in that the basic configuration of velocity contours will not change on reanalysis if identification of the most important arrivals is correct [see *Blundell*, 1984].

TRANSECT LINE

Models A, B, and C

Model A (Figures 3 and 4*a*) is the preferred model for the Transect line. Model B (Figure 4*b*) is an alternate model for the middle crust beneath the Chugach and southern Peninsular terranes, and model C (Figure 4*c*) is an alternate model for the lower crust of the whole Transect line. We shall describe the features of these models from the surface downward and then examine salient features of the data (Figures 5–10) that constrain the models. For a layer-by-layer discussion of model constraints and uncertainties and for additional data recorded along the Transect line, the reader is referred to Appendix A.

Upper crust (0- to 9-km depth). The surficial layer, layer 1 (1.8–3 km/s), corresponds to unconsolidated glaciofluvial deposits. Layer 2 corresponds to near-surface bedrock (weathered with open cracks; 4.2–5.2 km/s) except in the Copper River basin where it corresponds to consolidated Mesozoic and Cenozoic sedimentary rocks (2.8–4.6 km/s). Layer 1 is thickest in the Copper River basin and patchy elsewhere. Layer 2 has a poorly constrained velocity and thickness, both of which can in most places be traded off against each other (see Appendix A). In the Chugach Mountains, where it corresponds to bedrock, layer 2 is probably gradational into layer 3. In the Copper River basin the velocity and thickness of layer 2 is better controlled, especially in the northern Copper River basin (north of SP7) where well control and cross-line control (Glenn and Tok Highway lines, Figure 1 and Table 1) are available.

In the Prince William terrane, "basement" (layers 3 and 5) ranges in velocity from 5.2 to 6.0 km/s to 9-km depth. Velocities increase somewhat toward the north boundary of the terrane, the Contact fault (Figure 3). Orca Group flysch intruded by a few granitic plutons crops out along this part of the Transect line. The central and northern Chugach terrane is similarly underlain by "basement" (layers 3, 5, and 6) velocity of 5.5 to 6.0 km/s to 9-km depth. Valdez Group metaflysch and the McHugh complex (volcanic and sedimentary rocks and melange) crop out along the Transect line in this region. In the southern Chugach terrane, layers 3 and 6 terminate at or near a gently north dipping sequence of layers of low and high velocity (layers 7–12), and layer 5 thins and increases in velocity. The high-velocity (6.2-km/s) segment of layer 5 corresponds closely to outcrops of metabasalt.

Basement in the Peninsular terrane (layers 3, 4, and 6) has a velocity of 5.2–6.2 km/s. Wells penetrating to basement in

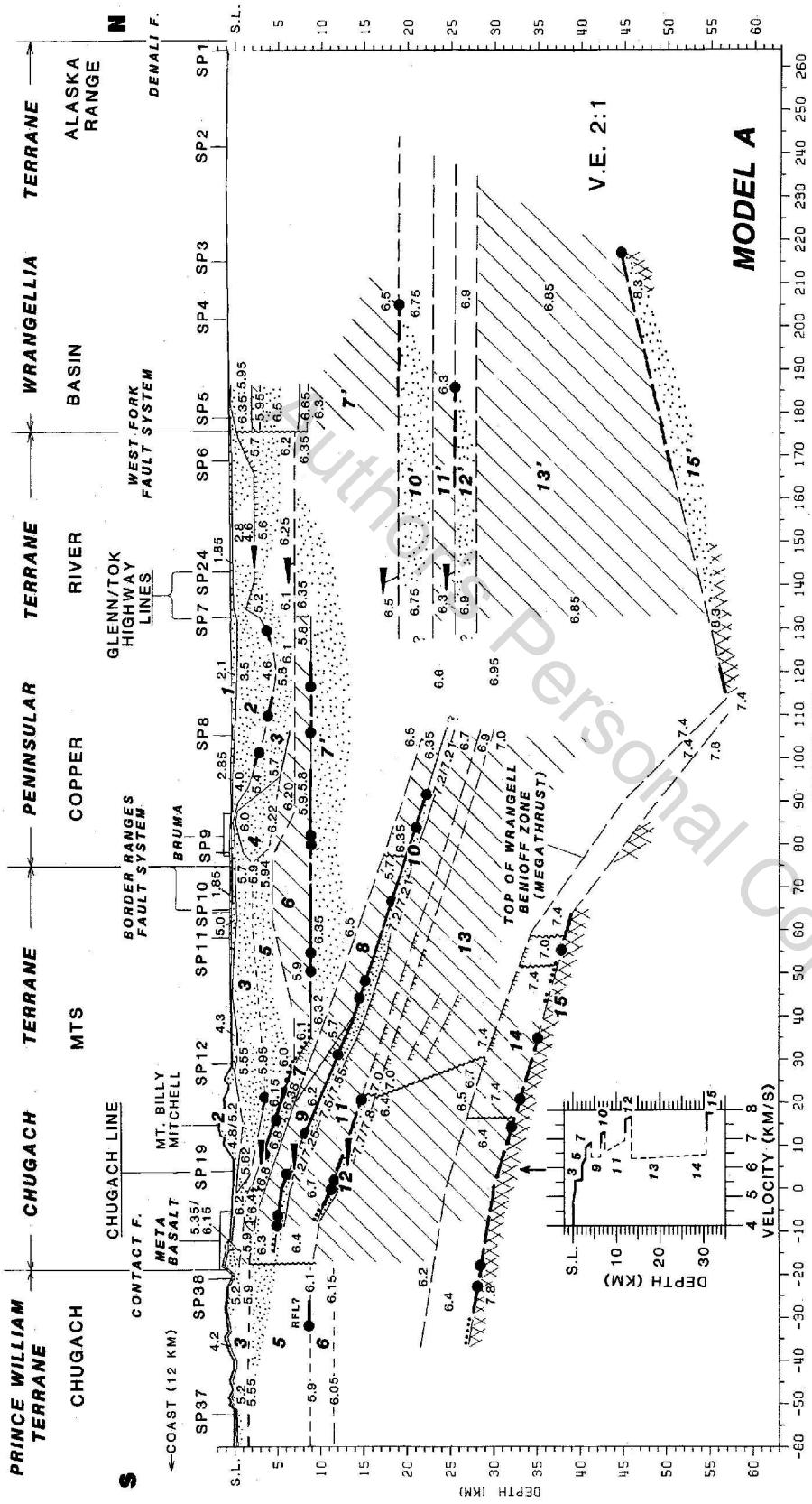

Fig. 3. Model A, preferred velocity model for the Transect line (see Figure 1 for location). Velocities (km/s) are given for top/bottom of each layer. Low-velocity zones (LVZs) are diagonally lined. Mantle is cross-hatched (except in regions of stipple pattern, see below). Layer numbers are in italics. Layer boundaries are (1) long-dashed where uncertain by more than about 1.5 km, (2) short dashed where they are second-order discontinuities, (3) hachured where controlled either in depth or dip by vertical incidence reflection data, or (4) wavy where they represent strong lateral changes. Regions controlled by bottoming refractions (not necessarily reversed) are stippled. Subsurface points of critical reflection are indicated by large dots; bottoming points for postcritical reflections are indicated by heavy lines (long-dashed, as above), and bottoming points for precritical reflections are indicated by rows of small dots. RFL? indicates an unmodeled reflector (?) Depths of corresponding interfaces on cross lines are indicated by heavy arrowheads and leaders. Beneath the northern Chugach Mountains and southern Copper River basin, model A is characterized by (1) a horizontal velocity discontinuity at 9-km depth, overlain by a low-velocity zone, both of which extend across the deep projection of the Border Ranges fault system, (2) gently north dipping layers of alternating low and high velocity that appear to be truncated by the (north dipping?) Contact fault, and (3) a north dipping subducting plate, consisting of 3–6 km of crust over a clearly defined Moho. Beneath the northern Copper River basin, the model is characterized by (4) subhorizontal low- and high-velocity layers in the middle crust that appear to extend across the deep (vertical) projection of the West Fork fault system and (5) a deep Moho. The blank region below 20-km depth between SP7 and SP8 indicates uncertainty in correlation of features between south and north halves of the model. The north dipping sequence 2 is interpreted to be sedimentary and metasedimentary rocks interlayered with fragments of oceanic crust and mantle of the Kula plate.

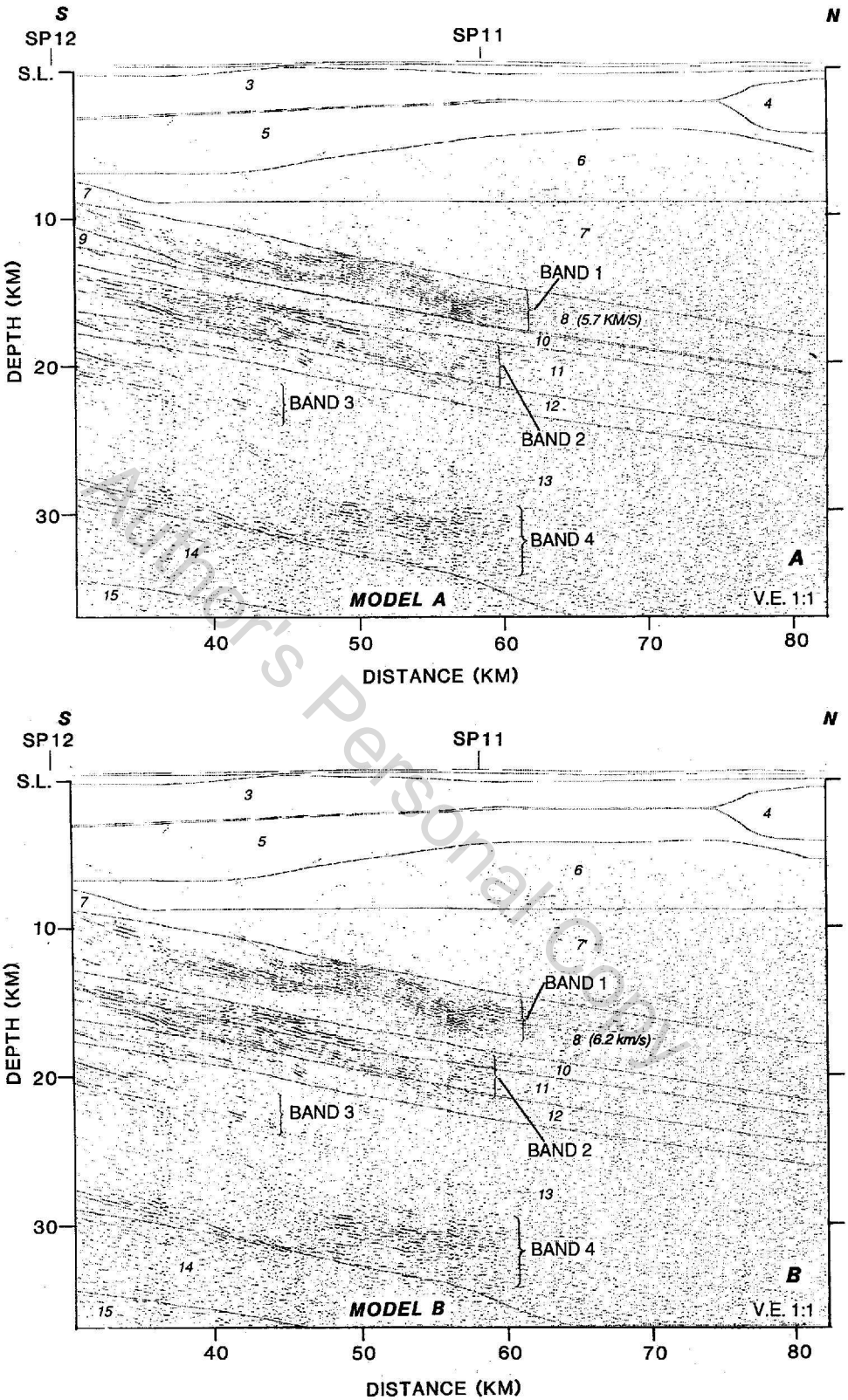

Fig. 4. (*a*) Model A superposed on vertical incidence reflection data that has been depth-converted using model A velocities. Note the close correspondence between layers 8 and 11 (LVZs) and reflection bands 1 and 2. (*b*) Model B, alternate model for the north dipping sequence, superposed on vertical incidence reflection data that has been depth-corrected using model B velocities. Layer 8 is faster (6.2 km/s) and thicker (4 km) than in model A. Layer correspondence with reflection bands is not as striking. (*c*) Model C, alternate model for the lower crust of the Transect line. Layers 13, 13′, and 14 are uniformly 6.4–6.6 km/s throughout the model. The location of Figures 4*a* and 4*b* is indicated in Figure 1 (RFL). Layer numbers are indicated in Figures 4*a*–4*c*. The format of Figure 4*c* is similar to that of Figure 3.

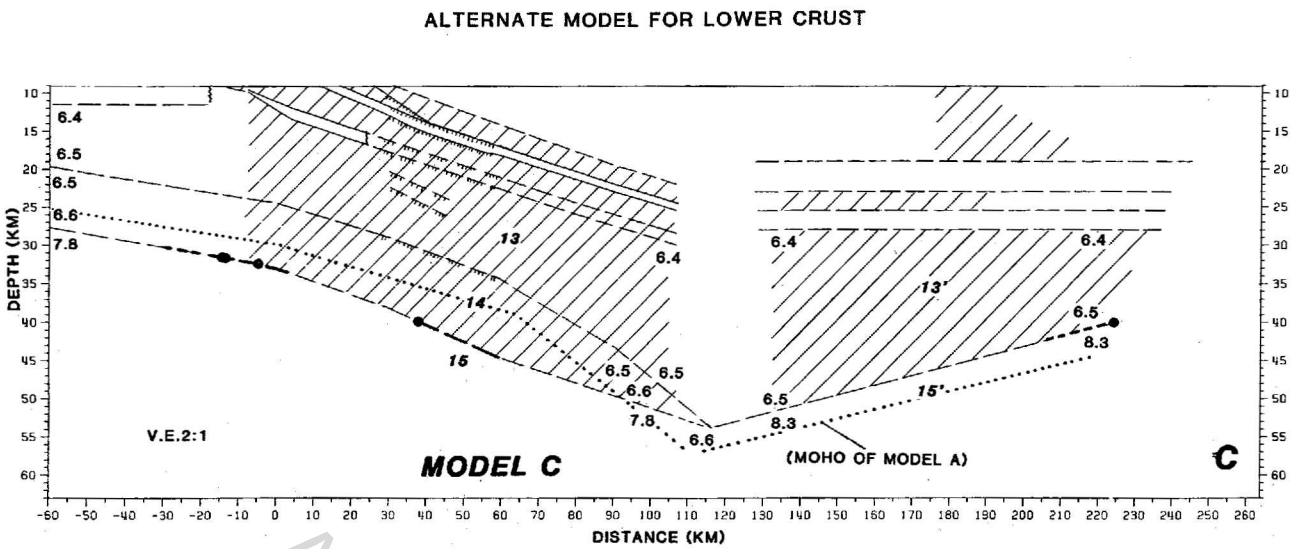

Fig. 4. (continued)

the Copper River basin indicate that at least its upper part is the Talkeetna Formation and possibly intrusive granitic rocks [*Alaska Geological Society*, 1970]. In the south part of the Peninsular terrane, corresponding to outcrops of the Border Ranges ultramafic-mafic assemblage (BRUMA), is a prism-shaped body with velocities of 6.0–6.2 km/s (body 4). A weak, low-velocity zone (LVZ, layer 6) is present in the lower part of the upper crust in both the Chugach and southern Peninsular terranes but appears to be absent in the northern Peninsular terrane. This LVZ is likewise absent in the central and northern parts of the Peninsular terrane on the Glenn and Tok Highway lines (Figure 1) [*Goodwin et al.*, 1989; E. L. Ambos et al., submitted manuscript, 1988].

A preliminary model of the upper crust of the Wrangellia terrane [*Colburn and Fuis*, 1986; R. H. Colburn and G. S. Fuis, unpublished model, 1988] has been included in the model in order that the deep crust and mantle beneath the Copper River basin may be modeled. The rudiments of that model include (1) velocities of about 6.0 km/s near the surface (6.35 km/s near the surface at the West Fork fault system), (2) a 6.5 km/s layer at about 3-km depth, overlain by a weak LVZ, and (3) a 6.65 km/s layer at about 8-km depth, overlain by a laterally discontinuous, weak LVZ (not present near the West Fork fault system in Figure 3).

Layer 7′. A layer of intermediate velocity (6.3–6.5 km/s; layer 7′) underlies the northern Chugach, Peninsular, and Wrangellia terranes (Figure 3). It extends without resolvable offset across the region beneath the Border Ranges fault system and perhaps also across the region of the West Fork fault system. In the northern Chugach and southern Peninsular terranes, its top is a clearly defined reflector that is accentuated in the data because of the overlying LVZ. In the northern Peninsular and Wrangellia terranes its top is not as clearly or uniquely defined, because layers above have similar or even higher velocities. This layer is truncated on the south by an LVZ of the north dipping sequence (layer 8).

North dipping layers in the upper and middle crust. The sequence of north dipping layers in the upper and middle crust beneath the Chugach and southern Peninsular terranes is controlled by data from the Transect and Chugach lines, which intersect at SP19, and by vertical incidence reflection data [*Fisher et al.*, 1989], which provides resolution between about SP11 and SP12 (Figures 3 and 4). The vertical incidence reflection data were used primarily to constrain the dips of interfaces.

Model A (Figure 3), or an alternate model, model B, to be discussed below, both produce better fits to the refraction/wide-angle reflection data for this sequence than did the models of *Page et al.* [1986] and *Fuis et al.* [1987]. The improvement came about from a recorrelation of layers beneath the central and southern Chugach terrane that was indicated by the vertical incidence reflection data.

The three high-velocity layers in the sequence (layers 7, 10, and 12) are separated by low-velocity zones (LVZs; layers 8/9 and 11). Layer 7 is traceable to within 2 km of the surface as a 6.8 km/s layer. If projected to the surface, it would correspond to the outcrops of metabasalt in the southern Chugach terrane. Layer 10 is clearly traceable for over 100 km as a high-velocity layer (7.2–7.5 km/s), from 5-km depth near the Contact fault to 25-km depth beneath the southern Peninsular terrane. Layer 12 is also traceable as a high-velocity layer (7.7 km/s) from near the Contact fault to a point beneath Mount Billy Mitchell, where it apparently decreases in velocity and becomes unresolvable in the LVZ created by layer 10 above. Layers 8/9 and 11 in this sequence are LVZs whose velocities are established indirectly using data from both the Transect and Chugach lines. We model considerable lateral velocity variation in layer 8/9, with a velocity as low as 5.7 km/s beneath the central and northern Chugach terrane. Layer 11 is modeled with an average velocity of 6.75 km/s.

In an alternate model for this north dipping sequence, model B (Figure 4*b*), layer 8/9 has a uniform velocity of 6.2 km/s, layer 10 is everywhere 1 km deeper than in model A, and layers 10 and 12 extend as far southward as points vertically beneath the trace of the Contact fault. This model fits the data from SP38 northward better than model A and fits other data somewhat worse than model A.

In model A, LVZs 8 and 11 correspond well with vertical incidence reflection bands 1 and 2, respectively, and high-velocity layers 10 and 12, with the thin, reflection-poor regions between bands 1, 2, and 3 (Figure 4*a*). In model B

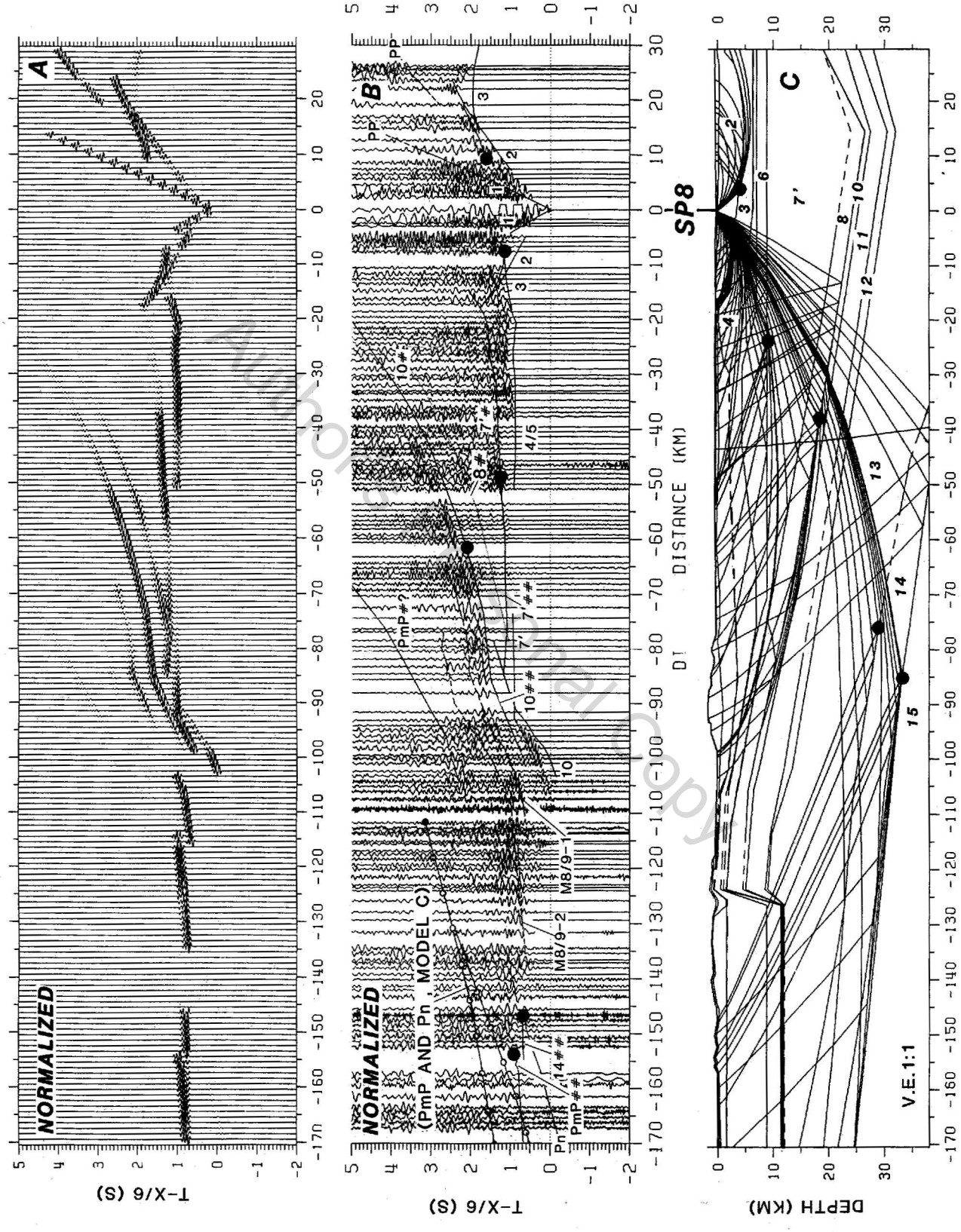

Fig. 5. Transect line: (*a*) Synthetic and (*b*) observed record sections and (*c*) ray diagram for model A from shot point 8 (SP8). Shot point is located at 0-km range. North is to the right. Synthetic seismograms in Figure 5*a* were calculated with the ray-density method of *McMechan and Mooney* [1980]. The record section in Figure 5*b* is trace-normalized, and travel times are reduced by distance/6 (km/s). Calculated travel times from model A (Figure 3) are superposed on the record section: solid lines are primary reflections and refractions; dashed lines are multiple reflections and refractions; the dotted line is a reflection from the top the major north dipping LVZ (layer 8); layer numbers are indicated for each branch; pound symbols indicate reflections: one symbol for a precritical reflection, two symbols for a postcritical reflection. Multiples are labeled "PP" and "PPP" for free-surface multiple refractions and "M8/9-1" and "M8/9-2", for example, for peg-leg multiples representing 1 and 2 reverberations in layers 8 and 9 combined. A question mark following a label indicates the predicted branch does not correspond to clear arrivals in the data. (In most cases, these questioned arrivals, such as "*PmP#*", have small predicted amplitudes, as can be seen by referring to Figure 5*a*). Large solid circles in Figure 5*b* are critical reflections corresponding to subsurface points in Figure 5*c*, also indicated by large solid circles. For comparison with *PmP* and *Pn* predicted by model A, *PmP* and *Pn* for model C are indicated by a line with open circles; a solid circle indicates the critical reflection. Differing apparent velocities for the prominent secondary arrival (10##) in this figure and in the reversing record section from SP12 (Figure 6) indicate a northward dip for layer 10, and a delay of this arrival from first arrivals indicates a major overlying LVZ (layer 8).

the correlation is not so clean. Models A and B have somewhat different geologic interpretations, as discussed below.

Lamination in the middle crust of the northern Copper River basin. The middle crust, between 19- and 28-km depth in the northern Copper River basin, consists of subhorizontal high-velocity layers (6.7 and 6.9 km/s; layers 10′ and 12′; Figure 3) and a sandwiched LVZ (layer 11′). These layers are constrained in depth and velocity by data on both the Transect line and the Glenn and Tok Highway cross lines; however, these data are much sparser than data for the north dipping sequence, and consequently, these layers are more poorly constrained. This laminated sequences can not be clearly correlated to the north dipping sequence, hence the blank zone between them in the model (Figure 3).

Lower crust and mantle. In the south half of the model, beneath the Prince William, Chugach, and southern Peninsular terranes, the lower crust consists of two layers (layers 13 and 14) separated by a boundary marking the top of the Wrangell Wadati-Benioff zone. This boundary is inferred to be the megathrust between the Northern American and Pacific plates [*Page et al.*, 1989]. In model A (Figure 3), both layers show marked lateral velocity changes (from 6.1 to 7.2 km/s on average for layers 13 and 6.4 to 7.4 km/s for layer 14), although these changes are poorly constrained. Mantle velocity, modeled at 7.8 km/s, is weakly constrained by modeling of amplitudes to be between 7.5 and 8.0 km/s (see Appendix A). No clear *Pn* arrivals constrain this velocity.

In the north half of the model, lower crustal layer 13′ is thick (16–26 km), and it velocity, modeled as 6.85 km/s, is poorly constrained. Moho dips gently (7°) southward to a maximum depth of 57 km beneath the southern Copper River basin. Mantle velocity, modeled as 8.3 km/s, appears to be between 8.0 and 8.5 km/s, in contrast to the subducting mantle to the south. *Pn* arrivals do constrain this velocity.

Much of the lower crust is poorly resolved, because it falls within LVZs created by high-velocity layers in the middle crust. In fact, a significantly different alternate model, model C (Figure 4*c*), is permissible which fits most of the refraction data as well as model A (Figure 3). Model C differs from model A in that layers 13 and 13′ have everywhere a velocity of 6.4–6.5 km/s, and layer 14 has a velocity of 6.5–6.6 km/s. Layer 14 is thicker (8 km) and also appears to thin northward, although such thinning is not well resolved in either models A or C. Because layer 13 is faster in the southern quarter of the model and slower in the north half of the model compared to model A, the Moho is corresponding deeper and shallower in those regions, respectively. In the intervening region, between Mount Billy Mitchell and the southern Copper River basin, the Moho is deeper than in model A owing to use of a different phase correlation.

Major Model Constraints in the Data

Constraints for major features in the upper crust and in the north dipping sequence beneath the Chugach and southern Peninsular terranes are best illustrated in record sections from SP8 and SP12 (Figures 5*b* and 6*b*). The primary constraints for the lower crust and Moho are record sections from SP37 and SP11 (Figures 7*b* and 8*b*) for the region beneath the Prince William and southern Chugach terranes and record sections from SP19 and SP1 (Figures 9*b* and 10*b*) for the region farther north. The remaining record sections

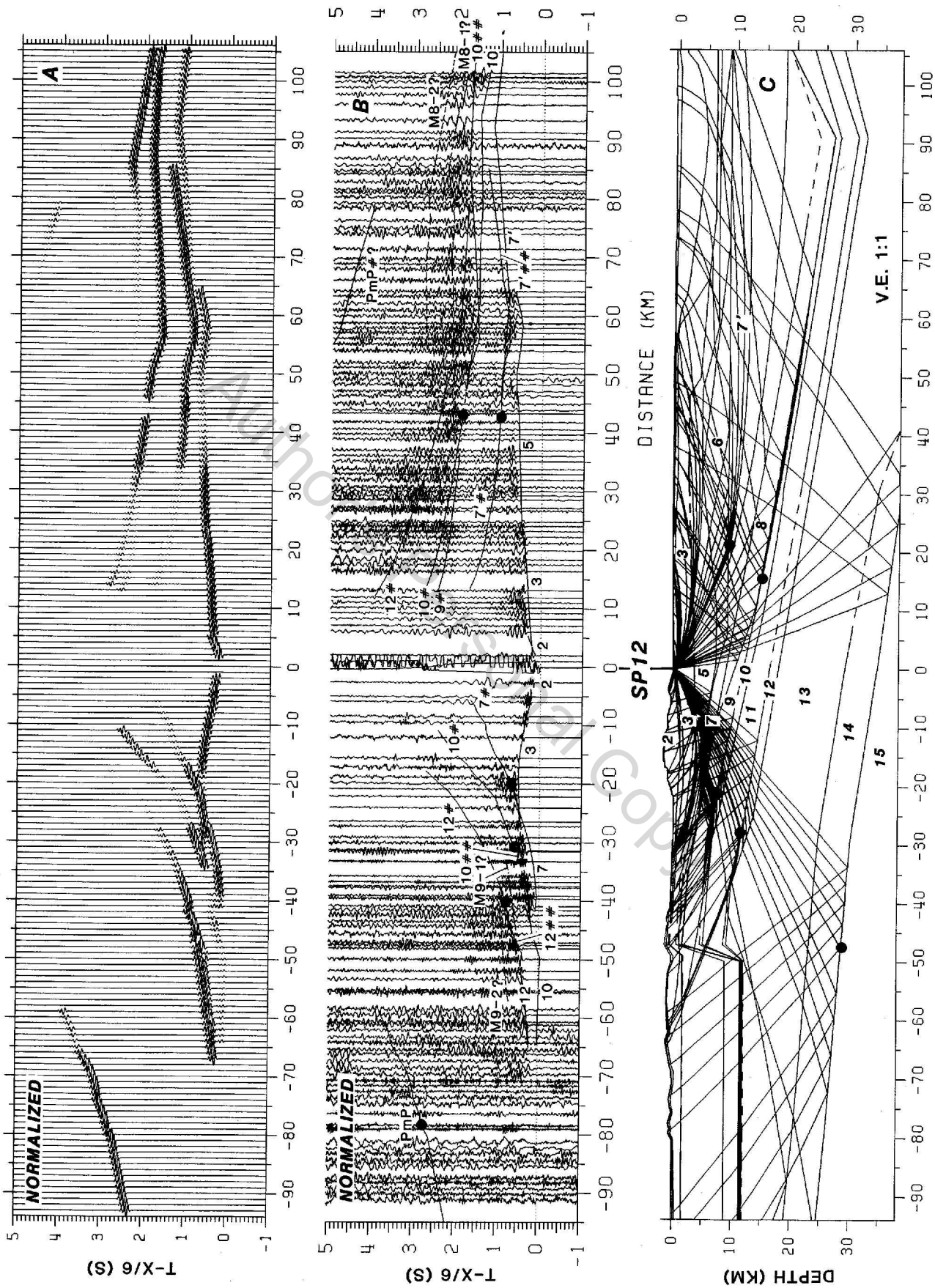

Fig. 6. Transect line: SP12. Format is the same as for Figure 5. Asymmetry of secondary branches (e.g., 10#, 12#) indicates shoaling of layers to the south.

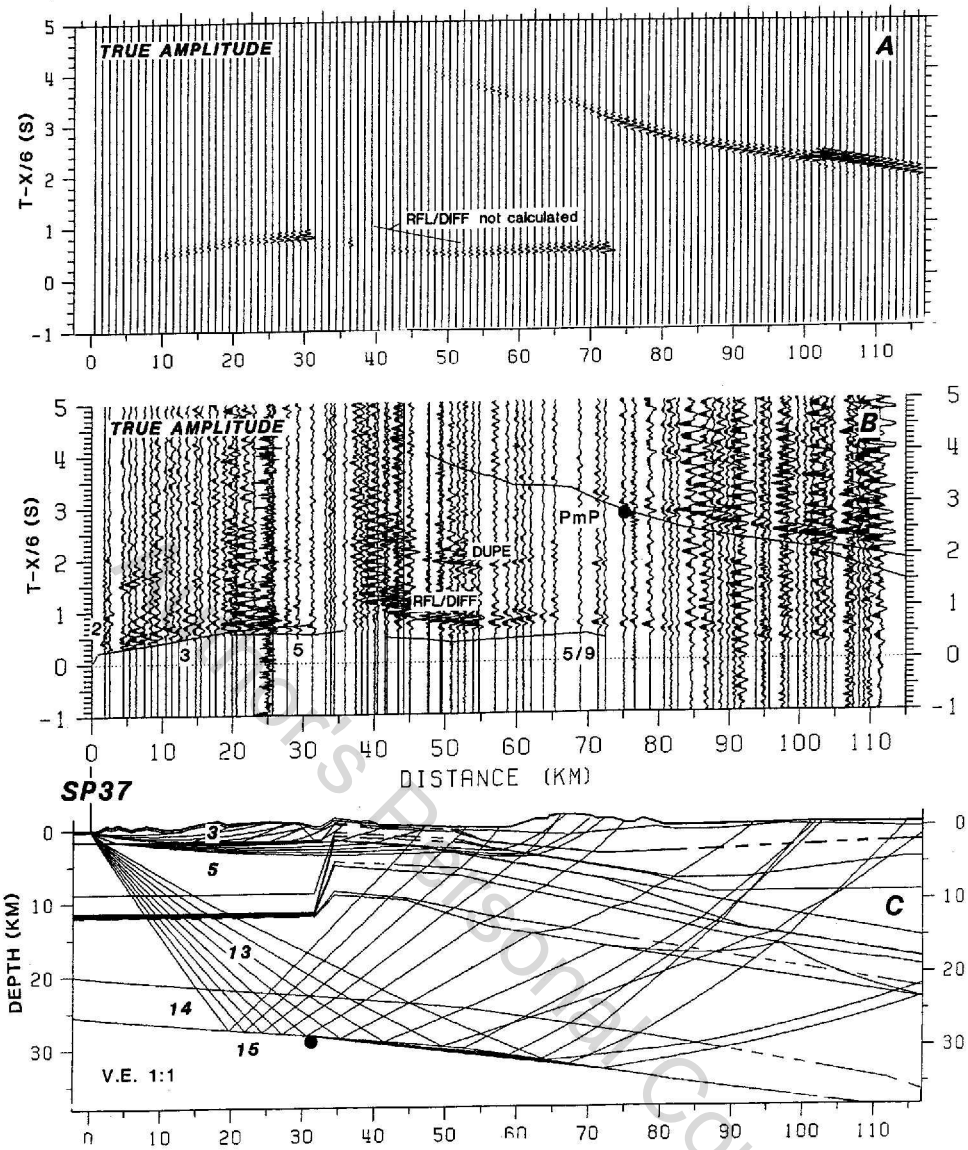

Fig. 7. Transect line: SP37. Format is the same as for Figure 5, but true relative amplitudes are shown. In Figure 7*a*, traces are scaled by distance; in Figure 7*b*, by distance raised to the power 1.5 (to compensate for scattering and attenuation). *PmP* from the subducting mantle (layer 15) is prominent. An unmodeled reflection (RFL?) is indicated; this feature might also be a diffraction from layers 10 or 12 beneath the Chugach terrane. A duplicate travel time curve (DUPE) is generated about 1 s after the lake explosion by collapse of the column of water raised by the explosion.

for the Transect line (except those for the North Richardson Highway line) are presented in Appendix A.

In the record section for SP8 (Figure 5*b*), travel time branches with relatively low apparent velocities (2.5–4.8 km/s) define asymmetric travel time curves about the shot point, indicating an increasing thickness of low-velocity rocks (layers 1 and 2) northward into the Copper River basin. An average velocity for "basement" near 6 km/s is seen south of the shot point between ranges of about 15 and 50 km, but basement arrivals become abruptly weak beyond 40-km range. Two branches of clear secondary arrivals are seen. The first, from layer 7′, has an apparent velocity of about 6.4 km/s, is strongest between ranges of about 40 and 50 km, and is delayed from first arrivals by as much as 0.4 s (Figure 5*b*, "7′#", "7′##"; quotation marks enclose labels seen on figures; the pound signs indicate precritical (#) and postcritical (##) reflections from the top of the given layer). The second, from layer 10, is the most prominent feature on the record section and is strongest between about 50- and 90-km range (Figure 5*b* "10#," "10##"; see also Figure A3). This branch is delayed from first arrivals at ranges beyond 75 km by as much 0.6 s, suggesting the presence of a major LVZ (layers 8 and 9) above layer 10. High-amplitude first arrivals, interpreted as refractions from layer 10, have a very high apparent velocity beyond 90-km range and become weak beyond 110-km range (Figure 5*b*, "10"). Echelon branches of high-amplitude secondary arrivals are seen between ranges of 100 and 140 km. These have travel times appropriate for peg-leg multiples within layers 8 and 9 (Figure 5*b*, "M8/9-1"). (Note that "M8/9-1" denotes 1 reverberation within layers 8 and 9 combined; "M8/9-2" denotes 2 reverberations; etc.) High-amplitude but somewhat incoherent secondary arrivals are seen beyond 140-km range that have appropriate travel times for *PmP*. The

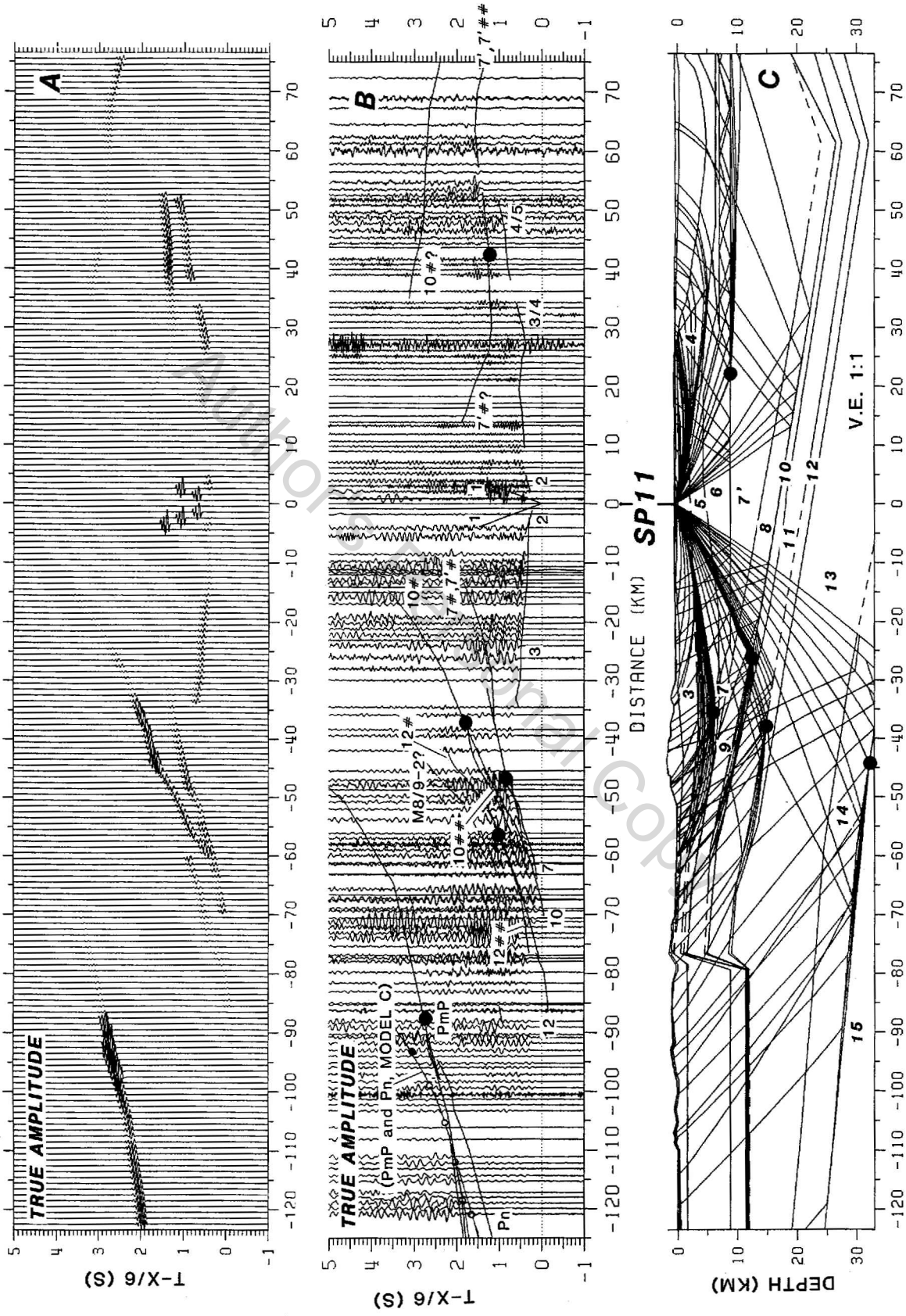

Fig. 8. Transect line: SP11. Format is the same as for Figures 5 and 7; true relative amplitudes are shown. Asymmetry of branches similar to that of SP12 (Figure 6) is seen. *PmP* from the subducting mantle (layer 15) is prominent.

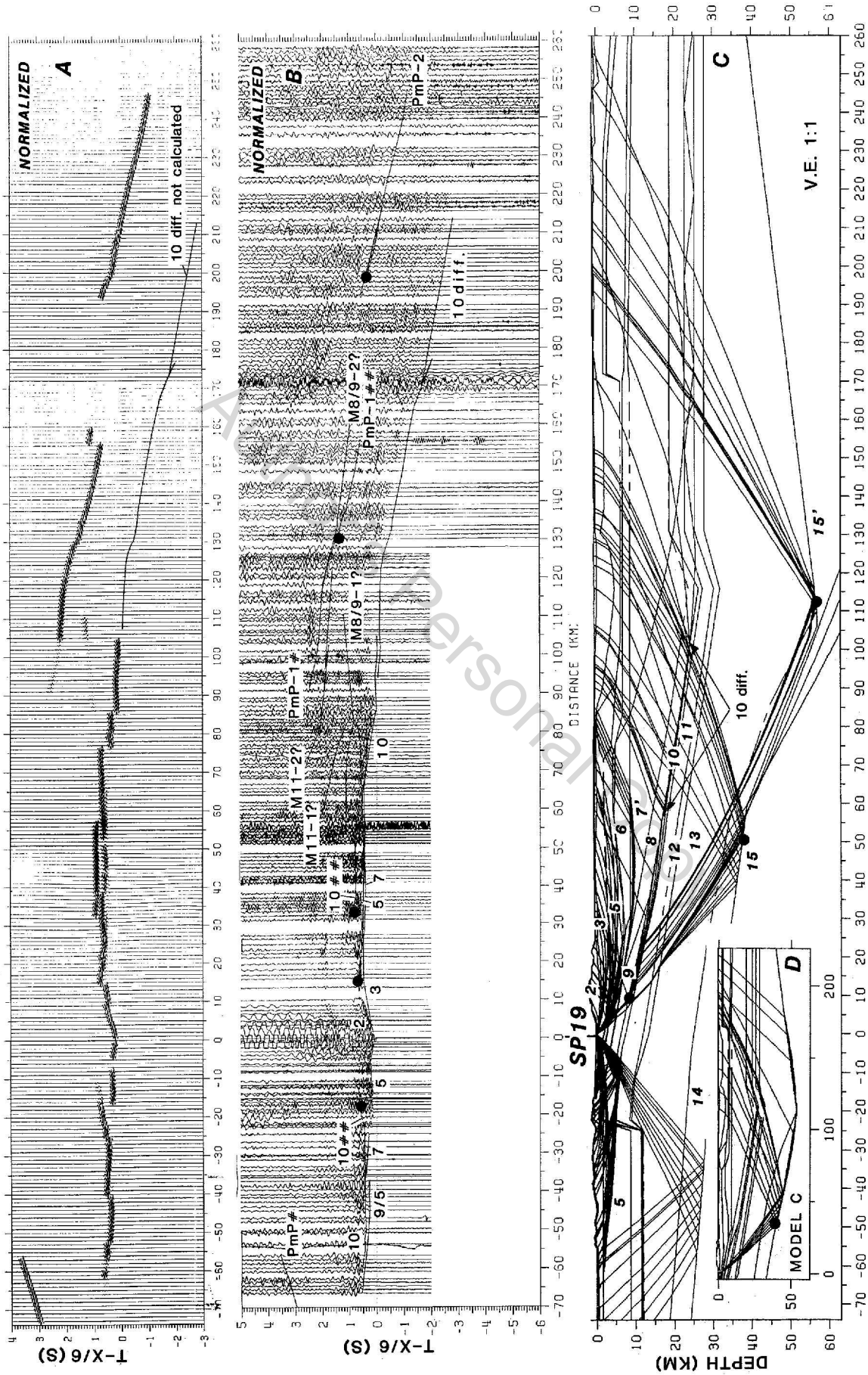

Fig. 9. Transect line: SP19. Format is the same as for Figure 5, but an additional ray diagram (Figure 9*d*) is included to show *PmP* and *Pn* rays for model C. "*PmP*-1" is explained in model A as a simple reflection from the the subducting mantle (layer 15). "*PmP*-2" is explained as a reflection from the mantle of the North American plate (layer 15′) that undergoes an intermediate reflection or refraction in the steeply dipping part of the subducting plate (layers 14 and 15; see Figure 9*c*). "10 diff." is diffracted first arrivals from layer 10. This branch is modeled as originating in the interval between the two arrows in Figure 9*c*; it is not calculated in Figure 9*a*.

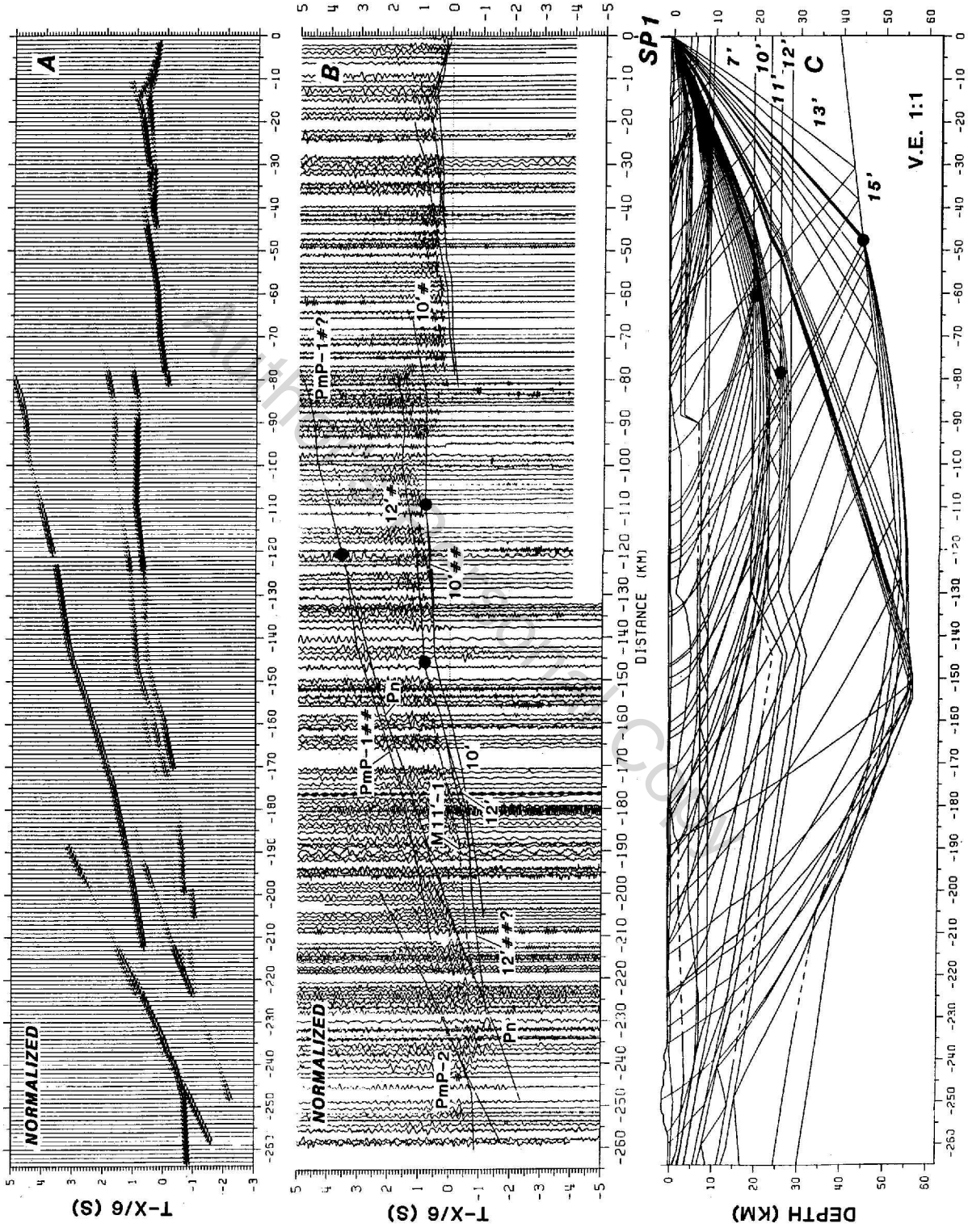

Fig. 10. Transect line: SP1. Format is same as for Figure 5. Prominent phases from both midcrustal layers (layers 10′ and 12′) and from mantle of the North American plate (layer 15′) are seen. The late mantle phases imply a deep Moho.

primary constraints for *PmP*, however, are seen on record sections from other shot points. Note that there are no clear arrivals along the *PmP* branch predicted by the alternate model, model C (Figure 4*c*).

The data from SP12 northward (Figure 6*b*) reverse some of the data from SP8. These, too, display a prominent band of secondary energy (between ranges of 20 and 100 km), from layer 10, that is significantly delayed from earlier branches. Differences between this record section and that from SP8 include (1) higher-velocity first-arrival branches near the shot point, (2) a basement branch with an apparent velocity less than 6 km/s, a drop in amplitudes beyond 37 km, but clear arrivals to 70-km range, (3) a weaker analog of the layer-7′ reflection, and (4) generally lower apparent velocities for the prominent band of secondary arrivals from layer 10.

The data from SP12 southward are quite asymmetric with respect to the data to the north. Between ranges of about 35 and 60 km, one sees two prominent echelon arrival branches with high apparent velocities and low reduced travel times (0–0.7 s). The first branch is interpreted as a superposition of reflections and refractions from layers 7 and 10 (Figure 6*b*, "7", "10", "10##") and the second, reflections and refractions from layer 12 (Figure 6*b*, "12", "12##"). Weak secondary arrivals are seen beyond 80-km range at 2–2.5 s reduced travel time that are consistent with *PmP*.

The Moho is best constrained by data from SP37 and SP11 (Figures 7*b* and 8*b*). From SP37, *PmP* is clearly traceable northward from 60-km range to the end of the record section, with large amplitudes beginning at about 85 km. Clear onset of *PmP* begins southward from SP11 at 90-km range and persists to the end of the record section, with large amplitudes beginning at 110-km range. However, a later branch of arrivals, predicted by the alternate model, model C, can also be observed (best seen on a normalized record secction, not shown). The apparent velocity of *PmP* approaches a relatively low value near the ends of the record sections from both SP37 and SP11, implying a relatively low velocity for the layer immediately above the Moho (layer 14) in the region where these reflections bottom (between SP38 and Mount Billy Mitchell, Figure 3). We have modeled layer 14 with a velocity of about 6.4 km/s in this region.

Record sections from SP19 and SP1 constrain the middle and lower crust of the Copper River basin and Moho north of about SP11 (Figures 3, 9*b*, and 10*b*). From SP19 northward, clear, low-amplitude first arrivals with an average apparent velocity near 7 km/s are seen from 125- to 220-km range and become faint at greater ranges (Figure 9*b*, "10 diff."). These have been modeled as diffractions from layer 10 (see Figure 9*c*), although alternative explanations are possible. Two branches of secondary arrivals are clearly visible: one, with a low apparent velocity (near 6 km/s) is seen at 2 s and 100- to 120-km range (Figure 9*b*, "*PmP*-1#"); the second, with a high apparent velocity (more than 8.5 km/s), is seen from 140- to 220-km range and is 2.5–4.5 s later than first arrivals (Figure 9*b*, "*PmP*-2"). The first is modeled as a precritical reflection from Moho near the sharp elbow in the subducting plate (see Figures 3 and 9*c*). The second is modeled as energy that refracts or reflects from the steeply dipping segment of the subducting plate, beneath the interval, SP11 to SP8, and reflects a second time from the south dipping Moho beneath the Copper River basin (see Figures 3 and 9*c* and Appendix A). Model A succeeds in matching the first branch and the distal part of the second branch. The alternative model, model C, cannot explain the first branch but can explain the entire second branch more simply as *PmP* from the subducting plate (see Figure 9*d*).

From the reversing shot point, SP1, a series of echelon arrival branches with high apparent velocities (more than 8 km/s) are seen in the range interval 100–200 km (Figure 10*b*, "10′", "12′", and "M11′-1"). These arrivals, together with similar arrivals on the Glenn/Tok Highway cross line of *Goodwin et al.* [1989] and E. L. Ambos et al. (submitted manuscript, 1988), document the existence of layering in the middle crust beneath the Copper River basin (layers 10′, 11′, 12′, Figure 3). In addition, strong secondary arrivals with a high apparent velocity (more than 8.5 km/s) are seen at 0.5 to −0.5 s and 195- to 230-km range. Weak first arrivals seem to extend this branch to the end of the record section, and a short branch of second arrivals at 3 s and 140- to 150-km range may represent the initiation of this branch. We interpret this branch to be combination of *Pn* and *PmP* (Figure 10*b*). Both models A and C explain this branch equally well.

Comparison of Model A With High-Resolution Velocity Models and Reflection Data in the Copper River Basin

Reflection data collected in the Copper River basin by the oil industry (R. Shafer, written communication, 1985) and by the U.S. Geological Survey [*Brocher et al.*, 1989*a*] have been used to construct a composite high-resolution velocity model that we can compare with model A (Figure 11). The south two-thirds of this composite model (Figure 11, coordinates 70–135 km) are taken chiefly from *Brocher et al.* [1989*a*], and the north third (Figure 11, coordinates 135–150 km) is taken chiefly from *Colburn and Fuis* [1986, also unpublished modeling, 1988]. The composite high-resolution model makes use of common shot gathers, stacked sections, and a sonic log from an exploration oil well near SP7.

Layer boundaries in model A and in the high-resolution model generally agree within 0.2–0.3 km in the northmost Chugach Mountains (Figure 11, coordinates 70–95 km) but diverge in the southern Copper River basin (coordinates 95–135 km). Shallow layer boundaries agree well at SP8, as they should; however, the high-resolution model incorporates an extra layer of relatively low velocity (2.3–3.2 km/s) and indicates considerably shallower basement (as much as 2 km shallower) in the Copper River basin. Unfortunately, reversed coverage of the basement was not obtainable from the common shot gathers that were used, hence the question marks on that boundary. The apparent discrepancy in basement depth between the models results primarily from inclusion of the 2.3–3.2 km/s layer in the high-resolution model; both models produce similar travel time delays for basement arrivals in the Copper River basin.

Two sets of prominent reflections can be seen in the Copper River basin north of coordinate 110 km (Figure 11). The upper set is seen at approximately 1 km below sea level. North of SP7, the base of this set cooresponds to a velocity boundary, 3.0–4.5 km/s, in the high-resolution model. South of SP7, this set may correlate with a velocity boundary, 3.2–3.6 km/s (Figure 11, coordinates 112–120 km). The deeper set of reflections corresponds in the high-resolution model to a velocity boundary, 4.6–5.2 km/s. This set of reflections has been identified in the well near SP7 as the top of the Talkeetna Formation (chiefly andesite flows and related sedimentary rocks). A sonic log from the well indi-

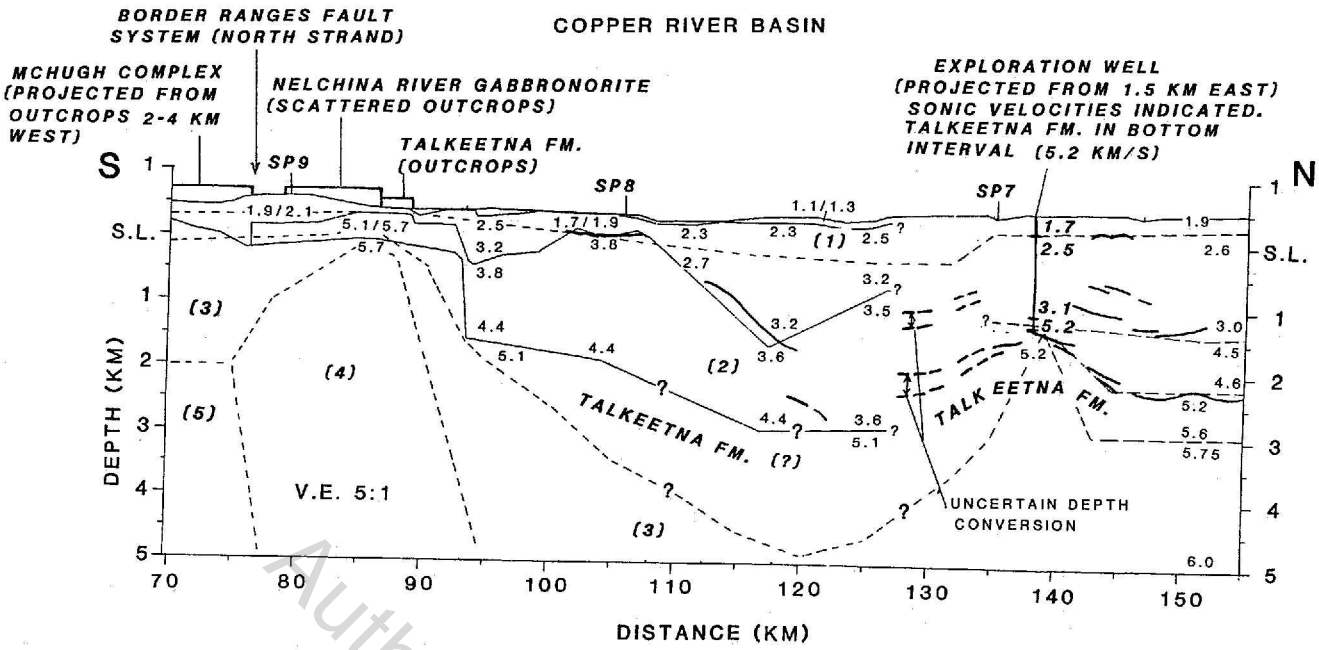

Fig. 11. Comparison of model A with high-resolution seismic refraction and reflection results from the Copper River basin. Solid light boundaries from 70–127 km are from *Brocher et al.* [1989*a*]. Dashed light lines are from model A (Figure 3). Solid heavy lines are reflections interpreted from oil industry data supplied by R. Shafer (written communication, 1985) that were converted from time to depth sections using refraction velocities. Light numbers are refraction velocities (in km/s). Heavy italic numbers in parentheses are layer numbers for model A. The distance coordinate system is similar to that of Figure 3 but is expanded to follow the roads from 70 to 127 km. Between SP8 and SP7, a shallower basin depth (3 km versus 5 km) is predicted by the high-resolution results than by our model A. Outcrops south of SP8 and well data near SP7 sugggest that 5.1 km/s basement beneath the Copper River basin is the Talkeetna Formation (see text).

cates a 5.2 km/s average interval velocity for the Talkeetna Formation. A similar interval velocity is documented for the Talkeetna Formation in another exploration well about 10 km to the northwest (E. L. Ambos et al., submitted manuscript, 1988). The apparent fault shown at about coordinate 95 km in the high-resolution model brings the Talkeetna Formation to the surface, where its model velocity is again 5.1 km/s.

To summarize, the high-resolution model contains three layers above basement, with velocities (1) less than 2 km/s, (2) roughly 2–3 km/s, and (3) 4–4.5 km/s. Basement has a velocity of 5.1–5.2 km/s at its top. Prominent reflections are seen in some places between the second and third layers and at the top of basement, which is identified as the Talkeetna Formation. In the northmost Chugach Mountians, model A agrees with the high-resolution model, but in the southern Copper River basin, it differs from this model in lacking an extra layer (2.3–3.2 km/s) and in having a greater basement depth.

CHUGACH LINE

Model CGH

We shall describe the model for the Chugach line (model CGH, Figure 12*b*) and then examine salient features in the data (Figures 13–16) that constrain the model. For a layer-by-layer discussion of model constraints and uncertainties the reader is referred to Appendix B.

Upper crust (layers 1–5). In model CGH, layers are numbered to be consistent with the models of the Transect Line (models A–C, Figures 3 and 4). Layers 1 and 2 are surficial layers. Layers 3 and 5 are "basement." Layers 7, 10, and 12A/12B are high-velocity layers, and layers 9 and 11A/11B are intervening LVZs.

Layers 1 and 2 represent unconsolidated glaciofluvial deposits and surficial bedrock, respectively. Layer 1 (1.8–1.9 km/s) is present in significant thickness only in a basin near Valdez (Figure 12*b*). Layer 2, as on the Transect line, has a poorly constrained velocity (4.2–5.0 km/s) and thickness, both of which can be traded off against each other. In many places, layer 2 is probably gradational into layer 3, although it is modeled as a discrete layer. "Basement" (layers 3 and 5) changes in average velocity, velocity gradient, and thickness from west to east (Figure 12*b*). Between SP17 and SP18, layer 3 is 6.1 km/s at its top with a low gradient (less than 0.1/s), but east of SP18, it is 5.6 km/s at its top with a higher gradient that increases progressively eastward (to a maximum of 0.34/s at SP20). Layer 5, on the other hand, has a fairly uniform velocity throughout the model (6.4–6.6 km/s) but thins markedly, from 6 km in the west to 1.5 km in the east. Like layer 3, the velocity gradient in layer 5 increases eastward. In fact, there is no clear evidence in the data (reflections) to indicate that the top of layer 5 is a sharp boundary. The average velocity of layers 3 and 5 on the Chugach line is everywhere higher than on the Transect line. This difference is consistent with laboratory measurements of anisotopy within the metaflysch of the Chugach terrane (Table 2; see interpretation and discussion section below).

Layers 7–12. On the Transect line, layers 7–12 compose a north dipping sequence. On the Chugach line between SP19 and SP20 these layers are subhorizontal. West of SP19,

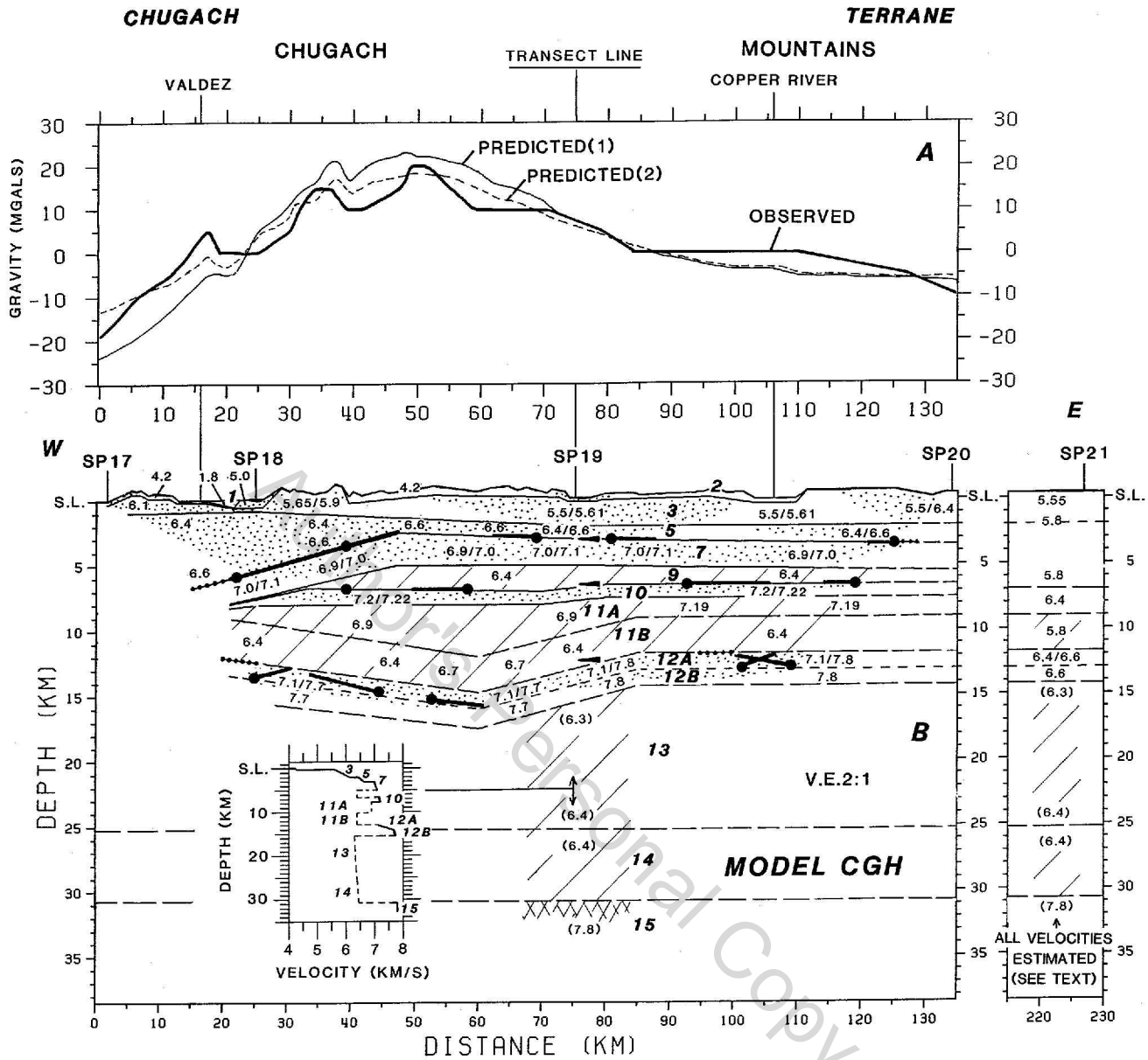

Fig. 12. (*a*) Observed and predicted Bouguer gravity profiles along the Chugach line. Observed data were kindly supplied by D. L. Barnes (written communication, 1986). Predicted curve 1 was calculated using a $2\frac{1}{2}$-dimensional gravity algorithm and the following layer densities (in g/cm^3): layer 1, 2.35; layer 3, 2.67–2.70 (depending on average velocity); layer 5, 2.75 (see Table 2); layer 7, 3.00; layer 9, 2.75; layer 10, 3.10; layer 11A, 3.00; layer 11B, 2.80; layers 12A and 12B, 3.15. Layer extensions in and out of the page are consistent with Figure 3 (see Appendix B). Predicted curve 2 was calculated in the same way, but layers 7, 10, and 11A all had a density of 2.92 g/cm^3. (*b*) Model CGH, velocity model for the Chugach line (see Figure 1 for location). Format is the same as for Figure 3. Layers are numbered as on the Transect line, but layers 11 and 12 are subdivided (see text). Layers 7–12 constitute the gently north dipping sequence on the Transect line and are interpreted as sedimentary and metasedimentary rocks interlayered with fragments of oceanic crust and mantle of the Kula plate. The gravity mimics the shape of layer 7, and a linkage between the two is inferred (see text). A drastic change in velocity structure is required between SP20 and SP21 in layers above 15-km depth, but the details of the structure that we show at SP21 are speculative. The lower crust and Moho are controlled only on the Transect line. (In layer 12A, heavy lines are bottoming points not for reflections, as at the tops of other layers, but for rays turning sharply in a high velocity gradient.)

some layers dip west (layer 7), some dip west then east (layers 11B, 12A, and 12B), and some thicken and then pinch out (layers 9, 10, and 11A). Layer 7 has a velocity (6.9–7.1 km/s) that is marginally higher than that on the Transect line. Layers 10 and 12 have velocities similar to those on the Transect line, at least near the junction with that line, but a high gradient has been included in the upper part of layer 12 (sublayer 12A) to be consistent with the results of *Flueh et al.* [1989]. Velocities in the LVZs (layers 9 and 11) were modified from *Flueh et al.* [1989]. The latter velocity details are accurate only for the region east of about SP19, where the study by *Flueh et al.* [1989] was concentrated, and are less certain to the west.

Lower crust and mantle. Lower crust and mantle in

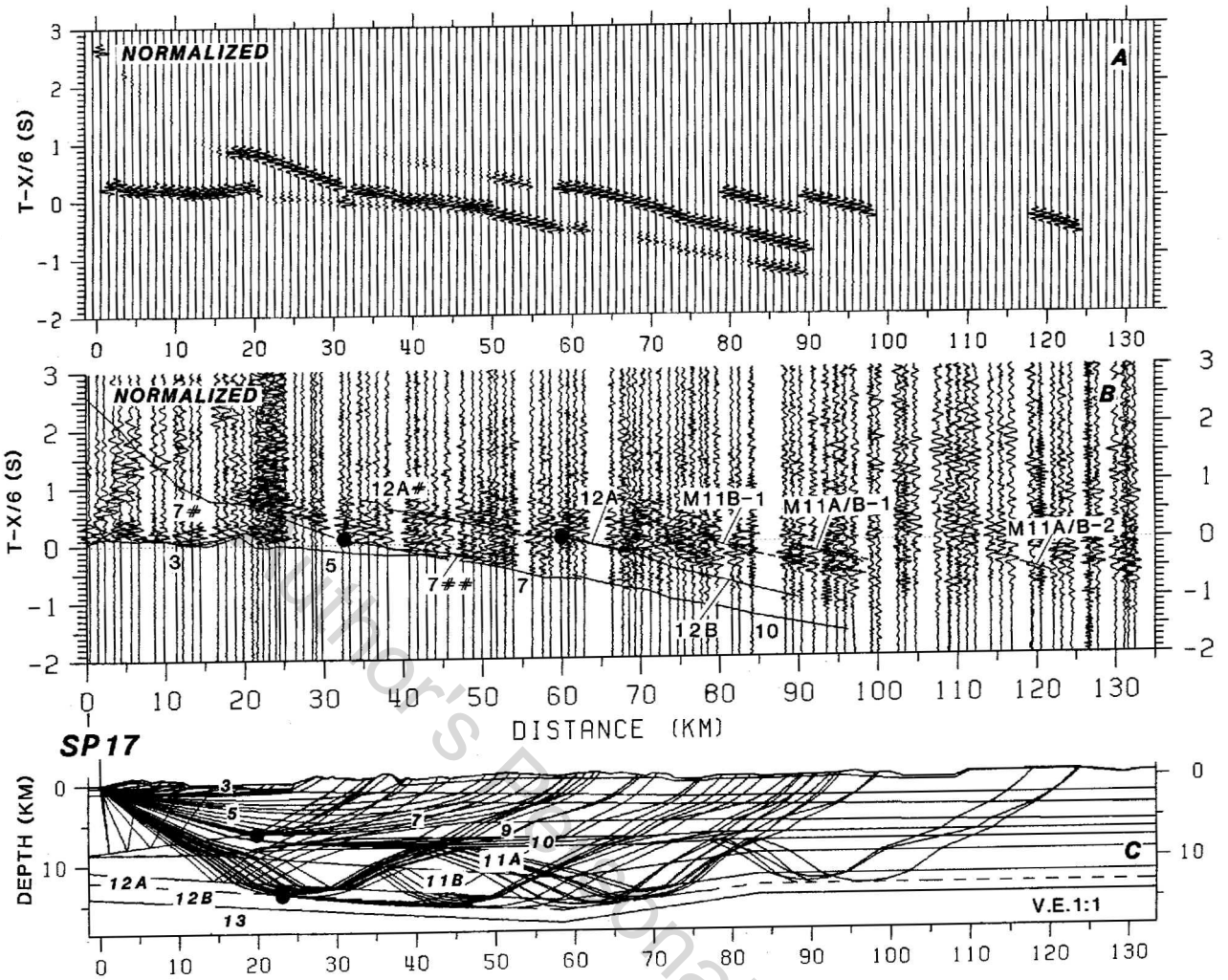

Fig. 13. Chugach line: SP17. Format is the same as for Figure 5, but the ray diagram (Figure 13*c*) includes ray paths for peg-leg multiples in layer 11. Echelon secondary arrivals in Figures 13*a* and 13*b* include both primary reflections ("12A#" and "12A") and peg-leg multiples ("M11B-1" and "M11A/B-1"). (See Figure 5 for definitions of symbols in quotes.) East is on the right.

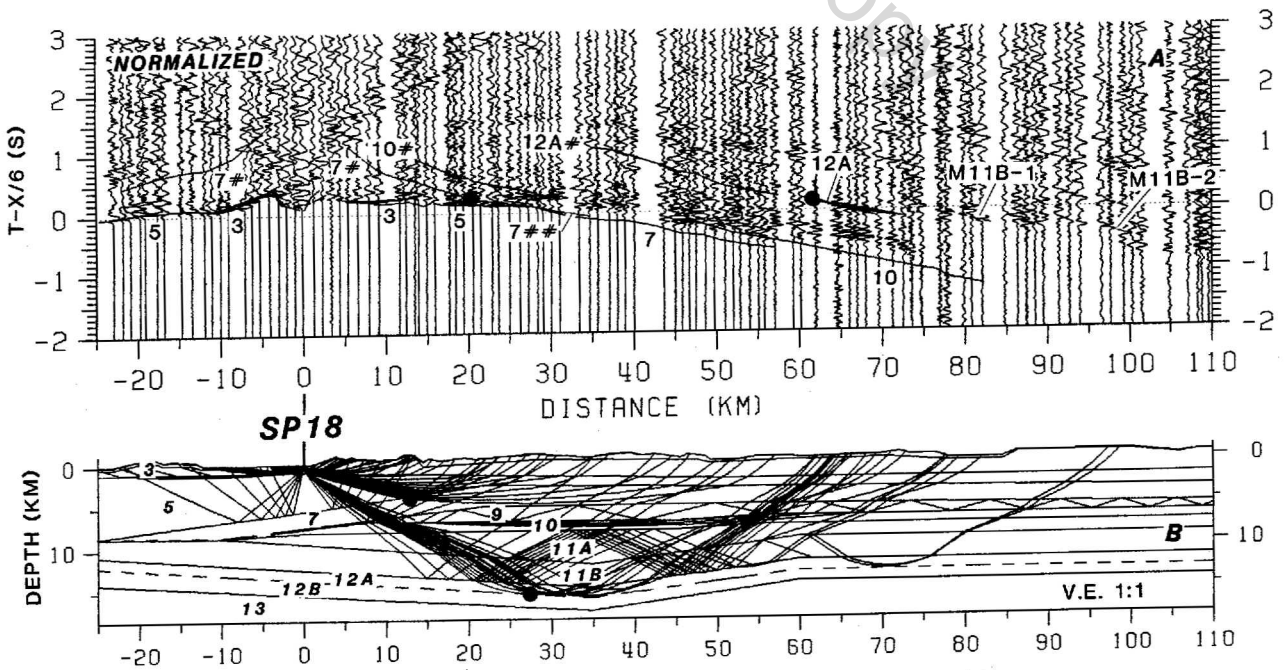

Fig. 14. Chugach line: SP18. Format is the same as for Figures 5 and 13.

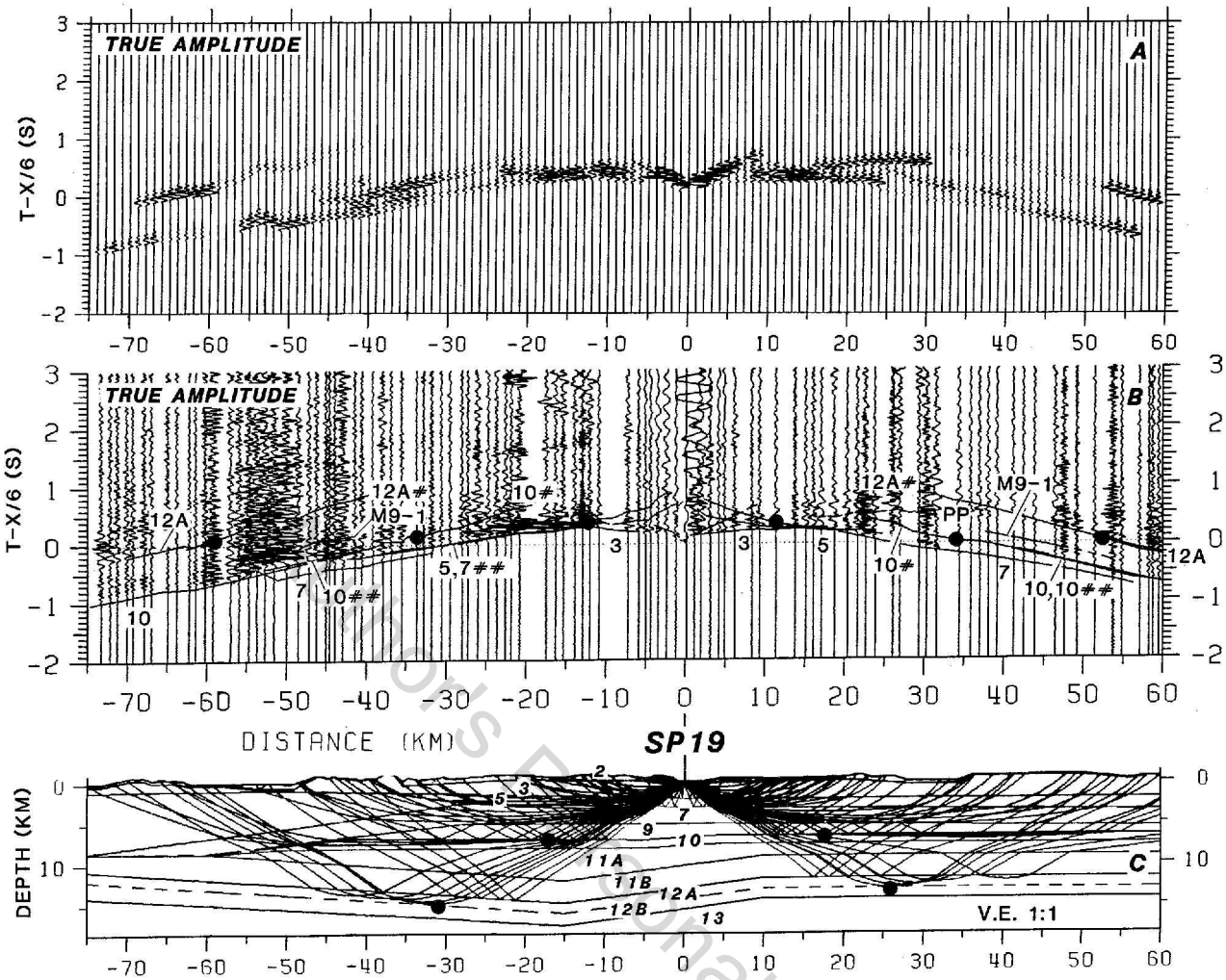

Fig. 15. Chugach line: SP19. Format is the same as for Figure 7 (true amplitudes shown). Asymmetry in the branch 12A indicates different depths for layer 12 east and west of SP19.

model CGH are taken without modification from model A of the Transect line. Unfortunately, the high velocity of layer 12 and velocity changes eastward of SP20 prevent perceptible energy from layers 13–15 from reaching the surface from any of the shotpoints.

Major Model Constraints in the Data

Unlike data recorded on the Transect line (e.g., Figures 5*b* and 6*b*), the data from SP17 through SP20 on the Chugach line are grossly similar (Figures 13–16). Superposing first-arrival picks for all shot points out to 60 km, the scatter does not exceed about 0.3 s. Generally high apparent velocities (near 6 km/s) are seen near the shot points, due to the lack of unconsolidated sedimentary rocks along the line. First arrivals with apparent velocities between 6.4 and 7.2 km/s are seen between ranges of about 20 and 50–60 km, and echelon secondary arrivals with somewhat higher apparent velocities are seen beginning at ranges as little as 20 km. From all shot points but SP17, the first clear secondary arrival begins at 30- to 40-km range and is delayed from first arrivals by only a few tenths of a second (Figures 13–16, "10", "10##"). From all shot points a prominent secondary arrival, inferred to be a reflection, begins at 50- to 70-km range and is delayed from first arrivals by 0.6–0.7 s (Figures 13–16, "12A"). From SP20, a low-amplitude branch, inferred to be a refraction, emerges from this prominent branch with a high apparent velocity (7.7 km/s; Figure 16*b*, "12B"). A similar arrival is seen less clearly from SP17 (Figure 13*b*, "12B"). The large delay of branch "12A" from the first arrivals suggests the presence of a major LVZ (layer 11). Beginning at 70- to 90-km range from all shot points is a third prominent echelon arrival delayed from the second one by 0.5–0.6 s (Figures 13, 14, and 16, "M11B-1"). Studies by *Flueh et al.* [1989] indicate that this arrival is a peg-leg multiple generated in layer 11 (specifically, layer 11B). Additional echelon arrivals are seen at greater ranges and are interpreted as successive reverberations within layer 11.

When examined in detail, the data differ significantly from shot point to shot point both in the apparent velocity of first arrivals and in travel times and amplitudes of secondary arrivals. One of the most important differences is the fact that a strong secondary arrival beginning at about 20 km for SP17 and also SP18 westward (Figures 13*b* and 14*a*, "7#") is not seen for other shot points. For SP18 eastward, a similar phase begins at 10- to 15-km range, giving the data from SP18 a distinctly asymmetrical appearance and suggesting marked eastward shoaling of a reflector (layer 7; Figure 14*a*, "7#"). Another important difference is the

greater range of onset (10 km greater) for the strong "12A" secondary arrival for SP17, SP18, and SP19 westward compared to SP19 eastward and SP20 (Figures 13–16). This difference is seen most clearly in the marked asymmetry in the record section for SP19 (Figure 15*b*) and suggests a greater depth for layer 12 west of SP19 than east of SP19. Thus, in spite of the gross data similarity among the several shot points, there is clear evidence for lateral velocity changes along the Chugach line.

An offset shot for the Chugach line at SP21 (Figure 2) provided unreversed coverage of deep layers in the Chugach Mountains. The data from SP21 (Figure 17), like the data from other shot points, are characterized by echelon arrival branches that begin with strong secondary arrivals, continue as weak first arrivals, and disappear at greater ranges. The branches are delayed from one another by large fractions of a second (0.45 s on average) and have high apparent velocities of 7.1–8.3 km/s (Figure 17*a*, "12B", "M11B-1" through "M11B-4"). The latest clear branch on the record section begins at about 130-km range and is continuous over a larger range interval (100 km) than earlier branches (Figure 17*a*, "P_L").

The velocity in all layers above 15-km depth must decrease strongly from SP20 to SP21 (Figure 12*b*). If the velocity structure at SP20 were projected eastward with no change, arrivals from SP21 would be 0.7–1.0 s early compared to the data. This conclusion is surprising given the increase in metamorphic grade eastward from SP20. Without data in the interval between SP20 and SP21, we can only constrain the structure in broad terms. The reader is referred to Appendix B for a detailed discussion of the structure near SP21.

The latest phase seen from SP21 (Figure 17*a*, "P_L") is not *PmP* or *Pn* but is interpreted as an upper mantle reflection possibly from the base of the subducting lithosphere. Interestingly enough, *PmP* is not visible in the data, nor is more than a short branch segment predicted. A westward increase in the velocity of layer 12 between SP21 and SP20 (Figure 12*b*) creates a waveguide whose top is layer 12 and whose base is the Moho (Figure 17*b*). Little energy leaks out of this waveguide; *PmP* and *Pn* are in most places reflected postcritically downward from the base of layer 12. Thus the weak peg-leg multiples ("M11B-1", etc.) are not overprinted and obscured by these phases. On the other hand, energy from the reflector within the mantle, represented by the "P_L" branch, arrives at the base of layer 12 at steeper angles than *PmP* and *Pn* and is not trapped in the waveguide. (See also the discussion by *Flueh et al.* [1989].)

Multiples

Branches "M11B-1", etc., seen from most shot points and best displayed from SP21, are interpreted as peg-leg multiples generated in the second LVZ, layer 11 (specifically sublayer 11B), as stated above. Peg-leg multiples generated in the first LVZ, layer 9, are so early in time on the Chugach line, in contrast to the Transect line, that they are largely obscured by primary phases (see for example Figures 15*b* and 16*b*, "M9-1").

In an earlier interpretation [*Page et al.*, 1986; *Fuis et al.*, 1987] that has now been abandoned, branches "M11B-1", etc., were interpreted as primary reflections from successively deeper layers, below layer 12. Although ray theory permitted the earlier interpretations, *Flueh et al.* [1989] have shown using the reflectivity method that high-velocity refractions from each such layer would persist to much larger ranges and earlier travel times than seen in the data.

Gravity Ridge: A Link to Layer 7

The Chugach line lies largely on the crest of an east-west trending Bouguer gravity high with a maximum relief of 50–60 mGal and a maximum width of about 50 km [*Barnes*, 1977]. This ridge terminates at about Valdez, with a small prong extending southwestward, so that SP17 is off the ridge. The gravity profile along the Chugach line (Figure 12*a*) mimics the shape of layer 7 and thus (1) supports the configuration of this layer in model CGH and (2) suggests layer 7 is primarily responsible for the gravity ridge. On the Transect line, layer 7 projects to the surface at outcrops of metabasalt. These outcrops and the gravity ridge along the southern Chugach terrane are coextensive for 650 km eastward from our transect, further confirming the link of layer 7 to the gravity ridge. The greatest relief on the gravity profile along the Chugach line occurs between SP18 and SP19, over a region where layers 7–12 are thickest, suggesting that deeper layers in this sequence are also weakly linked to the gravity ridge. The gravity profile predicted from our velocity model (Figure 12*b*) matches the observed profile as closely as 5 mGal for an appropriate choice of layer densities (see Figure 12; Appendix B).

Comparison With the Model of Wolf and Levander [1989]

There is agreement between our model CGH and that of *Wolf and Levander* [1989] on the existence of 3 high velocity layers beneath the Chugach Mountains (our layers 7, 10, and 12; their layers 3, 5, and 7), which are separated by LVZs of varying definition. Velocities agree well (generally within ±0.05 km/s) for the upper two layers, but their deepest layer is 0.3–0.4 km/s slower than ours. The configuration of the layers differs more or less significantly between the models, however. The layers of *Wolf and Levander* [1989] are largely horizontal with a trough-shaped deepening (by about 2 km) of the second and third layers east of SP19. In contrast, model CGH shows a marked deeping of the uppermost layer (layer 7) and a trough-shaped depression of the deepest layer (layer 12) west of SP19. *Wolf and Levander* [1989] accomplish travel time matches for the upper-layer arrivals west of SP19 by introducing a westward velocity decrease in this layer. They explain the prominent phase we have termed "7#" from SP17 (Figure 13) as a reflection from the base of this layer, but unfortunately predicted amplitudes are too small compared to first arrivals to strongly support this interpretation. In support of their proposed trough-shaped deepening of the lower layers east of SP19, they have explained the prominent phases we have termed "12A" (Figures 15 and 16) with reflections from the base of the middle layer. Again, predicted amplitudes are too small compared to other phases to support this configuration.

INTERPRETATION AND DISCUSSION

Interpretation of the compositions of the many layers in our models depends on conversion of modeled compressional wave seismic velocities to rock types. Since this conversion is nonunique, particularly in the absence of such

data as shear wave velocities, densities, or magnetic properties, surface and drill hole geologic information must be used. We shall discuss shallow layers (layers 3–5) briefly in each terrane, from south to north, and then speculate on the compositions of deeper layers.

Shallow Layers

Prince William terrane. In the Prince William terrane along the Transect line, Orca Group rocks, consisting of deformed and lightly metamorphosed flysch (zeolite to lower greenschist facies), are exposed. A large body of tholeiitic basalt (10 km wide in plan view) is exposed a few kilometers west of the line between SP37 and SP38 (*Winkler and Plafker* [1981]; not shown in Figure 2), and a large granitic pluton is parallel to and a few kilometers east of the line (Figure 2). Model velocity-depth curves for the Prince William terrane best match preliminary laboratory velocity data for flysch, granite, and metagraywacke but are a bit slow for tholeiitic basalt (Figure 18*a*). Velocity anisotropy in flysch of the Orca Group is not as marked in laboratory measurements or in model refraction velocities as it is in metaflysch of the Chugach terrane (see below). Velocities reported by *Taber et al.* [1986] on the Montague line, parallel to the structural grain in the Prince William terrane and at an angle of about 55° to the Transect line (Figure 1), are similar to velocities reported in this study near SP37.

Chugach terrane. The Valdez Group metaflysch (phyllite and metagraywacke) of the Chugach terrane crops out along the Transect line between SP11 and SP19 and along the entire Chugach line (Figure 2). Foliation planes strike generally east-west and dip steeply. A model velocity-depth curve for the Transect line at SP12 matches well laboratory velocity curves for phyllite and metagraywacke that were obtained from measurements perpendicular to foliation planes (a direction, Table 2; Figure 18*b*). On the other hand, a model velocity-depth curve for the Chugach line near SP17 best matches laboratory curves obtained from measurements parallel to foliation planes (b direction, Table 2; Figure 18*c*). Thus our model velocities for the Chugach metaflysch are consistent with laboratory results indicating anisotropy in these rocks. *Brocher et al.* [1989*a*] have also demonstrated anisotropy in Chugach terrane rocks using shot gather data from reflection profiling in the vicinity of SP12 along the Transect line.

Comparing model curves for the Transect and Chugach lines at SP19, one observes that basement (layers 3 and 5, Figure 18*d*) is slower on the Transect than Chugach line, as expected; however, the average basement velocity gradients for both curves are higher than predicted by either set of laboratory curves for phyllite and metagraywacke (a and b curves, Figure 18*d*), indicating a probable change in composition with depth at SP19. In a "down structure" direction from SP19, to the south toward the outcrops of metabasalt (Figure 2), one does indeed see an increase in metabasalt and metatuff in the section [*Winkler and Plafker*, 1981].

Layer 7 projects to the surface at the outcrops of metabasalt in the southern Chugach terrane (Figure 3), and indeed, preliminary laboratory velocity measurements of these metabasalts match well the model velocity for layer 7. A high-velocity segment of layer 5 intervenes between layer 7 and the outcrops. We interpret this high-velocity segment as a zone of open cracks and weathering in the metabasalt. Layer 7 appears to be slightly anisotropic (Figure 18*d*). (Note that the calculated depths to layers 7 and 10 are slightly less on the Transect line than on the Chugach line owing in part to anisotropy in the layers above them.)

Peninsular terrane. The Transect, Glenn, and Tok Highway lines cross the Peninsular terrane where it includes sedimentary rocks of the Copper River basin (Figures 1 and 2; layers 1 and 2, Figure 3; *Plafker et al.* [1989]). For a detailed discussion of these sedimentary rocks, the reader is referred to E. L. Ambos et al. (submitted manuscript, 1988).

Wells that penetrate to basement in the central Copper River basin (layer 3, Figure 3) and outcrops in the southern Copper River basin indicate that basement is, at least in its upper part, chiefly the Talkeetna Formation (Figure 11) [*Alaska Geological Society*, 1970; E. L. Ambos et al., submitted manuscript, 1988]. However, at least one well encountered "syenite" [*Alaska Geological Society*, 1970], and outcrops of Jurassic granodiorite have been mapped in the northern Copper River basin [*Nokleberg et al.*, 1986]. Interval velocities measured in wells that penetrate the Talkeetna Formation (5.2 km/s) and our model velocities for the upper part of basement (5.1–5.8 km/s) are in approximate agreement (Figures 3 and 11). However, laboratory velocity measurements for the Talkeetna Formation are higher (6.1 km/s for andesite breccia and 6.5 km/s for andesite flow, at 100 MPa, Table 2). Thus the Talkeetna Formation in the Copper River basin (1) consists of more clastic rocks than lava flows, (2) is highly fractured, and/or (3) is mixed with rocks of lower velocity. Outcrops certainly indicate that the Talkeetna Formation is fractured [*Plafker et al.*, 1989; *Nokleberg et al.*, 1989]. In addition, the well and outcrop information cited above indicate some admixture of granitic rocks.

Aeromagnetic data in the Copper River basin suggest strongly the presence of granitic rocks in the basement. A broad but strong aeromagnetic high is observed that trends east-west and has its axis at about the latitude of shot point 7 [*Godson*, 1984]. This feature has been modeled by making basement in the Copper River basin highly magnetic, as discussed by *Campbell and Barnes* [1985] and *Campbell* [1987]. Measurements of magnetic susceptibility for rocks of the Talkeetna Formation [*Burns*, 1982] indicate that this unit could not be responsible for the aeromagnetic high. Rocks that might produce such a high include Jurassic granitic rocks or the BRUMA, both of which produce strong aeromagnetic anomalies where they crop out in the northern Chugach Mountains (compare the detailed aeromagnetic map by the *U.S. Geological Survey* [1979] with the geological map by *Winkler et al.* [1981]. Our refraction velocities would appear to rule out BRUMA (Table 2). Thus it would appear that Jurassic granitic rocks are a significant component of layer 3.

Body 4 (6.0–6.22 km/s) underlies a region of sparse outcrops of the Nelchina River Gabbronorite (upper part of BRUMA; Figures 3 and 11). Laboratory velocity measurements are not yet available for these rocks, but a layered gabbro of the Tonsina ultramafic-mafic suite to the south (lower part of BRUMA) has velocities ranging from 6.4 to 7.2 km/s in a direction perpendicular to foliation and higher velocities within the foliation (Table 2; see measurements at 10–100 MPa). Rays bottoming in body 4 would be traveling roughly perpendicular to steeply north dipping foliation in the BRUMA, if outcrop attitudes can be projected to depth [see *Nokleberg et al.*, 1989; *DeBari and Coleman*, 1989]. To

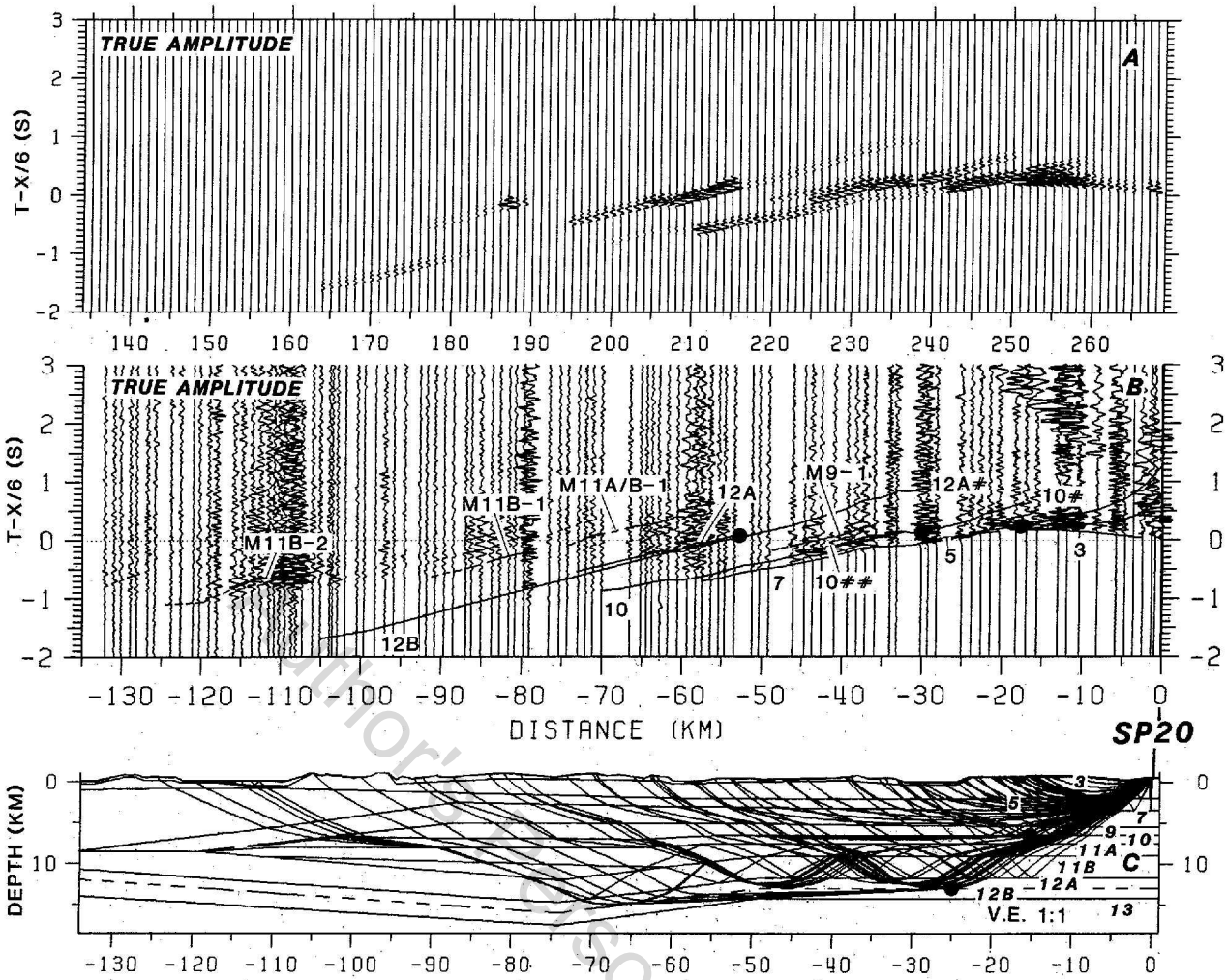

Fig. 16. Chugach line: SP20. Format is the same as Figure 7 (true amplitudes shown), but the ray diagram (Figure 16*c*) includes ray paths for peg-leg multiples in layer 11.

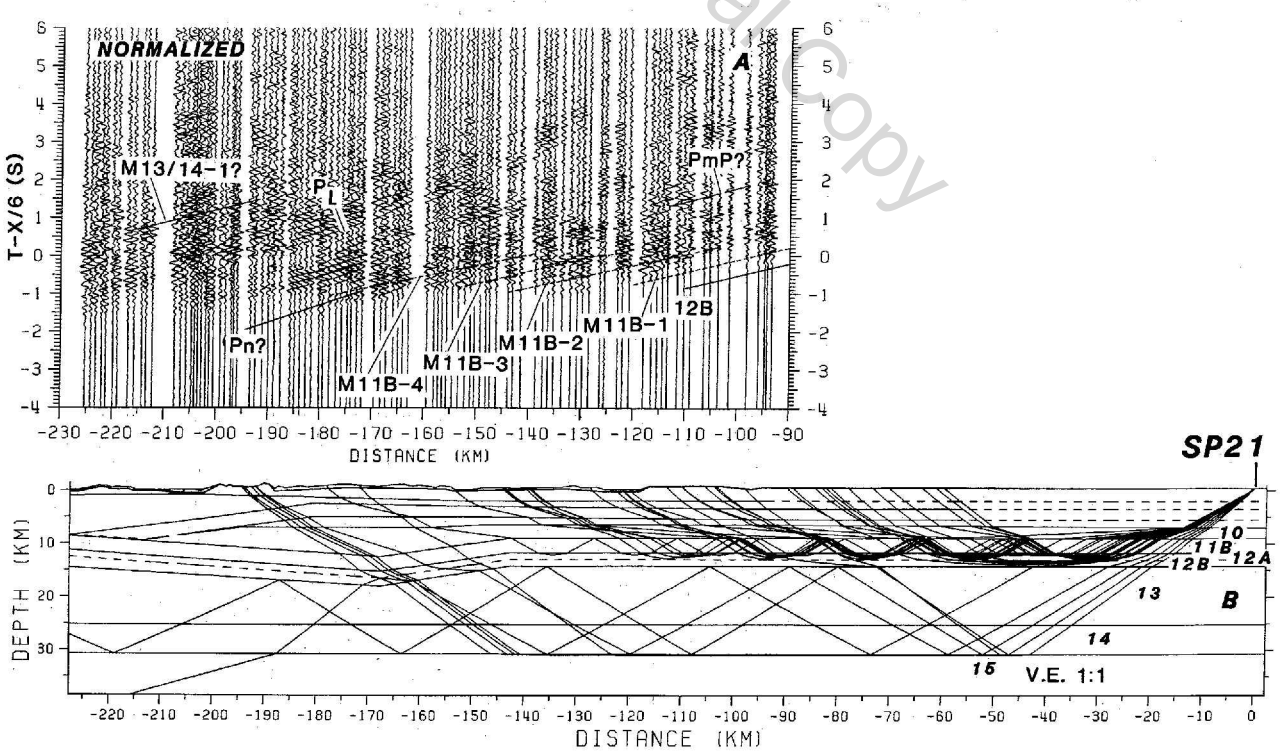

Fig. 17. Chugach line: SP21. Format is the same as Figure 5, but the ray diagram (Figure 17*b*) includes ray paths for peg-leg multiples in layer 11. A marked increase in the velocity of layer 12 westward from SP21 creates a waveguide that postcritically reflects most upgoing *PmP* and *Pn* energy at the base of layer 12; no clear *PmP* or *Pn* arrivals are observed in the data. P_L is an inferred reflection from within the mantle. East is on the right.

TABLE 2. Compressional Wave Velocities and Densities of Selected Rocks Along the Southern TACT Route at Pressures to 1000 MPa

		Chugach Terrane					Peninsular Terrane			
		Valdez Group			Schist of Liberty Creek		Tonsina Ultramafic-Mafic Suite		Talkeetna Formation	
Pressure, MPa	Sample Orientation*	TA-1 $\rho = 2734$ Phyllite	TA-8 $\rho = 2767$ Meta-graywacke	TA-5 $\rho = 2779$ Metatuff	TA-9 $\rho = 3022$ Blue-schist	TA-11 $\rho = 2990$ Green-schist	TA-30 $\rho = 3140$ Serpentinized Dunite	TA-31 $\rho = 3234$ Layered Gabbro	TA-25 $\rho = 2886$ Andesite Flow	TA-26 $\rho = 2686$ Andesite Breccia
10	a	5.31	5.02	5.62	5.74	6.13	7.14	6.37	5.96	5.63
	b	6.27	6.06	6.71	6.60	7.36	6.70	6.78	6.27	5.64
	c	6.18	5.52	6.41	5.80	6.46	6.87	6.87	6.12	5.86
	mean	5.92	5.53	6.25	6.05	6.65	6.90	6.67	6.12	5.71
100	a	5.80	5.93	6.30	6.41	6.45	7.34	6.92	6.42	6.15
	b	6.53	6.45	6.85	7.00	7.48	6.85	7.33	6.53	6.00
	c	6.44	6.14	6.59	6.39	6.75	7.01	7.42	6.48	6.10
	mean	6.26	6.17	6.58	6.60	6.89	7.07	7.22	6.48	6.08
200	a	5.90	6.05	6.38	6.60	6.53	7.41	7.04	6.51	6.29
	b	6.58	6.54	6.90	7.13	7.52	6.91	7.43	6.61	6.11
	c	6.51	6.24	6.65	6.57	6.83	7.06	7.52	6.56	6.20
	mean	6.33	6.28	6.64	6.77	6.96	7.13	7.33	6.56	6.20
300	a	5.96	6.11	6.42	6.69	6.57	7.45	7.10	6.56	6.35
	b	6.61	6.57	6.92	7.19	7.55	6.95	7.47	6.65	6.17
	c	6.54	6.29	6.68	6.65	6.86	7.09	7.55	6.60	6.25
	mean	6.37	6.32	6.67	6.84	6.99	7.16	7.37	6.60	6.26
400	a	6.00	6.15	6.45	6.74	6.59	7.48	7.13	6.60	6.39
	b	6.63	6.60	6.94	7.23	7.57	6.99	7.49	6.68	6.20
	c	6.57	6.33	6.70	6.70	6.89	7.12	7.57	6.64	6.28
	mean	6.40	6.36	6.70	6.89	7.02	7.20	7.40	6.64	6.29
500	a	6.03	6.18	6.48	6.78	6.62	7.50	7.16	6.62	6.42
	b	6.64	6.62	6.96	7.25	7.58	7.01	7.51	6.70	6.23
	c	6.59	6.35	6.72	6.74	6.91	7.15	7.59	6.66	6.29
	mean	6.42	6.38	6.72	6.92	7.04	7.22	7.42	6.66	6.32
1000	a	6.13	6.28	6.55	6.90	6.69	7.57	7.26	6.71	6.52
	b	6.68	6.68	7.01	7.34	7.63	7.10	7.57	6.77	6.31
	c	6.65	6.44	6.78	6.85	6.97	7.23	7.64	6.74	6.34
	mean	6.49	6.47	6.78	7.03	7.10	7.30	7.49	6.74	6.39
Sample location										
Latitude		61°07′11″	61°15′09″	61°10′21″	61°36′34″	61°36′18″	61°35′10″	61°36′05′	61°46′55″	61°46′55″
Longitude		146°21′30″	145°16′46″	145°39′29″	144°27′41″	144°27′15″	145°07′21″	145°01′02″	145°11′02″	145°11′02″

*Sample orientation: a, perpendicular to foliation; b, parallel to foliation and lineation; c, parallel to foliation, perpendicular to lineation.

Velocities (km/s) were measured at confining pressures to 1000 MPa (equivalent to crustal depths of approximately 35 km) using the method described in detail by *Christensen* [1985]. Three mutually perpendicular cores (orientations a, b, and c) were taken from each sample, cut to right circular cylinders and polished flat and parallel to within 0.008 cm. Typical sample dimensions after preparation were 2.54 cm in diameter and 4.00 cm in length. Bulk densities (kg/m^3) were determined from the weights and dimensions of the cores. Prior to the velocity runs, the samples were jacketed with copper foil to exclude the pressure medium from the pore spaces.

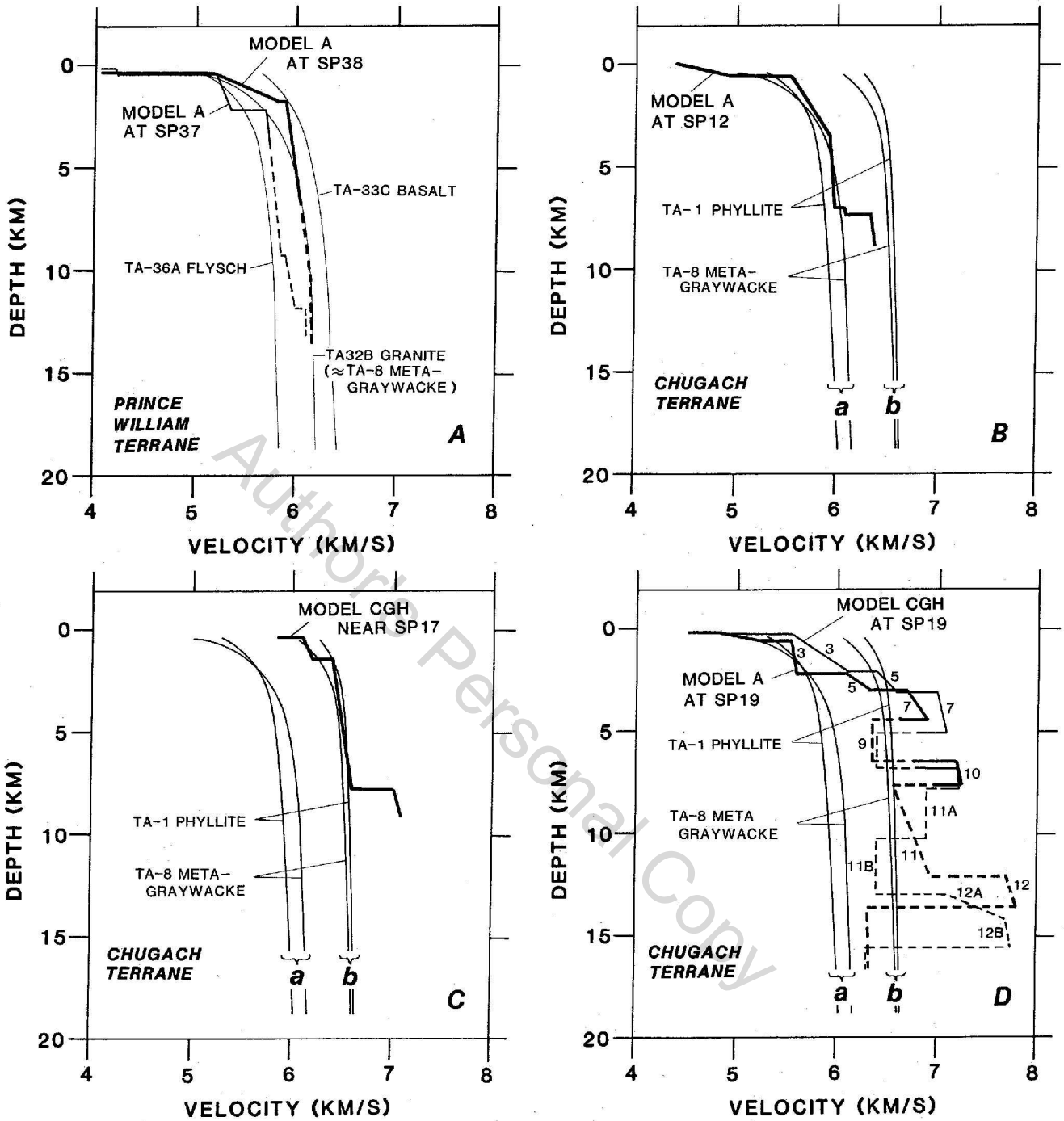

Fig. 18. Comparisons of velocity-depth curves derived from refraction data (model A, see Figure 3) and laboratory measurements for characteristic rock types in the Prince William terrane (Figure 18*a*) and Chugach terrane (Figures 18*b*, 18*c*, and 18*d*) (see Table 2). In Figure 18*a*, the model curve at SP37 is bracketed by laboratory curves for granite or metagraywacke (TA-32B or TA-8) and flysch (TA-36A), and the model curve at SP38 matches closely the curve for granite or metagraywacke below 5-km depth. (Model curves are dashed where uncertain.) Both model curves are lower in velocity, however, than the laboratory curve for basalt (TA-33C). In Figures 18*b* and 18*c*, phyllite (TA-1) and metagraywacke (TA-8) are highly anisotropic and are each represented by two laboratory curves, one for velocity measured perpendicular to foliation (a direction, Table 2) and one, parallel to foliation (b direction, Table 2). The curve at SP12 (Figure 18*b*) on the Transect line matches the a curve, and the curve near SP17 (Figure 18*c*) on the east-west Chugach line matches the b curve. These results are expected because of the orientation of the two lines with respect to foliation in the terrane. In Figure 18*d*, model curves for the Transect line (model A, Figure 3) and the Chugach line (model CGH, Figure 12) are compared with each other and with laboratory curves for phyllite and metagraywacke. Layers 3, 5, and 7 of model A are systematically slower than similar layers of model CGH. In neither model does the curve for layers 3 and 5 ("basement") agree closely with the laboratory curves, and the high overall velocity gradient for the combined layers 3 and 5 suggests a change in composition with depth. See text for further discussion.

explain this important discrepancy, we postulate any of five possibilities: (1) that the mafic and ultramafic rocks are intruded extensively at depth by granitic rocks, (2) that ultramafic rocks increase in proportion with depth and are largely serpentinized, (3) that metamorphic wall rocks increase in proportion with depth, (4) that the mafic and ultramafic rocks are extensively brecciated (and altered) at depth, and (5) that an intermediate-velocity body of rock has been tectonically emplaced beneath the mafic and ultramafic rocks. West of the transect, Jurassic granitic rocks that intrude the Nelchina River Gabbronorite make up 40% of the outcrops [*Burns*, 1985]. Similar intrusions are also seen along the transect, but their proportion in outcrop is unknown. Preliminary laboratory measurements of a sample of one such intrusion give a velocity of 6.2 km/s, arguing strongly for possibility 1. Also west of the transect, a 4-km-thick melange zone containing largely serpentinized ultramafic rocks, gabbronorite, and rocks of the McHugh Complex occurs along the south boundary of the Nelchina River Gabbronorite [*Winkler et al.*, 1981]. The existence of such a melange argues for a combination of possibilities 2 and 4; however, no such zone is observed on the transect. Furthermore, serpentinite and ultramafic rocks are relatively minor in proportion on the transect, and rocks are not extensively fractured or brecciated [*Plafker et al.*, 1989]. Possibilities 3 and 5 are difficult to assess. On one hand, west of the transect are exposed scant outcrops of metamorphic wall rocks, into which the ultramafic and mafic rocks are intruded [*Burns*, 1985]. On the other hand, exposed thrust faults of the Border Ranges fault system [*Plafker et al.*, 1985, 1989] certainly admit the possibility of deeper thrust faults.

Modeled thicknesses for the magnetic rocks along the south flank of the Peninsular terrane range from 3 to 10 km, depending on the magnetic susceptibilities used [*Burns*, 1982; *Campbell and Barnes*, 1985; *Campbell*, 1987]. Smaller thicknesses result from using higher susceptibilities, which are actually most similar to those measured in rock samples [*Burns*, 1982]. Our modeled thickness for body 4 is about 5 km (Figure 3).

Wrangellia terrane. We defer to a later paper discussion relating outcrop in the Wrangellia terrane to our velocity model for the Transect line. The reader is referred to *Goodwin et al.* [1989] for such a discussion for the Tok Highway line. Our model of the Wrangellia terrane is used in this paper merely as a means to investigating deep structure beneath the Copper River basin.

Deeper Layers

Layer 6. Layer 6 (Figure 3) is analogous to upper-crustal LVZs that have been interpreted at depths ranging from 8 to 15 km in a number of locations around the world that include the U.S. Basin and Range province, the Alpine foreland basin and Rhinegraben region of southern Germany, and the Canadian shield (e.g., *Landisman et al.*, 1971; *Berry and Mair*, 1977]. Commonly, the velocity in the layer above the LVZ is 5.9–6.2 km/s; the interpreted velocity in the LVZ is about 5.5 km/s; and the velocity in the layer below is 6.1–6.7 km/s. Explanations for this LVZ include (1) granitic sills [e.g., *Landisman et al.*, 1971], (2) a zone where pore pressure approaches lithostatic pressure [e.g., *Nur and Simmons*, 1969; *Christensen*, 1989], (3) a zone of brecciation, gouge, serpentization, or alteration associated with a subhorizontal fault zone, and (4) an effect of normal temperature increase with depth in rocks of uniform composition [*Christensen*, 1979]. Possibilities 2–4 are not, of course, mutually exclusive. Layer 6 lies between dissimilar layers: a heterogenous upper layer (layers 5, 4, and 3) and a homogeneous lower layer (layer 7′). This fact leads us to speculate that layer 6 represents a fault zone, as in possibility (3). Perhaps high pore pressure also contributes to the existence of the LVZ, but the limited spacial extent of layer 6 indicates that such a high-pressure zone cannot be a regional feature in southern Alaska.

Layer 7′. Layer 7′, of intermediate velocity (averaging about 6.4 km/s, Figure 3), may represent one of at least three possibilities: (1) island arc rocks (including intermediate granitic rocks, metavolcanic rocks, metasedimentary rocks, and minor gabbro and metagabbro) that are the roots of the Peninsular and Wrangellia terranes, (2) metasedimentary and metavolcanic rocks that are the continuation of the Chugach terrane (Valdez Group rocks) beneath the Peninsular terrane, or (3) different rocks in different places. Island arc rocks, such as seen as in the Sierran foothills of California and inferred beneath the sedimentary sequence in the adjacent Great Valley [*Saleeby*, 1986], have model velocities (6.2–6.7 km/s) spanning those of the layer in question [*Spieth et al.*, 1981; *Colburn and Mooney*, 1986; *Holbrook and Mooney*, 1987]. On the other hand, Valdez Group rocks (exclusive of metabasalt) have velocities of 5.9–6.6 km/s (Table 2), also spanning velocities of layer 7′.

In spite of the fact that layer 7′ appears continuous across the deep projection of the Border Ranges fault system it may indeed represent different rocks in different places, as in possibility 3 above: it may represent Chugach terrane rocks south of the fault and Peninsular/Wrangellia terrane rocks north of the fault. The differing strength of the reflector at its top in these two locations supports such an interpretation. Unfortunately, vertical incidence reflection data failed to resolve structure beneath the Border Ranges fault system, and our wide-angle data do not provide a definitive picture.

Layers 7–12. The north dipping sequence, consisting of layers 7–12 (Figure 3), is inferred to be fragments of oceanic crust (basalt, gabbro, and metamorphosed equivalents) and mantle interlayered with sedimentary and metasedimentary rocks. Layer 7 correlates with metabasalt that is interbedded and interfaulted with metaflysch of the Chugach terrane. These rocks are interpreted to be near-trench extrusive rocks [*Plafker et al.*, 1989]. Thus layer 7 must be considered part of the Chugach terrane. Lower layers (8–12), however, are separated from layers 7 and 7′ and also from each other by major velocity discontinuities that are most likely faults. We interpret these layers to have been tectonically underplated in a subduction zone. Justification for this interpretation includes the following facts:

1. The layers dip north (at about 10°), subparallel to the top of the present Wrangell Wadati-Benioff zone, inferred to be the top of the currently subducting plate. This parallelism is, of course, suggestive only, as underplating occurred in the late Mesozoic or early Tertiary and involved the convergence between a different pair of plates than the current ones.

2. The layers can be traced in our models for considerable distances: over 100 km in a north-south direction (Figure 3) and over 200 km in an east-west direction (Figure 12*b*). In addition, other evidence suggests that some of this

sequence extends for much greater distances both to the east and west. Outcrops of metabasalt and the gravity ridge associated with layer 7 can both be traced 650 km eastward from our transect. Four hundred kilometers to the southwest, *Fisher et al.* [1983] see a package of strong landward dipping reflections on a marine multichannel seismic reflection line extending from the Alaskan shelf northwestward into Cook Inlet. The top of this package dips between 5- and 9-s two-way travel time. Nearby, in a study of earthquakes and surface blasts on the southern Kenai Peninsula, *Stephens et al.* [1987, 1990] also see evidence for a marked velocity discontinuity at 15- to 18-km depth. If these separate features are linked to the north dipping sequence in the Chugach Mountains, a large areal extent for the sequence is implied. It seems likely that only the subduction of an oceanic plate and overlying sedimentary rocks could produce layers of the dimensions apparent for such a sequence.

3. Velocities of layers 8–12 are consistent with those of sedimentary and metasedimentary rocks, oceanic crustal layers, and mantle. Layers 8 and 9 (5.7–6.35 km/s, Figure 3) have velocities appropriate for sedimentary, metasedimentary, and volcanic rocks, as well as numerous other rocks (Table 2) [*Christensen*, 1982]. However, layer 8 has structures appropriate for sedimentary rocks. It coincides in whole (model A) or in part (model B) with reflection band 1 (Figures 4*a* and 4*b*). *Fisher et al.* [1989] have interpreted a slight obliquity of reflections within band 1 as evidence of duplex structure within (presumably) sedimentary rocks. Duplex structure has been documented, for example, in sedimentary rocks accreted in the Chugach terrane on Kodiak Island, southwest of our study area [*Sample and Moore*, 1987]. Velocities in layers 8 and 9 are also appropriate for the bottom part of oceanic layer 2, inferred to consist of metabasalt and brecciated dikes [see *Salisbury and Christensen*, 1978].

Layer 10 (7.2–7.5 km/s, Figure 3) has velocities appropriate for the bottom part of oceanic layer 3, or the so-called "basal layer." Evidence for a "basal layer" is ambiguous in most marine seismic investigations [*Spudich and Orcutt*, 1980], but the layer is definitely present in some exposed ophiolite sections. *Salisbury and Christensen* [1978], for example, demonstrate that the basal 2.5 km of the Bay of Islands ophiolite complex consist of pyroxene and olivine gabbro and troctolite having a velocity of 6.9–7.4 km/s. The top part of oceanic layer 3, which averages about 6.8 km/s [*Shor et al.*, 1970; *Spudich and Orcutt*, 1980] is clearly missing among layers 8, 9, and 10. (In fact, the lack of such a layer and the juxtaposition of layers of lower and higher velocities give rise to the exceptional reflections observed on the Transect line.)

Layer 11 has an average velocity of about 6.75 km/s on both the Transect and Chugach lines and could conceivably represent oceanic layer 3 (Figures 3 and 12*b*). On the Chugach line, however, this layer is subdivided into a higher-velocity upper part (11A, 6.9–7.2 km/s, Figure 12*b*) and a lower-velocity lower part (11B, 6.4 km/s). This subdivision is poorly constrained, but it does not resemble expected structure within oceanic layer 3. Layer 11A might indeed represent oceanic layer 3, but layer 11B might represent metasedimentary rocks, possibly similar to metaflysch of the Chugach terrane.

On the Transect line, the velocity of layer 12 (7.7 ± 0.3 km/s) is well constrained where it exceeds that of layer 10 (Figure 3). Along the greater part of its length on the Transect line, however, it can not be clearly seen in the refraction data, although vertical incidence data suggest its presence. On the Chugach line, this layer has a well-constrained velocity ranging in different places from 7.7 ± 0.2 to 7.8 ± 0.2 km/s between SP17 and SP20, but at SP21, its velocity must be much lower (6.6? km/s, Figure 12*b*). Where its velocity is 7.7 km/s, this layer is almost certainly ultramafic rocks, possibly a fragment of oceanic mantle. Where its velocity is lower, it may include mafic oceanic rocks (oceanic layer 3).

In summary, because of its dip, areal extent, and layer velocities, the part of the northern dipping sequence consisting of layers 8–12 appears to be sedimentary and metasedimentary rocks and fragments of oceanic crust and mantle that were underplated during subduction.

The age and identity of the north dipping sequence (layers 7–12) can be determined as follows. The metabasalts linked to layer 7 are interbedded with metaflysch of Late Cretaceous age (Campanian? and Maestrichtian [*Plafker et al.*, 1989]). Layers 7–12 all terminate at or north of the north dipping Contact fault; we infer that they are truncated by this structure. The Contact fault is intruded by 50-Ma granitic rocks (Figure 2) [*Winkler and Plafker*, 1981]. Thus underplating of layers 8–12 occurred during the interval Late Cretaceous to early Tertiary. The oceanic plate that was subducting beneath Alaska during this time span was the Kula plate [*Engebretson*, 1982]. It would appear, then, that the inferred fragments of oceanic crust and mantle in the north dipping sequence, including layers 7, 10, 12, and possibly others, are fragments of the Kula plate [see also *Fuis and Plafker*, this issue].

By its link to metabasalt of the Valdez Group, layer 7 is part of the Chugach terrane. Layer 8 may be linked to either the Chugach or Prince William terrane, given its low velocity and interpreted sedimentary composition. Layers 8–12 might be viewed as one or more separate underplated "terranes." These layers are apparently fault-bounded on the south by the Contact fault and on the top by an inferred fault (a fossil megathrust?) at the base of layers 7 and 7′. Of course, other layers in the sequence also appear to be separated by major faults (fossil megathrusts?). It may be reasonable to postulate that layers 8–12 represent a terrane similar to both the Chugach and Prince William terranes that was underplated, or accreted, at a time during or between times of accretion of those two terranes.

Layers 10′–12′. Layer 10 of the north dipping sequence can be carried northward with certainty to a point beneath the southern Peninsular terrane (northernmost dot on layer 10, Figure 3). Layer 10′ of the laminated sequence beneath the northern Copper River basin can be carried southward with certainty to the Glenn/Tok Highway line (arrowhead on layer 10′, Figure 3). These two layers, and other layers in the sequences of which they are a part, can not be clearly connected, hence the blank area in model A between about SP7 and SP8 (Figure 3).

Layer 10′ appears to extend across the deep (vertical) projection of the West Fork fault system, although such a relationship must be regarded as poorly resolved, given the uncertainties on layer boundaries here (Figure 3; Appendix A). It is possible that layer 10′ and also deeper layers were emplaced after strike-slip faulting between the Peninsular and Wrangellia terranes, in the Late Jurassic to mid-

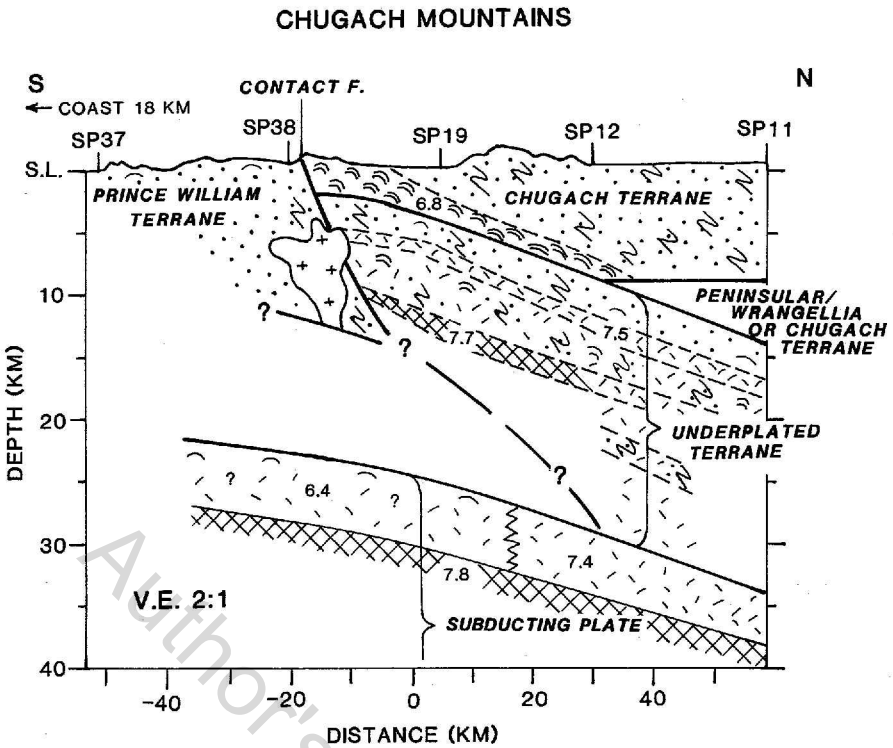

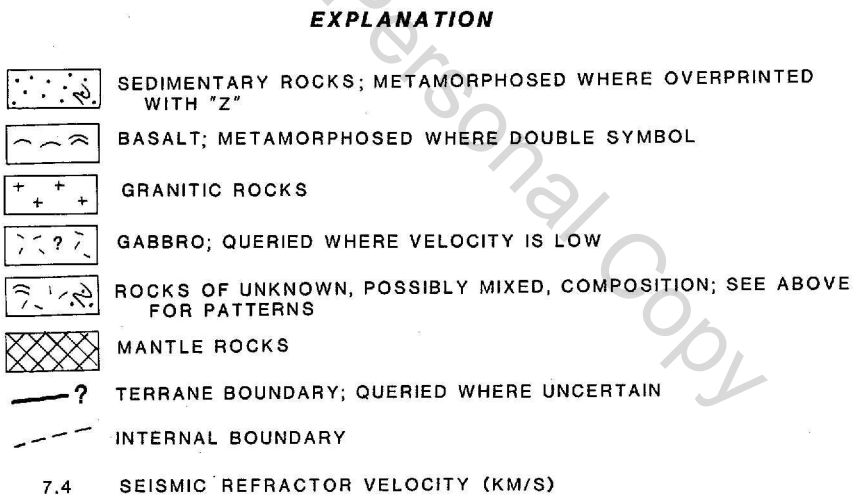

Fig. 19. Interpretive cross section for the Chugach Mountains, showing the relationships among the Prince William, Chugach, and underplated terranes and the subducting plate.

Cretaceous. The origins of layers 10′–12′ have been linked to the origin of layer 13′ (*Fuis and Plafker* [this issue]; see discussion of layer 13′ below).

Layers 13 and 13′. Layer 13, in the south half of the model, is partly imaged by vertical incidence data and would appear to be underplated rocks similar to layers 8–12 above. Reflection band 3, within layer 13, has a dip similar to bands 1 and 2, which are associated with layers 8 and 11 (Figures 4*a* and 4*b*). In model A (Figure 3) a marked velocity decrease southward in layer 13, from 7.2 km/s beneath the northern Chugach terrane to 6.2 km/s beneath the Prince William terrane, would appear to indicate a marked change in composition that may represent a deep terrane boundary. This terrane boundary could be an extension of the Contact fault or could be a younger fault (Figure 19). In model C, however (Figure 4*c*), no lateral change is modeled in layer 13, and hence no clear terrane boundaries would appear to be present.

Layer 13′, in the north half of the model, represents part of a thick crustal root. *Fuis and Plafker* [this issue] present at least three alternative origins for this root. In the first, the root, including the current Moho, was derived from the North American Continent and moved into place during or after the underplating of layers 8–12, in the Late Cretaceous or early Tertiary. In the second, the root consists in part of underplated fragments similar to layers 8–12 but lacking in seismic definition owing to metamorphic overprint(s) or irregularities due to folding and/or intrusion. In a third

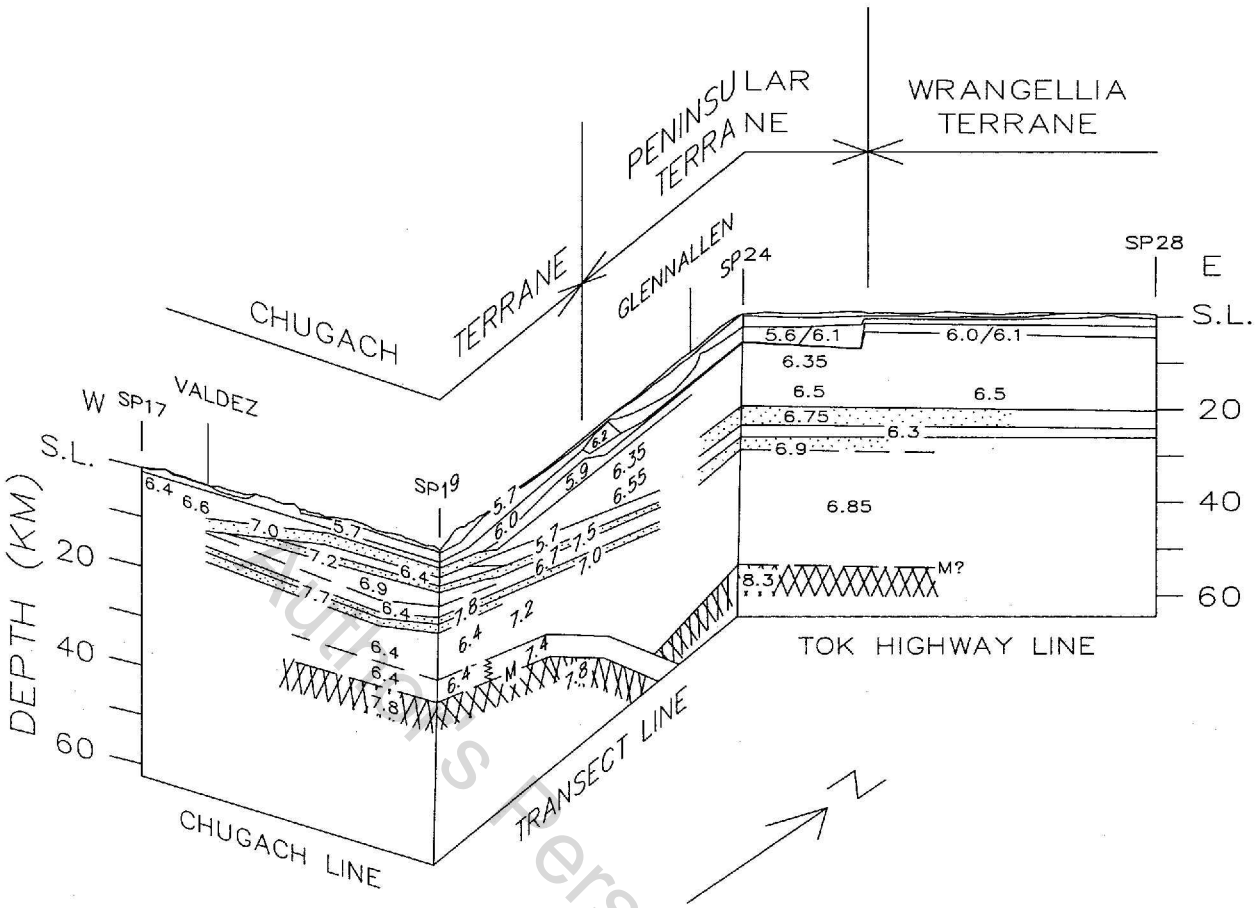

Fig. 20. Fence diagram integrating results for the Transect, Chugach, and Tok Highway lines; viewed from the southeast. Panels are taken from Figures 3 and 12*b* and Figure 8 of *Goodwin et al.* [1989]. (See Figure 1 for locations.) Numbers above panels are shot points; numbers on panels are average velocities (in km/s). High-velocity refractors are stippled; mantle is cross-hatched. "M" is Moho.

interpretation, the root was created in large part by magmatic underplating.

Layer 14. Layer 14 is interpreted as subducting oceanic crust. In model A (Figure 3), its velocity ranges from 6.4 (±0.3) km/s south of Mount Billy Mitchell to 7.4 (±0.3) km/s north of Mount Billy Mitchell. North of the elbow in the subducting plate the velocity is more uncertain. This lateral velocity distribution is somewhat puzzling. A 6.4 km/s velocity is too low for standard oceanic layer 3, and a 7.4 km/s velocity is too high. In model C, however (Figure 4*c*), the velocity in layer 14 averages 6.55 km/s and is constant.

Layer 14 could be the subducting Pacific plate or subducting Yakutat terrane (see discussion by *Bruns* [1985] and *Plakfer* [1987]). The lower part of the Pacific plate has a velocity structure similar to that of layer 14. At a point about 400 km southeast of the Transect line, the Pacific plate consists of 2 km of sediments, 1 km of basalt (5.5 km/s), and 3.5–5 km of oceanic layer 3 (6.73 km/s) [*von Huene et al.*, 1979]. The lower part of the Yakutat terrane also has a velocity similar to that layer 14. At a point about 100 km southeast of the Transect line, this terrane consists of 5–7 km of sedimentary rocks, 3–5 km of basalt, and a lower part with a velocity of 6.4–7.2 km/s and unknown thickness [*Bayer et al.*, 1978].

Recent reflection and refraction data collected 50 km south of the Transect line [*Brocher et al.*, 1989*b*] will shed more light on the interpretation of both layers 13 and 14.

SUMMARY

In this and companion studies [*Taber et al.*, 1986; *Brocher et al.*, 1989*a*; *Fisher et al.*, 1989; *Flueh et al.*, 1989; *Goodwin et al.*, 1989; E. L. Ambos et al., submitted manuscript, 1988] we have used seismic refraction and reflection data to examine in three dimensions the Prince William, Chugach, Peninsular, and Wrangellia terranes of southern Alaska (Figures 3, 4, 11, 12, and 20). The velocity structure of the upper crust (less than 9-km depth) is different from terrane to terrane. In contrast, the middle and lower crust contains several layers that extend across deeply projected terrane boundaries.

Upper Crust

In the Prince William terrane, laboratory and model refraction velocities indicate the Transect line is underlain to at least 5-km depth by flysch and metaflysch (Orca Group) or granitic rocks but not by significant amounts of tholeiitic basalt (Figure 18*a*). Laboratory velocity measurements indicate no marked velocity anisotropy in the flysch and neither do model refraction velocities on the Transect and Montague

lines, which are at an angle of about 55° to one another. In the Chugach terrane, laboratory and model refraction velocities are consistent with an upper crust of metabasalt in the south and metaflysch in the central part of the terrane. The McHugh Complex (basalt and minor sedimentary rocks and melange), in the north part of the terrane, can not be distinguished from Valdez Group metaflysch on the basis of velocity. Velocity anisotropy (as much as 10%) within the Valdez Group metaflysch is confirmed by both laboratory and model refraction velocities.

Mesozoic and Cenozoic sedimentary rocks in the Copper River basin are as much as 3–5 km deep. The Lower Jurassic Talkeetna Formation apparently forms the upper part of "basement" (5.2–6.2 km/s, layer 3) beneath the basin and is exposed to the south in the Chugach Mountains. A magnetic component to this basement might include Jurassic granitic rocks.

On the north flank of the Chugach mountains, the Peninsular terrane contains a body with velocities, 6.0–6.22 km/s, that extends from near the surface to about 5-km depth and correlates with outcrops of the BRUMA. The shape of this body is deduced in part from models of aeromagnetic data. As the modeled velocities for this body are significantly lower than expected for rocks of the BRUMA, this body may be extensively intruded at depth by intermediate plutonic rocks, although other explanations are also plausible. The BRUMA is believed to be the uplifted base of the Peninsular terrane.

Deeper Crust

A strong reflector at the top of an intermediate-velocity layer (6.4 km/s, layer 7′, Figure 3) at 9-km depth extends beneath the deep projection of the Border Ranges fault system, between the Peninsular and Chugach terranes. This relationship suggests that the upper parts of the Peninsular and Chugach terranes are detached, although an alternate explanation, involving no detachment, is possible. We have postulated that layer 7′ is either the roots of the Peninsular and Wrangellia terranes (island arc rocks) or the roots of the Chugach terrane (metaflysch). An LVZ above this layer in some places (layer 6) may be a fault zone.

A north dipping high-velocity layer (6.8–7.1 km/s, layer 7, Figure 3), projects to the surface at outcrops of metabasalt in the basal part of the Chugach terrane. Laboratory velocity measurements of the metabasalt at 100–200 MPa match the model refraction velocities for this layer. The metabasalt is interbedded and interfaulted with Chugach terrane metaflysch, of Late Cretaceous age, and is inferred to be oceanic crust of the Kula plate. Layer 7 is linked to a gravity ridge in the southern Chugach terrane that, together with outcrops of the metabasalt, persists for over 650 km eastward from our transect. Layers beneath layer 7 also dip north, have a wide inferred areal extent, and have alternating low and high velocities (5.7–7.8 km/s, layers 8–12). Prominent bands of vertical incidence reflections correlate in part or in whole with the LVZs in this sequence. These layers are inferred to be tectonically underplated sedimentary and metasedimentary rocks and fragments of oceanic crust and mantle of the Kula plate. The underplating occurred during the Late Cretaceous and/or early Tertiary.

In the middle crust of the northern Peninsular and Wrangellia terranes, a laminated sequence (6.3?–6.9 km/s, layers 10′–12′, Figure 3) appears to extend across the deep (vertical) projection of the West Fork fault system, between the Peninsular and Wrangellia terranes, although a crosscutting relationship can not be clearly resolved. This sequence may have been emplaced after strike-slip faulting between the Peninsular and Wrangellia terranes.

Details of velocity structure in the lower crust of the four terranes we have examined are uncertain, because high-velocity layers in the middle crust largely mask observations of the lower crust. Lower crust beneath the Prince William, Chugach, and southern Peninsular terranes is divided into two layers by the top of the north dipping Wrangell Wadati-Benioff zone, inferred to be the current megathrust, but this layer division is distinguishable only in vertical incidence reflection data. The upper layer (layer 13, Figure 3) exhibits a prominent reflection band similar to those observed in layers 8–12 and, like those layers, probably represents tectonically underplated rocks. The lower layer (layer 14, Figure 3) is interpreted to be subducting oceanic crust. Its velocity is variable (6.4–7.4 km/s) but poorly resolved, and its thickness is 3–8 km. The Moho of the subducting plate is clearly seen. Lower crust beneath the northern Peninsular and Wrangellia terranes (6.85? km/s, layer 13′, Figure 3) extends from about 28-km depth, the base of the laminated sequence (layers 10′–12′), to a south dipping Moho at 45- to 57-km depth. Layers 10′–13′ constitute a "root" that appears to abut the underplated oceanic lithospheric fragments to the south. This root consists of (1) lower crust from the North American continent that moved into place during or after tectonic underplating, (2) underplated rocks that have lost the clear seismic layering visible in the south, or (3) magmatically underplated rocks.

Our interpretation of the crust of southern Alaska indicates that tectonic underplating has played a major role in the process of accretion and continent formation.

APPENDIX A

The following is a layer-by-layer discussion of the constraints for models A, B, and C (Figures 3 and 4). The reader will need to refer to Figures 3–10 as well as supplementary Figures A1–A5.

Layers 1 and 2

Two distinctly different surficial layers (layers 1 and 2) are recognized in model A (Figure 3). Layer 1 (1.85–2.85 km/s) corresponds to glaciofluvial cover in both the Copper River basin and Chugach Mountains (thin patches in the latter). Layer 2 (2.8–5.2 km/s) corresponds in the Chugach Mountains to cracked and weathered bedrock and in the Copper River basin to Mesozoic sedimentary rocks. The best constraints on velocity and thickness of layer 1 are first and second arrivals from SP7, SP8, and SP9 (Figures 5*b*, A2, and A4*b*), and the best constraints on the velocity and thickness of layer 2 are first arrivals from SP11, SP12, and SP19 (Figures 6*b*, 8*b*, and 9*b*). The maximum thickness of layer 2 is nearly 3 km beneath Mount Billy Mitchell, but thickness and velocity can be traded off in modeling this layer between shotpoints. Layer 2 in the Copper River basin has a moderate velocity gradient that is controlled not only by the curved first arrival branches but also by free-surface multiple refractions (Figures 5*b* and A4*b*, "*PP*", "*PPP*"). Although this layer would appear to be well modeled, at least to about

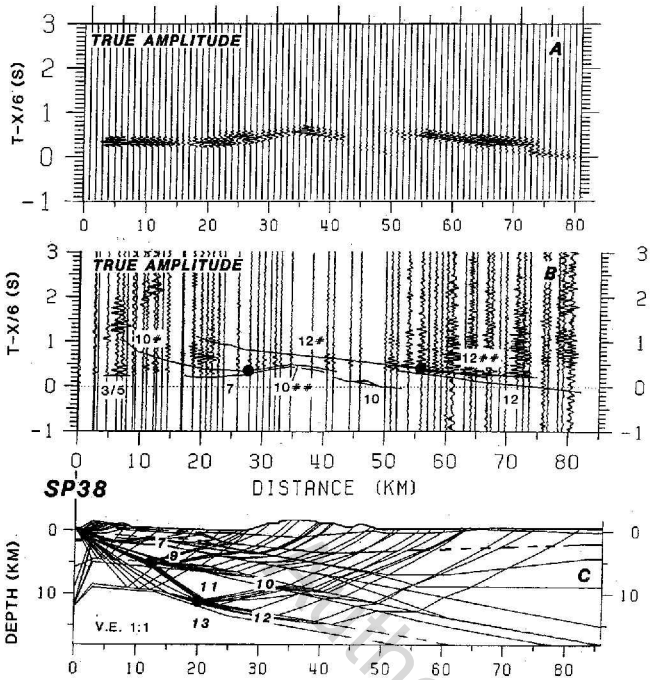

Fig. A1. Transect line: SP38. Format is the same as for Figure 7 (true amplitude). These data constrain layers 10 and 12 near their southern terminations, near the Contact fault. North is on the right.

3-km depth where penetration by multiple refractions provides a check, modeling by *Brocher et al.* [1989*a*], using shot point gathers from vertical incidence reflection data, indicates a subdivision of this layer into two layers and a lesser overall thickness than in our model (see discussion in text). Thus we indicate a relatively large uncertainty in basin depth in the south part of the Copper River basin.

Layers 3–6 ("Basement")

Layers 3–6 are referred to collectively as "basement." Layer 3 is well sampled by reversing travel paths throughout model A, and layer 4, restricted in extent, is also well sampled (Figures 3, 5*c*–9*c*, and A4*c*). On the other hand, layer 5 is well sampled only in the Chugach terrane between about SP19 and SP9 (Figures 6*c*, 8*c*, and 9*c*). In the Prince William terrane, only the top kilometer or so of layer 5 has reversed coverage (Figures 7*c* and 9*c*). Layer 6, an LVZ in the Chugach and southern Peninsular terranes, is, of course, not sampled directly, but its boundaries and velocities are adjusted to provide travel time and amplitude matches to the data for arrivals from layers above and below.

Trial-and-error modeling of travel times indicates the average velocity within layer 3 is certain to about 0.1 km/s in the Chugach terrane and perhaps to 0.2 km/s in the Prince William and Peninsular terranes. The gradient, on the other hand, is poorly known but was adjusted to produce appropriately large amplitudes to ranges of 30–40 km from most shot points (e.g., compare Figures 5*a* and 5*b* and 6*a* and 6*b*).

The geometry of the prism-shaped body beneath outcrops of BRUMA, body 4, is constrained in part by modeling of magnetic data [*Campbell and Barnes*, 1985; *Campbell*, 1987]. The south dipping upper interface of this body is well constrained to about 2-km depth. The north dipping upper interface was modified in this study to a steeper dip than in the model of *Campbell and Barnes* [1985] in order to better separate higher-velocity rocks (6.0–6.22 km/s) beneath the BRUMA outcrops from lower-velocity basement rocks to the north beneath the Copper River basin. BRUMA outcrops are associated, at least near their northern boundary, with localized early arrivals on all record sections (e.g., Figure 5*b*, 20-km range south; Figure 6*b*, 60-km range north). The lower interface of body 4 was added in this study to truncate first arrivals beyond about 50 km from SP8 southward and SP11 northward (Figures 5*a*, 5*b*, 5*c*, 8*a*, 8*b*, and 8*c*). The velocity of this body is certain to within about 0.1 km/s, as numerous travel paths crisscross within it. The initial trial velocity was 6.5 km/s; the final velocity, 6.0–6.2 km/s, is surprisingly low, given laboratory velocities for the BRUMA (Table 2).

The average velocity of layer 5 is certain to within 0.15–0.2 s within the Chugach terrane but is more poorly known in the Prince William terrane. The reduced gradient in this layer produces the decrease in amplitude of first arrivals observed for most shotpoints beyond a range of 30–35 km (e.g., compare Figures 6*a* and 6*b*).

Thickness and velocity of layer 6 can be traded off to produce the total observed delay of about 0.4 s from SP8 and SP12 between refractions from layer 5 and reflections from layer 7′ (Figures 5*b* and 6*b*). The top of layer 6 rises northward between SP12 and SP9 in order to truncate first arrivals from SP12 at 65-km range. Although layer 6 is modeled in two sublayers beneath body 4, with velocities of 6.2 and 5.8–5.9 km/s, only an average velocity of about 6.0

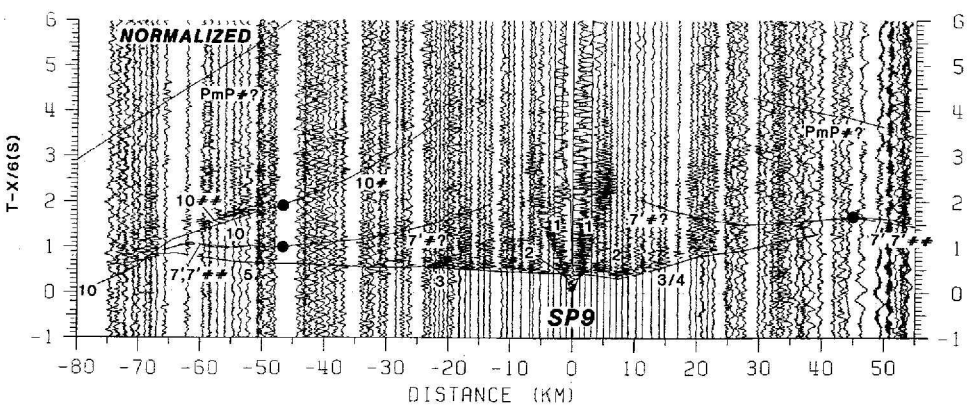

Fig. A2. Transect line: SP9. Format is the same as for Figure 5.

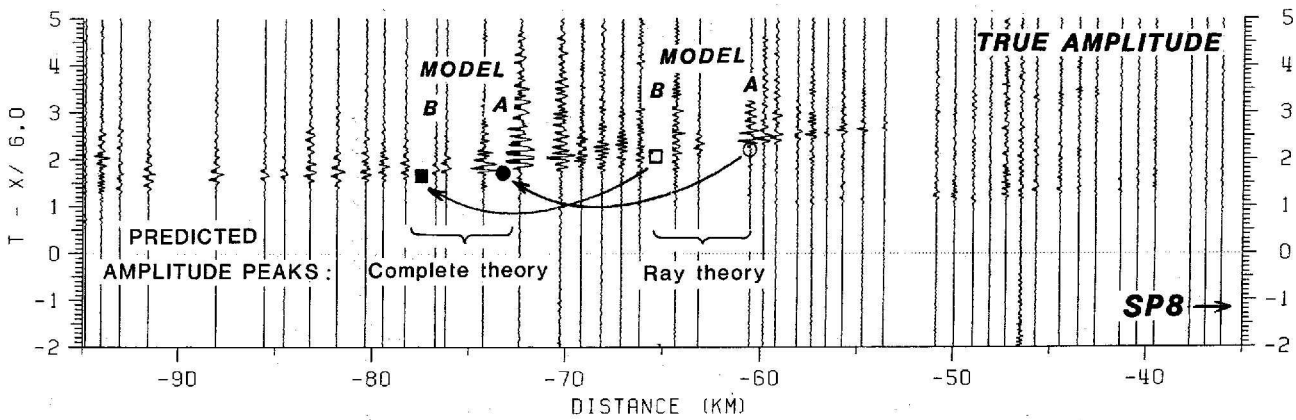

Fig. A3. Transect line: SP8. True-amplitude data from SP8 with amplitude peaks (points of critical reflection) predicted by ray theory and estimated for a more complete (full wave) theory using the results of *Flueh et al.* [1989] for both models A and B. The estimated peak for model A matches the amplitude peak in the data marginally better than the estimated peak for model B.

km/s, slightly higher than that for the rest of the layer, is certain. The travel times of reflections recorded beyond ranges of 35 km for SP8 southward and SP11 northward constrain this average velocity in this area (Figures 5*b* and 8*b*, "7′#" and "7′##"). Layer 6 is not seen in the northern Peninsular terrane on the Glenn and Tok Highway lines [*Goodwin et al.*, 1989; E. L. Ambos et al., submitted manuscript, 1988] and must therefore terminate somewhere in the vicinity of SP7 (Figure 3). The southward termination of layer 6, near SP12, is well constrained by data from the Transect line.

Layer 7′

Reflections documenting the shape of the upper surface of layer 7′ are seen clearly southward from SP7, SP8, and SP24 (Figures 5*b*, A4*b*, and A5*b*) and northward for SP11 and SP12 (Figures 6*b* and 8*b*), and bottoming points are shown on model A (Figure 3). Relative amplitudes are well predicted for reflections that bottom beneath the Peninsular terrane (e.g., Figures 5*a* and 8*a*), but predicted amplitudes are somewhat too large compared to the data for reflections that bottom beneath the Chugach terrane (e.g., Figure 6*a*). There would appear to be some unmodeled change in character of this reflector from the Peninsular to the Chugach terrane. In addition, there would appear to be some unmodeled reflectors in layer 6 beneath the region of the Border Ranges fault system that produce arrivals at 35- to 40-km range north of SP11 and 0.2 s ahead of the reflection from layer 7′ (Figure 8*b*).

Refractions that document the velocity of layer 7′ are seen clearly from SP7, SP8, and SP24 southward (Figures 5*b*, A4*b*, and A5*b*) and ambiguously from SP12 and SP19 northward (Figures 6*b* and 9*b*). The phases are weak for SP12 and not clearly separated from other phases for SP19, where travel time curves are bunched together. An error estimate for the velocity of layer 7′ based on trial-and-error fitting of travel time curves to the data is ±0.1 km/s. The velocity at the base of the layer is not constrained by refractions that bottom there (Figure 3) and is probably uncertain by ±0.2 s.

The average velocity of layer 7′ beneath the northern Peninsular and Wrangellia terranes is constrained primarily by the combined Glenn and Tok Highway lines to be 6.35 ± 0.15 km/s (Figure 20) [*Goodwin et al.*, 1989]. Since layer 7′ beneath Wrangellia falls within an LVZ, its features cannot be known directly, but its velocity has been adjusted to produce the correct traveltimes, amplitudes, and points of critical reflection for arrivals from layer 10′ (Figure 10*b*).

Layers 7–12 (North Dipping Sequence)

Reflections that document the upper surface of layer 7 are seen clearly from SP12 southward but are not clearly separated from other phases for SP19 northward (Figures 6*b* and 9*b*, "7#" and "7##"). This layer has an average velocity of 6.8 km/s beneath SP19 and the southern flank of Mount Billy Mitchell that is constrained within about ±0.1 km/s by first arrivals from SP12 and SP19 (Figures 6*b* and 9*b*, "7"). The layer decreases in velocity both downdip and updip of this interval by about 0.4 km/s. The downdip decrease, certain to about ±0.2 km/s, is required by first arrivals at ranges beyond about 30 km from SP19 northward (Figure 9*b*, "7"). The updip decrease and the local LVZ just north of the Contact fault are less certain and are required to match the complex travel time curves from SP19 southward and SP38 northward (Figures 9*b* and A1*b*, "7").

Layer 8, part of a major LVZ (Figure 3), has a velocity and thickness adjusted to produce the observed delay of 0.6–0.7 s between reflections from layer 10 and refractions from layer 7′. This delay is best observed at 75- to 90-km range southward from SP8 (Figure 5*b*). Model A (Figure 4*a*) produces this delay with a 3-km-thick LVZ, of velocity 5.7 km/s, and the alternate model, model B (Figure 4*b*), produces this delay with a 4-km-thick LVZ, of velocity 6.2 km/s. In both models A and B a slight decrease in the delay produced by layer 8 for shot points north of SP8 is modeled by a northward increase in LVZ velocity (see Figures A4*b* and A5*b*).

Points of critical reflection from layer 10 are shifted away from shotpoints by amounts ranging from 0 to 5 km for model B, compared to model A, owing largely to the greater depth of layer 10 in model B. For most shot points, model A predicts points of critical reflection at or near the onset of regions of large amplitudes that commonly extend for 15–20 km, and model B predicts points of critical reflection within these regions. For a complete theory of wave propagation in

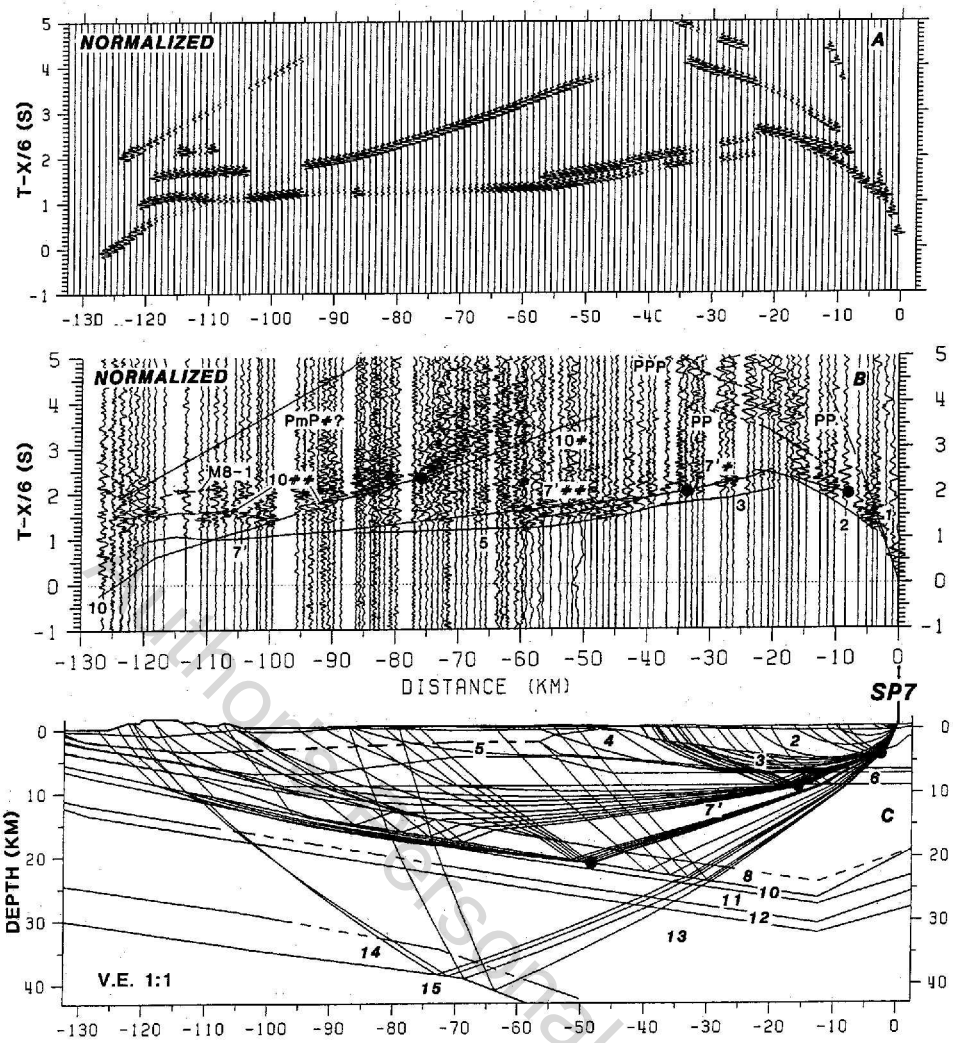

Fig. A4. Transect line: SP7. Format is the same as for Figure 5. Phases seen are similar to those of Figure 5.

which the effects of finite frequencies are taken to account, a peak in reflection amplitudes is expected at a point more distant from the source than for the ray theory used herein [*Červený et al.*, 1977]. For example, for 5–10 Hz energy, similar to that of our signal, the predicted amplitude peak for layer 10 reflections is expected 10–15 km farther than the ray theory peak [see *Flueh et al.*, 1989]. Examining true-amplitude data from SP8 southward (Figure A3), we see that model A predicts the observed amplitude peak, at 70–75 km, marginally better than model B.

Layer 9, also part of the major LVZ, has a model velocity (6.2–6.3 km/s) similar to that determined by *Flueh et al.* [1989] from peg-leg multiples in this layer on the Chugach line. Similar multiples generated on the Transect line from SP8 southward agree well in travel time with observed echelon branches of large-amplitude arrivals at 0.5–1.0 s and 100–140 km (Figure 5*b*, "M8/9-1" and "M8/9-2"). (Note that "M8/9-1" indicates one reverberation within layers 8 and 9 combined; "M8/9-2" indicates two reverberations.) Large observed amplitudes do not, however, persist along the entire predicted travel time curves; they are seen only at the distal ends. A similar phenomenon has been confirmed by *Flueh et al.* [1989]. Another possible example of this phenomenon is seen in the data from SP11 southward. Large-amplitude arrivals at 0.2–0.4 s and 70–100 km occur along a distal projection of the travel time curve for M8/9-2 (Figure 8*b*). Agreement in travel time between predicted and observed peg-leg multiples from SP8 and SP11 indicates that the velocity for layer 9 is well determined, as the majority of the travel path for the observed multiples, at the distal ends of the travel time curves, is in layer 9. In contrast, from SP19 northward and SP12 northward, no clear arrivals can be seen along the predicted traveltimes curves for peg-leg multiples (or even distal projections of these curves; Figures 6*b* and 9*b*, "M8/9-1?", etc.).

The boundary between layers 8 and 9 was placed so as to explain an apparent precritical reflection that is observed to be slightly earlier than the one from the top of layer 10 (Figure 6*b*, "9#"). This boundary corresponds to reflections in the southern part of band 1 of the vertical incidence data that converge upon reflections at the base of the band (Figure 4*a*). *Fisher et al.* [1989] interpreted such convergent reflections as evidence of duplex structure in band 1.

Wide-angle reflections constraining the upper surface of layer 10 have bottoming points from just north of the Contact fault to a point beneath the southern Peninsular terrane; this boundary is well controlled over a distance of more than 100 km (Figure 3). As indicated above, however, the depth to

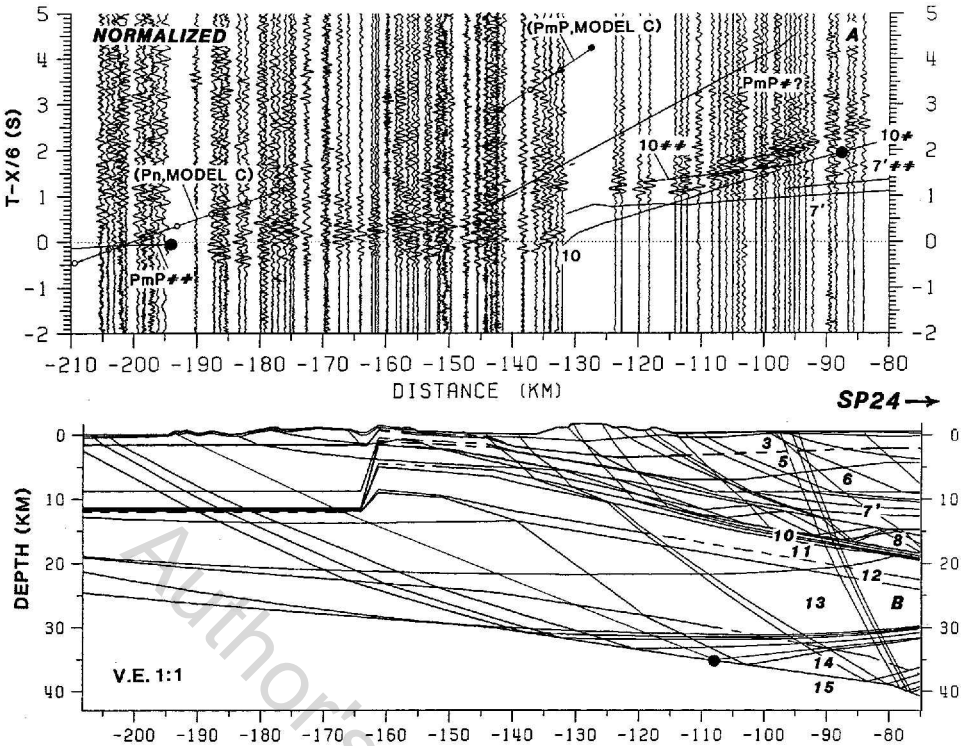

Fig. A5. Transect line: SP24. Format is same as for Figure 5. Phases are similar to those of Figure 5.

this boundary is uncertain by at least 1 km (compare models A and B; Figures 4*a* and 4*b*). Although we have modeled lateral velocity variation within layer 10, this variation is barely resolved in both models A and B. In model A (Figure 3), we show a velocity of 7.5 km/s over a 20-km segment of the layer northward from Mount Billy Mitchell, and 7.2 km/s north and south of this segment. In model B (Figure 4*b*), the velocity is 7.2 km/s south of Mount Billy Mitchell but 7.5 km/s everywhere north of Mount Billy Mitchell. Trial and error perturbations of these velocity distributions indicate permissible velocity ranges of ±0.1 km/s for the higher-velocity segments and ±0.2 km/s for the lower-velocity segments in both models. Primary constraints are first arrivals from SP8 and SP19 (Figures 5*b* and 9*b*, "10"). Note that a 7.2 km/s velocity is required in layer 10 beneath SP19 in order to be consistent with the results of *Flueh et al.* [1989] and our own results from modeling the Chugach line. The southern termination of layer 10 can not be more precisely determined than some point in an interval 0–15 km north of the Contact fault, given the fact that models A and B differ on this feature (see text). In model A, although bottoming points for reflections from layer 10 can be traced to within 5 km of the fault, high velocity in this layer (7.2 km/s) must terminate at least 10 (±5) km north of the fault. In model B, high velocity in layer 10 is permissible all the way to the fault. The northern termination of layer 10 and the relationship of this layer to the subhorizontal layers 10′ and 12′ beneath the northern Copper River basin are unknown.

The velocity gradient in layer 10 is uncertain but was adjusted to produce the correct relative amplitudes for refractions from all shotpoints (e.g., compare Figures 5*a* and 5*b*, "10"). The thickness of the layer was reduced in successive steps to a final value near 1 km in order to truncate refractions as near to observed locations as possible. For example, observed refractions from SP19 northward and SP8 southward are truncated at about 90 and 110 km, respectively, and predicted refractions are truncated at 104 and 103 km, respectively (Figures 5*b* and 9*b*, "10"). Note that oscillations are permitted in the lower boundary of this layer, but the layer must be as thin as about 1 (±0.5) km in at least a few key places in order to cut off rays and thereby truncate refractions as observed.

The velocities of layers 11 and 12 and the depth of layer 12 are relatively poorly constrained by Transect line data and have been adjusted to be consistent, to the extent possible, with models of Chugach line data by *Flueh et al.* [1989] and this study. Uncertainties in velocity and depth for layers 11 and 12 are greater than for layers 8/9 and 10, because (1) they are deeper, (2) layer 12 has only a short (30 km) high-velocity segment (7.7–7.8 km/s), and (3) layer 12 appears to dip westward as well as northward (Figures 3 and 12*b*). We estimate the uncertainty in the average velocity of these layers to be ±0.3 km/s and uncertainty in the depth to layer 12 to be ±2 km.

The southern termination of layer 12, like that of layer 10, lies in an interval 0–15 km north of the Contact fault, given the fact that models A and B differ on this feature (see text). Bottoming points for reflections from the top of this layer can be traced to within 10 km of the fault, but high velocity in the layer (7.8 km/s) may extend all the way to the fault (model B) as long as (1) the layer is thin (less than about 1 km) or (2) the velocity gradient is high (greater than 0.05–0.1/s). If the latter conditions are not met, a first-arrival branch from SP11 would extend well beyond observed first arrivals to excessively early travel times (see Figure 8*b*). Even model A, where layer 12 terminates 10 km north of the fault, has this problem, but predicted amplitudes for the excessively early arrivals are small and are permitted by the

data (compare Figures 8*a* and 8*b*, "12"). The northern extent of layer 12 is certain only to the subsurface point of critical reflection from SP11 southward, beneath Mount Billy Mitchell (Figure 3). For shot points north of SP11, arrivals from layer 12 are either not present or are masked by the reflection from layer 10. If the blank region below band 2 in the vertical incidence reflection data can be interpreted as evidence of layer 12, then this layer would appear to extend northward to at least SP11 (Figures 3 and 4*a*). We were forced to reduce the velocity of this layer to 7.0 km/s in this region, however, in order that *Pn* arrivals from SP1, observed clearly to at least 230-km range (Figure 10*b*), could penetrate the north dipping sequence. (If layer 12 had a 7.7 km/s velocity in this region, *Pn* would be reflected downward postcritically from the base of the layer).

The velocity gradient and thickness of layer 12 are uncertain except at the southern termination of the layer as outlined above.

Layers 10′–12′ (Midcrustal Layers in the Northern Copper River Basin)

Layer 10′ is best constrained in velocity on the combined Glenn and Tok Highway lines to be 6.75 ± 0.15 km/s (Figure 20) [*Goodwin et al.*, 1989]. On the Transect line, arrivals from this layer from SP1 are clear, but arrivals from the reversing direction, from SP7 and SP8, are emergent or were not recorded at the proper range. There is weak evidence for at least one deeper layer (layer 12′) on the combined Glenn and Tok Highway lines and on the Transect line, at a depth of about 25 km. The velocity of layer 12′ is uncertain, but the apparent point of critical reflection, about 150 km from shot point 1, is best matched using a velocity that is only slightly increased (by 0.2 km/s) from that of layer 10′. An LVZ (6.3? km/s, layer 11′) is included to produce the observed delay (0.4–0.5 s) between the layer 12′ reflection and the layer 10′ refraction; however, the evidence for this feature is not compelling. Arrivals following those from layer 12′ are explained as peg-leg multiples generated in the LVZ (Figure 10*b*, "M11′-1").

Layers 13, 13′, and 14 (Lower Crust)

The velocities of layers 13 and 13′ are poorly constrained. In fact, two significantly different models of these layers, models A and C (Figures 3 and 4*c*), are permissible, but these alternate models also require different phase correlations. The velocity of layer 14, the subducting crust, is somewhat better constrained, at least in the region south of Mount Billy Mitchell, by the tails of the *PmP* branches from SP37 and SP11 (Figures 7*b* and 8*b*). However, this layer, too, is subject to an alternate interpretation in model C (Figure 4*c*). Together layers 13, 13′, and 14 produce the big delays (1.5–3.5 s) between *PmP* and refractions (or diffractions) from midcrustal layers (Figures 7–10).

In the south half of model A, considerable lateral velocity variation is interpreted in layer 13 (Figure 3). Average layer velocity increases from 6.1 km/s near the Pacific coast to 6.5 km/s beneath Mount Billy Mitchell, jumps to 7.2 km/s (on average) beneath Mount Billy Mitchell, and remains constant to some poorly defined point beneath the Copper River basin. This landward increase in velocity is required if one assumes that the Moho is subparallel to the top of the Wrangell Wadati-Benioff zone, as defined by *Page et al.* [1989]. If this assumption is relaxed, then other structures are possible, as trade-off is permitted between Moho depth and layer 13/14 velocity. If one assumes instead that the velocity of layer 13 is constant, say 6.4 km/s, then Moho is subhorizontal beneath the Chugach Mountains, and the subducting crust (layer 14) tapers to 0-km thickness beneath about SP11. If one further drops the requirement that the phase "*PmP*-1#" from SP19 northward be fitted (Figure 9*b*), then model C is permitted. In model C the subducting crust is 8–10 km thick beneath the Chugach Mountains, although thinning is required farther north, beneath the Copper River basin. In the north halves of models A and C, layer 13′ is modeled as an LVZ in an attempt to reproduce the observed truncation of layer 12′ refractions beyond about 185 km from SP1 (Figure 10*b*, "12′"), (Refractions are indeed truncated at the proper locations, but, unfortunately, predicted wide-angle reflections from the top of this layer persist into the observed shadow (Figure 10*b*, "12′##?"), indicating that further tailoring of the upper interface of layer 12 is warranted.) In model A, layer 13′ was arbitrarily assigned an average velocity (6.85 km/s), only slightly less than that inferred for layer 12′ (6.9 km/s). A lower average velocity (6.45 km/s in model C) is also permitted, but Moho must be elevated compared to model A (Figure 4*c*).

The top of layer 14 is defined by the top of earthquakes in the Wrangell Wadati-Benioff zone and is equated to the megathrust between the Pacific and North American plates [*Page et al.*, 1989]. Between SP11 and SP12 this interface coincides with band 4 in the vertical incidence reflection data. Owing to the finite thickness of this band and errors in earthquake location, this interface has an estimated uncertainty in depth of a few kilometers. In the region south of Mount Billy Mitchell, the velocity of layer 14 is determined, within perhaps ±0.3 km/s for both models A and C, to be 6.4 km/s, from the asymptotic *PmP* velocities observed from SP37 and SP11 (Figures 7*b* and 8*b*). In the region north of Mount Billy Mitchell, a velocity of 7.4 (±0.3) km/s is required in model A to fit *PmP* travel times from SP19, SP8, and SP24 (Figures 5*b*, 9*b*, and A5*b*). North of the elbow in this layer, relatively high velocities are also required in order to transmit energy northward for the "*PmP*-2" phase (Figure 9*b* and 9*c*, see below). In the region north of Mount Billy Mitchell, velocities in model C are poorly determined.

Layers 15 and 15′ (Mantle)

The large-amplitude phases beginning at 2–2.5 s and 80- to 100-km range from SP37, SP19 northward, and SP11 southward are all modeled as reflections from layer 15, or mantle of the subducting plate (Figures 7–9, "*PmP*", "*PmP*-1#"; see note below). In addition, the large-amplitude phases beginning at 3–4 s and 140-km range from SP19 northward and SP1 southward are modeled as reflections from layer 15′, or mantle of the North American plate (Figures 9*b* and 10b, "PmP-2", "PmP-1##"). (Note that for SP19 and SP1, "*PmP*-1" indicates a simple mantle reflection, from either layers 15 or 15′, and is eqivalent to "*PmP*". "*PmP*-2" indicates a complex ray path that includes travel through the steeply dipping part of layer 14 and reflection from layer 15′.) In model C, on the other hand, the later large-amplitude phase from SP19 ("*PmP*-2") is modeled as a reflection from Moho of the subducting plate, thus making the subducting

Moho several kilometers deeper than in model A (Figure 4*c*). The earlier large-amplitude phase from SP19 (*PmP*-1#") is not explained in model C, as stated above.

In the south halves of both models A and C, layer 15 dips northward, although its depth is uncertain by 3–5 km, depending on velocities assumed for layers 13, 13′, and 14. No *Pn* arrivals are clearly observed, but mantle velocity is estimated from the positions of points of critical reflection and from the strength of reflections to be in the range 7.5–8.0 km/s (see Figures 7*a* and 8*a*).

In the north halves of both models A and C, layer 15′ dips southward (7°), and its depth differs by about 3 km between the two models because of differing model velocities for layer 13′. The maximum Moho depth is 57 km, beneath the southern Copper River basin. Mantle velocity is constrained by reversing refractions and/or diffractions and by the apparent position of points of critical reflection from SP19 and SP1 (Figures 9 and 10). The permissible range for *Pn* is estimated to be 8.0–8.5 km/s. In model C, mantle refractions weakly constrain a tapering of the subducting crust beneath the southern Copper River basin (Figure 9*d*).

At least two problems with our modelling of mantle phases should be mentioned. (1) Predicted reflections from layers 15 and 15′ (considering only simple reflections, "*PmP*" and "*PmP*-1") are larger than those observed for all shot points except SP37 (e.g., compare Figures 7*a* and 7*b* and 8*a* and 8*b*). (2) "*PmP*-2" arrivals are influenced strongly by small structural details in the steeply dipping part of layer 14. For problem 1 the Moho may be a more complex boundary than the simple velocity step in our model (Figure 3). For problem 2, asymptotic ray theory generally predicts more pronounced foci and shadows than are observed, since diffracted energy is not included.

APPENDIX B

The following is a layer by layer discussion of constraints for model CGH (Figure 12*b*). The reader will need to refer to Figures 12–17.

Layers 1 and 2

Layers 1 and 2 (Figure 12*b*) represent unconsolidated glaciofluvial deposits and surficial bedrock, respectively. The only location where layer 1 attains significant thickness is a basin just east of Valdez. The layer velocity (1.8–1.9 km/s) was not determinable from Chugach line data but was assumed to be similar to the velocities for this material determined by E. L. Ambos et al. (submitted manuscript, 1988), although glaciofluvial deposits in the Copper River basin may differ somewhat. The velocity of layer 2 (cracked and weathered bedrock) is poorly constrained by Chugach line data but somewhat better constrained by Transect line data (see above). The thickness of this layer is adjusted to produce the appropriate local delays in the travel time curves; however, a trade-off between velocity and thickness is permissible in locations away from shot points.

Layers 3 and 5 ("Basement")

Layer 3 changes in velocity and velocity gradient from west to east. Between SP17 and SP18 it is 6.1 km/s at its top with a low gradient (less than 0.1/s, but east of SP18 it is 5.6 km/s at its top with a high gradient (about 0.17/s) that increases progressively eastward (to about 0.34/s at SP20). The eastward decrease in velocity is a well-resolved feature and is reflected in the a progressive eastward decrease in apparent velocities in the range interval 5–10 km from each shotpoint. The eastward increase in gradient is indicated by the onset of free surface multiple refractions at SP19 (Figure 15*b*, "*PP*"). These multiple refractions are seen from SP19 eastward, but geometric irregularities in the surficial layers immediately west of SP19 suppress multiples in that direction. Similar irregularities (not modeled) near SP20 either suppress these multiples from SP20, or the gradient is not as high as modeled in that region.

Layer 5 has fairly uniform velocity throughout the model, 6.4 (±0.1) km/s at its top and 6.6 (±0.15) km/s at its base, except in the model coordinate interval 47–65 km, where its top is 0.2 km/s faster. (Errors are estimated from trial-and-error modeling, as in Appendix A). Layer thickness, on the other hand, changes dramatically, from 6.5 km in the west to 1.5 km in the east. The consequent eastward increase in velocity gradient is apparent in an eastward increase in amplitude and decrease in branch length for layer 5 refractions; these features are well reproduced in synthetic record sections (compare Figures 13*a* and 13*b* and 15*a* and 15*b*, "5"). In its eastward increasing velocity gradient, this layer mimics layer 3. In fact, there are no clear reflections in the data to indicate that layers 3 and 5 are separate layers. The difference in average velocity of layers 3 and 5 between the Chugach and Transect lines (0.2–0.3 km/s, Figure 18*d*) is fairly well resolved and is consistent with laboratory determinations of anisotropy for metaflysch of the Chugach terrane (see Table 2, text).

Layers 7–12

In the region between SP17 and SP19, strong reflections, both precritical and postcritical, outline the top surface of layer 7 (Figures 13*b* and 14*a*, "7#"; Figure 15*b*, "7##"). In the region between SP19 and SP20, reflections from the top of the layer are not clearly separated from other arrivals. Reversed refractions from all shot points determine the velocity of this layer (6.9–7.1 km/s) quite accruately (±0.1 km/s) in the region east of about Valdez. The velocity gradient (0.05/s) and thickness (2 km) appear to be modeled approximately correctly as amplitudes and branch terminations match the data fairly closely (compare Figures 13*a* and 13*b*, 15*a* and 15*b*, and 16*a* and 16*b*, "7"). The difference in velocity of layer 7 between the Chugach and Transect lines (about 0.2 km/s, Figure 18*d*) is marginally resolved. Thicknesses agree well, within error.

The velocity of layer 9 was adopted from reflectivity modeling by *Flueh et al.* [1989] and the thickness of the layer was adjusted to produce the small delay (0.2–0.3 s) between refractions from layer 7 and reflections from layer 10. From SP17, there are no clear reflections from layer 10, and the refractions from layers 7 and 10 are nearly continuous, leading to our interpretation that layer 9 pinches out before reaching SP17 (Figure 12*b*).

Strong reflections from all but SP17 outline the top of layer 10 (Figures 14–16, "10#" and "10##"). Trial-and-error modeling on the Transect line indicates the top of this layer is no more accurately known than about 1 km (compare Figures 4*a* and 4*b*). Reversed refractions from all shot points on the Chugach line determine the velocity of this layer (7.2 km/s) quite accurately (±0.1 km/s) over its entire extent. The

velocity gradient (0.02/s) and thickness (1 km) were adjusted to produce the correct amplitudes and branch terminations, although a short interval of focused energy from SP17 (80- to 90-km range) does not match the data well (compare Figures 13*a* and 13*b* and 16*a* and 16*b*, "10"). The velocity and thickness of layer 10 agrees well with that determined on the Transect line (Figure 18*d*).

The average velocity of layer 11 (about 6.7 km/s) is a bit higher than that determined from reflectivity modeling by *Flueh et al.* [1989]. Layer 11 was subdivided in an attempt to more closely match peg-leg multiple travel times observed from SP17. Reverberations within layer 11B come closer to matching in traveltime the observed arrivals at 85- to 100-km range from SP17 than reverberations within the entire layer (Figure 13*b*, compare "M11B-1" and "M11A/B-1"). Amplitudes and range intervals over which multiples are strongest are not necessarily well predicted using ray theory (Figures 13*a* and 16*a*). Velocity details of layer 11 await further testing using a finite element algorithm.

Reflections from the top of layer 12 from SP17, SP18, and SP19 westward occur at about 10-km greater range than for SP19 eastward and SP20 (Figures 13–16, "12A") requiring that layer 12 deepen in the west half of the model. (If layer 12 were flat, the reflections from SP17, SP18, and SP19 westward would be 0.3 s too early.) Trial-and-error modeling on both the Chugach and Transect lines indicates that the top of layer 12 is no more accurately known that 1–2 km. Refractions from this layer, seen clearly from SP20 and ambiguously from SP17 (Figures 13*b* and 16*b*, "12B"), determine the layer velocity to be 7.7 ± 0.2 km/s in the west part of the model and 7.8 ± 0.2 km/s in east part (Figure 12*b*). A zero velocity gradient is required between SP19 and SP20 to produce the observed low amplitude of the refraction from SP20 (Figures 16*a* and 16*b*, "12B"). In fact, *Flueh et al.* [1989] model a negative velocity gradient in the lower half of layer 12 in this region to reproduce the observed amplitudes.

Layers 13–15 (Lower Crust and Mantle)

Velocities and depths of layers 13–15 were adopted from the Transect line, as no clear arrivals from these deeper layers are observed on the Chugach line. The reader is referred to the text for a discussion of these deeper layers and also a discussion of a "P_L" reflection from within the upper mantle.

Gravity Model

Predicted gravity for model CGH was calculated using a $2\frac{1}{2}$-dimensional algorithm and average densities for each layer taken from the velocity-density data of J. E. Nafe from *Dobrin* [1976] (predicted curve 1, Figure 12*a*). By reducing densities of layers 7 (3.00 g/cm^3), 10 (3.10 g/cm^3), and 11B (3.00 g/cm^3) to 2.92 g/cm^3, the agreement with the observed data can be brought to within about 5 mGals (predicted curve 2, Figure 12*a*). The predicted gravity curves are not too sensitive to layer dimensions in and out of the plane of the model; these dimensions have been chosen to be consistent with model A (Figure 3). For example, layer 7 in the gravity model extends 25 km northward (into the page, Figure 12*b*) and 20 km southward (out of the page, Figure 12*b*). Reducing both dimensions by 10 km reduces the predicted gravity by less than 3 mGal. Increasing both dimensions by 80 km increases the predicted gravity by less than 3 mGal. Lesser effects are seen by changing dimensions of layers 10 and 11B, as only 5–10 mGal of the total relief of the gravity ridge (30–40 mGal) is due to those layers.

Velocity Structure at SP21

As discussed in the text, the velocity of all layers above about 15-km depth must decrease in velocity eastward from SP20 to SP21 in order to produce the observed traveltimes (Figure 17*a*). Without data from the interval between SP20 and SP21, the structure can only be constrained in broad terms. These constraints are as follows: (1) a delay of about 0.7 s is required near SP21; (2) a strong LVZ (layer 11) is required to produce the peg-leg multiples seen from SP21; (3) the rocks at the surface at SP21 are felsic gneisses of amphibolite grade; (4) a detailed gravity map of the Chugach Mountains (D. F. Barnes, written communication, 1986) indicates that SP21 is north of the gravity ridge that characterizes most of the Chugach line (Figure 12*a*). We have chosen a structure at SP21 (Figure 12*b*, "SP21") in which the upper crust, to 7-km depth, has a velocity as low as reasonable for felsic crystalline rocks (constraint 3; see, for example, *Birch* [1960]) in order to achieve the required delay (constraint 1). In order to create an LVZ (constraint 2) we added a "lid" between depths of about 7 and 9 km (layer 10, 6.4 km/s) and an LVZ (layer 11, 5.8 km/s) between depths of 9 and 11.5 km. Notably absent is layer 7, which is linked to the gravity ridge (constraint 4; see text). The structure that we have chosen for SP21 produces an acceptable fit to the data (Figure 17*a*) but is, of course, poorly constrained. At least one group of alternate models was attempted and rejected: models in which the velocity of the layer 12 remained constant between SP20 and SP21 but the layer dipped eastward.

Acknowledgments. We estimate that data collection, data analysis, and writing of this manuscript consumed more than 18 man-years of effort since 1983. More than half of this effort was expended by persons other than the authors, and without their effort this manuscript could not have been written. We therefore gratefully acknowledge the work of Patricia Berge, Robert Colburn, Edward Criley, Edward Cruz, Margaret Daley, Stephen Gallanthine, Charles Gilbert, Laurie Hodgen, Lester Hsu, Lorraine Hwang, Ronald Kaderabek, the late David Knapp, William Kohler, John Lahr, Kenneth LaJoie, Nan MacGregor-Scott, Robert McClearn, Patricia Meador, Janice Murphy, Robert Page, David Reneau, Donald Ruggery, Dale Russell, Leroy Scheirrl, Julie Shemeta, Christopher Stephens, John Taber, John VanSchaack, and Jeffrey Wilson. We are especially indebted to Edward Criley for managing the field operations in a difficult environment. This task included (1) contracting for drilling, explosives, helicopter, fuel, lodging, and transportation, (2) permitting shot point and instrument locations, and (3) coordinating the complex tasks of drilling, loading shot holes and lakes, and programming, deploying, and picking up instruments. We would like to thank a number of public and private agencies for their generous cooperation and interest in our study. They include the U.S. Park Service (Wrangell–St. Elias National Park; Charles Budge and Richard Martin), U.S. Forest Service (Chugach National Forest; Fred Arbogast and Leo Keeler), U.S. Bureau of Land Management (Kurt Kotter and Michael Green), Federal Aviation Administration (Harold Richardson and Robert Legg), National Marine Fisheries Service (Ronald Morris), U.S. Coast Guard (James Underwood and Gary Trucks), State of Alaska (Margaret Hayes), Ahtna, Inc. (Larry Lau and Joeneal Hicks), Alyeska Pipeline Service Company (Dennis Prendeville and James Harle), Kenai Air Alaska (Landis Lindgren and Monte Hough), Airlogistics (Raymond Anderson), and Temsco, Inc. (the late Ralph Yetka). We also thank

Robert Shafer of Amoco Production Company (Denver) for sharing with us proprietary reflection data from the Copper River basin. James Luetgert and William Kohler provided support for many of the computer programs used in the data analysis. Mark Goldman assisted in plotting the fence diagram (Figure 20). Roxanne Benbow, Marsha Green, and Steven Nelson assisted with Alaskan logistics. Suzan Hotop and Marty Sanders patiently typed the numerous drafts of this manuscript. Our interpretation of the seismic refraction data was aided by numerous discussions with George Plafker, Robert Page, David Campbell, Ernst Flueh, Thomas Brocher, Michael Fisher, Warren Nokleberg, Lorraine Wolf, and others. We thank Thomas Brocher, Robert Simpson, George Plafker, Alan Levander, and an anonymous reviewer for detailed reviews of earlier drafts of this manuscript. The entire TACT effort has been supported and encouraged by Robert Hamilton, Benjamin Morgan, David Russ, William Ellsworth, and Thomas Miller. Finally, it is a pleasure to acknowledge the selfless efforts of Robert Page in promoting and coordinating all aspects of the TACT multidisciplinary program.

REFERENCES

Alaska Geological Society, *Southwest to Northeast Stratigraphic Correlation Section, Eureka to Rainbow and Tazlina Unit to Moore Creek, Copper River Basin, Alaska*, Anchorage, 1970.

Andreason, G. E., W. J. Dempsey, J. R. Henderson, and F. P. Gilbert, Aeromagnetic map of the Copper River basin, Alaska, scale 1:125,000, *U.S. Geol. Surv. Geophys. Invest. Map, GP-156*, 1958.

Barnes, D. F., Bouger gravity map of Alaska, scale 1:250,000, *U.S. Geol. Surv. Geophys. Invest. Map, GP-913*, 1977.

Bayer, K. C., R. E. Mattick, G. Plafker, and T. R. Bruns, Refraction studies between Icy Bay and Kayak Island, eastern Gulf of Alaska, *U.S. Geol. Surv. J. Res.*, *6*, 625–636, 1978.

Berry, M. J., and J. A. Mair, The nature of the Earth's crust in Canada, in *The Earth's Crust: Its Nature and Physical Properties, Geophys. Monogr. Ser.*, vol. 20, edited by J. G. Heacock, pp. 319–348, AGU, Washington, D.C., 1977.

Birch, F., The velocity of compressional waves in rocks to 10 kilobars, 1, *J. Geophys. Res.*, *65*, 1083–1102, 1960.

Blank, H. R., J. H. Healy, J. Roller, R. Lamson, F. Fisher, R. McClearn, and S. Allen, Seismic refraction profile, Kingdom of Saudi Arabia, Field operations, instrumentation, and initial results, *Saudi Arabian Mission Proj. Rep. 259*, 49 pp., U.S. Geol. Surv., Reston, Va., 1979.

Blundell, D. J., The Zurich I model, how the interpretation fared, in Workshop Proceedings: Interpretations of Seismic Wave Propagation in Laterally Heterogeneous Structures, edited by D. M. Finlayson and J. Ansorge, *Rep. 258*, pp. 177–179, Bur. of Miner. Resourc., Geol., and Geophys., Commonwealth of Aust., Canberra, 1984.

Brocher, T. M., M. A. Fisher, E. L. Geist, and N. I. Christensen, A high-resolution seismic reflection/refraction study of the Chugach-Peninsular terrane boundary, southern Alaska, *J. Geophys. Res.*, *94*, 4441–4456, 1989*a*.

Brocher, T. M., P. E. Hart, and M. A. Fisher, Wide-angle recordings of the 1988 TACT MCS Survey in Prince William Sound, Alaska (abstract), *Eos Trans. AGU*, *70*, 1339, 1989*b*.

Bruns, T. R., Tectonics of the Yakutat Block, an allochthonous terrane in the northern Gulf of Alaska, *U.S. Geol. Surv. Open File Rep.*, *85-13*, 112 pp., 1985.

Burns, L. E., Gravity and aeromagnetic modelling of a large gabbroic body near the Border Ranges fault, southern Alaska, *U.S. Geol. Surv. Open File Rep.*, *82-460*, 66 pp., 3 plates, 1982.

Burns, L. E., The Border Ranges ultramafic and mafic complex, south-central Alaska: Cumulate fractionates of island-arc volcanics, *Can. J. Earth Sci.*, *22*, 1020–1038, 1985.

Campbell, D. L., Profiles showing models of magnetic structures in accreted terranes of south-central Alaska, scale 1:500,000, *U.S. Geol. Surv. Misc. Field Stud. Map, MF-1912*, 1987.

Campbell, D. L., and D. F. Barnes, Gravity and magnetic model of part of the 1984 TACT line, Chugach Mountains and southern Copper River Basin, in The U.S. Geological Survey in Alaska—Accomplishments During 1984, edited by S. Bartsch-Winkler, *U.S. Geol. Surv. Circ.*, *967*, 52–54, 1985.

Carey, S. W., The tectonic approach to continental drift—A symposium, report, pp. 177–355, Univ. of Tasmania, Geol. Dep., Hobart, Australia, 1958.

Červený, V., I. A. Molotkov, and I. Pšenčík, *Ray Method in Seismology*, 214 pp., Karlova University, Prague, 1977.

Christensen, N. I., Compressional wave velocities at high temperatures and pressures, critical thermal gradients, and crustal low-velocity zones, *J. Geophys. Res.*, *84*, 6849–6857, 1979.

Christensen, N. I., Seismic velocities, in *Handbook of Physical Properties of Rocks, II*, edited by R. S. Carmichael, pp. 1–228, CRC Press, 1982.

Christensen, N. I., Measurements of dynamic properties of rock at elevated pressures and temperatures, in *Measurements of Rock Properties at Elevated Pressures and Temperatures*, edited by J. Pincus and E. R. Hoskins, pp. 93–107, American Society for Testing and Materials, Philadelphia, Pa., 1985.

Christensen, N. I., Pore pressure, seismic velocities, and crustal structure, in Geophysical Framework of the Continental United States, edited by L. C. Pakiser and W. D. Mooney, *Mem. Geol. Soc. Am.*, *172*, 783–798, 1989.

Colburn, R. H., and G. S. Fuis, Velocity structure across the northern boundary of the Peninsular terrane, Copper River basin, Alaska (abstract), *Eos Trans. AGU*, *67*, 1198, 1986.

Colburn, R. H., and W. D. Mooney, Two-dimensional velocity structure along the synclinal axis of the Great Valley, California, *Bull. Seismol. Soc. Am.*, *76*, 1305–1322, 1986.

Coney, P. J., D. L. Jones, and J. W. H. Monger, Cordilleran suspect terranes, *Nature*, *288*, 329–333, 1980.

Csejtey, B., Jr., D. P. Cox, R. C. Evarts, G. D. Stricker, and H. L. Foster, The Cenozoic Denali fault system and Cretaceous accretionary development of southern Alaska, *J. Geophys. Res.*, *87*, 3741–3754, 1982.

Daley, M. A., E. L. Ambos, and G. S. Fuis, Seismic refraction data collected in the Chugach Mountains and along the Glenn Highway in southern Alaska in 1984, *U.S. Geol. Surv. Open File Rep.*, *85-531*, 32 pp., 10 plates, 1985.

DeBari, S. M., and R. G. Coleman, Examination of the deep levels of an island arc: Evidence from the Tonsina ultramafic-mafic assemblage, Tonsina, Alaska, *J. Geophys. Res.*, *94*, 4373–4391, 1989.

Dobrin, M. B., *Introduction to Geophysical Prospecting*, 3rd ed., 630 pp., McGraw-Hill, New York, 1976.

Engebretson, D. C., Relative motions between oceanic and continental plates in the Pacific basin, Ph.D. thesis, 211 pp., Stanford Univ., Stanford, Calif., 1982.

Fisher, M. A., R. von Huene, G. L. Smith, and T. R. Bruns, Possible seismic reflections from the downgoing Pacific plate, 275 kilometers arcward from the eastern Aleutian trench, *J. Geophys. Res.*, *88*, 5835–5849, 1983.

Fisher, M. A., T. M. Brocher, W. J. Nokleberg, G. Plafker, and G. L. Smith, Seismic reflection images of the crust of the northern part of the Chugach terrane, Alaska: Results of a survey for the Trans-Alaska Crustal Transect (TACT), *J. Geophys. Res.*, *94*, 4424–4440, 1989.

Flueh, E. R., W. D. Mooney, G. S. Fuis, and E. L. Ambos, Crustal structure of the Chugach Mountains, southern Alaska: A study of peg-leg multiples from a low-velocity zone, *J. Geophys. Res.*, *94*, 16,023–16,035, 1989.

Fuchs, K., and G. Mueller, Computation of synthetic seismograms with the reflectivity method and comparison with observations, *Geophys. J. R. Astron. Soc.*, *23*, 417–433, 1971.

Fuis, G. S., and E. L. Ambos, Deep structure of the Contact fault and Prince William terrane: Preliminary results of the 1985 TACT seismic-refraction survey, in The U.S. Geological Survey in Alaska—Accomplishments during 1985, edited by S. Bartsch-Winkler, *U.S. Geol. Surv. Circ.*, *978*, 41–45, 1986.

Fuis, G. S., and G. Plafker, Evolution of deep structure along the Trans-Alaska Crustal Transect, Chugach Mountains and Copper River Basin, southern Alaska, *J. Geophys. Res.*, this issue.

Fuis, G. S., E. L. Ambos, W. D. Mooney, R. A. Page, M. A. Fisher, T. M. Brocher, and J. J. Taber, Crustal structure beneath exposed accreted terranes of southern Alaska, *Geophys. J. R. Astron. Soc.*, *89*, 73–78, 1987.

Godson, R. H., Composite magnetic anomaly map of the United States, Part B—Alaska and Hawaii, scale 1:2,500,000, *U.S. Geol. Surv. Geophys. Invest. Map, GP-954B*, 2 sheets, 1984.

Goodwin, E. B., G. S. Fuis, W. J. Nokleberg, and E. L. Ambos,

The crustal structure of the Wrangellia terrane along the East Glenn Highway, eastern southern Alaska, *J. Geophys. Res.*, *94*, 16,037–16,057, 1989.

Hales, A. L., and T. Asada, Crustal structure in coastal Alaska, in *The Earth Beneath the Continents*, *Geophys. Monogr. Ser.*, vol. 10, edited by J. S. Steinhart and T. J. Smith, pp. 420–432, AGU, Washington, D. C., 1966.

Hanson, K., E. Berg, and L. Gedney, A seismic-refraction profile and crustal structure in central interior Alaska, *Bull. Seismol. Soc. Am.*, *58*, 1657–1665, 1968.

Healy, J. H., W. D. Mooney, H. R. Blank, M. E. Gettings, W. M. Kohler, R. Lamson, and L. E. Leone, Saudi Arabian seismic deep-refraction profile: Final project report, *Saudi Arabian Mission Open File Rep. 02-37*, 429 pp., U.S. Geol. Surv., Reston, Va., 1982.

Hillhouse, J. W., and C. S. Gromme, Northward displacement and accretion of Wrangellia: New paleomagnetic evidence from Alaska, *J. Geophys. Res.*, *89*, 4461–4467, 1984.

Holbrook, W. S., and W. D. Mooney, The crustal structure of the axis of the Great Valley, California, from seismic-refraction measurements, *Tectonophysics*, *140*, 49–63, 1987.

Hudson, T., and G. Plafker, Paleogene metamorphism in an accretionary flysch terrane, eastern Gulf of Alaska, *Geol. Soc. Am. Bull.*, *93*, 1280–1290, 1982.

Jones, D. L., N. J. Silberling, and J. Hillhouse, Wrangellia—A displaced terrane in northwestern North American, *Can. J. Earth Sci.*, *14*, 2565–2577, 1977.

Jones, D. L., N. J. Silberling, W. Gilbert, and P. Coney, Character, distribution and tectonic significance of accretionary terranes in the central Alaska Range, *J. Geophys. Res.*, *87*, 3709–3717, 1982.

Jones, D. L., N. J. Silberling, P. J. Coney, and G. Plafker, Lithotectonic terrane map of Alaska, scale 1:2,500,000, in Lithotectonic Terrane Maps of the North American Cordillera, edited by N. J. Silberling and D. L. Jones, *U.S. Geol. Surv. Open File Rep.*, *84-523*, A1–A12, 4 sheets, 1984.

Landisman, M., S. Mueller, and B. J. Mitchell, Review of evidence for velocity inversions in the continental crust, in *The Structure and Physical Properties of the Earth's Crust*, *Geophys. Monogr. Ser.*, vol. 14, edited by J. G. Heacock, Jr., pp. 11–34, AGU, Washington, D. C., 1971.

Luetgert, J. H., User's manual for RAY84/RAY83PLT, interactive two-dimensional ray tracing/synthetic seismogram package, *U.S. Geol. Surv. Open File Rep.*, *88-238*, 52 pp., 1988.

MacKevett, E. M., Jr., Geological map of the McCarthy quadrangle, Alaska, scale 1:250,000, *U.S. Geol. Surv. Misc. Invest. Ser. Map*, *I-1032*, 1978.

McMechan, G. A., and G. S. Fuis, Ray equation migration of wide-angle reflections from southern Alaska, *J. Geophys. Res.*, *92*, 407–420, 1987.

McMechan, G. A., and W. D. Mooney, Asymptotic ray theory and synthetic seismograms for laterally varying structures: Theory and application to the Imperial Valley, California, *Bull. Seismol. Soc. Am.*, *70*, 2021–2035, 1980.

Meador, P. J., E. L. Ambos, and G. S. Fuis, Data Report for the North and South Richardson Highway Profiles, TACT, seismic-refraction survey, southern Alaska, *U.S. Geol. Surv. Open File Rep.*, *86-274*, 51 pp., 1 plate, 1 magnetic tape, 1986.

Meissner, R., *The Continental Crust: A Geophysical Approach*, 426 pp., Academic, San Diego, Calif., 1986.

Mooney, W. D., Seismic methods for determining earthquake source parameters and lithospheric structure, in Geophysical Framework of the Continental United States, edited by L. Pakiser and W. D. Mooney, *Mem. Geol. Soc. Am.*, *172*, 11–34, 1989.

Nokleberg, W. J., D. L. Jones, and N. J. Silberling, Origin and tectonic evolution of the Maclaren and Wrangellia terranes, eastern Alaska Range, Alaska, *Geol. Soc. Am. Bull.*, *96*, 1251–1270, 1985.

Nokleberg, W. J., W. M. Wade, I. M. Lange, and G. Plafker, Summary of geology of the Peninsular terrane, metamorphic complex of Gulkana River, and Wrangellia terrane, north-central and northwestern Gulkana quadrangle, *U.S. Geol. Surv. Circ.*, *978*, 69–74, 1986.

Nokleberg, W. J., G. Plafker, J. S. Lull, W. K. Wallace, and G. R. Winkler, Structural analysis of the southern Peninsular, southern Wrangellia, and northern Chugach terranes along the Trans-Alaska Crustal Transect, northern Chugach Mountains, Alaska, *J. Geophys. Res.*, *94*, 4297–4320, 1989.

Nur, A., and G. Simmons, The effect of saturation on velocity in low-porosity rock, *Earth Planet. Sci. Lett.*, *7*, 183–193, 1969.

Page, R. A., G. Plafker, G. S. Fuis, W. J. Nokleberg, E. L. Ambos, W. D. Mooney, and D. L. Campbell, Accretion and subduction tectonics in the Chugach Mountains and Copper River basin, Alaska: Initial results of the Trans-Alaska Crustal Transect, *Geology*, *14*, 501–505, 1986.

Page, R. A., C. D. Stephens, and J. C. Lahr, Seismicity of the Wrangell and Aleutian Wadati-Benioff zones and the North American plate along the Trans-Alaska Crustal Transect, Chugach Mountains and Copper-River basin, southern Alaska, *J. Geophys. Res.*, *94*, 16,059–16,082, 1989.

Plafker, G., Regional geology and petroleum potential of the northern Gulf of Alaska continental margin, in *Geology and Resource Potential of the Continental Margin of Western North America and Adjacent Ocean Basins*, *Earth Sci. Ser.*, vol. 6, edited by D. W. Scholl, A. Grantz, and J. G. Vedder, pp. 229–268, American Association of Petroleum Geologists, Tulsa, Okla., 1987.

Plafker, G., D. L. Jones, and E. A. Pessagno, Jr., A Cretaceous accretionary flysch and melange terrane along the Gulf of Alaska margin, *U.S. Geol. Surv. Circ.*, *751-B*, B41–B43, 1977.

Plafker, G., W. J. Nokleberg, and J. S. Lull, Summary of 1984 TACT geologic studies in the northern Chugach Mountains and southern Copper River Basin, Alaska, in The United States Geological Survey in Alaska: Accomplishments During 1984, edited by S. Bartsch-Winkler, *U.S. Geol. Surv. Circ.*, *967*, 76–79, 1985.

Plafker, G., W. J. Nokleberg, J. S. Lull, S. M. Roeske, and G. R. Winkler, Nature and timing deformation along the Contact fault system in the Cordova, Bering Glacier, and Valdez quadrangles, in The U.S. Geological Survey in Alaska: Accomplishments in 1985, edited by S. Bartsch-Winkler, *U.S. Geol. Surv. Circ.*, *978*, 74–77, 1986.

Plafker, G., W. J. Nokleberg, and J. S. Lull, Bedrock geology and tectonic evolution of Wrangellia, Peninsular, and Chugach terranes along the Trans-Alaska Crustal Transect in the Chugach Mountains and southern Copper River basin, *J. Geophys. Res.*, *94*, 4255–4296, 1989.

Saleeby, J. B., C-2 Central California offshore to Colorado Plateau, *Centen. Continent/Ocean Transect 10*, scale 1:500,000, 2 sheets, 63 pp., Geol. Soc. of Am., Boulder, Colo., 1986.

Salisbury, M. H., and N. I. Christensen, The seismic velocity structure of a traverse through the Bay of Islands ophiolite complex, Newfoundland, an exposure of oceanic crust and upper mantle, *J. Geophys. Res.*, *83*, 805–817, 1978.

Sample, J. C., and J. C. Moore, Structural style and kinematics of an underplated slate belt, Kodiak and adjacent islands, Alaska, *Geol. Soc. Am. Bull.*, *99*, 7–20, 1987.

Shor, G. G., Jr., H. W. Menard, and R. W. Raitt, Structure of the Pacific Basin, in *The Sea*, *Part II*, *Regional Observations*, vol. 4, edited by A. E. Maxwell, pp. 3–27, Wiley-Interscience, New York, 1970.

Silberman, M. L., E. M. MacKevett, Jr., C. L. Connor, P. L. Klock, and G. Kalechitz, K-Ar ages of the Nikolai Greenstone from the McCarthy Quadrangle, Alaska: The "docking" of Wrangellia, *U.S. Geol. Surv. Circ.*, *823-B*, B61–B63, 1981.

Sisson, V. B., L. S. Hollister, and T. C. Onstott, Petrologic and age constraints on the origin of a low pressure/high temperature metamorphic complex, southern Alaska, *J. Geophys. Res.*, *94*, 4392–4410, 1989.

Spieth, M. A., D. P. Hill, and R. J. Geller, Crustal structure in the northwestern foothills of the Sierra Nevada from seismic refraction experiments, *Bull. Seismol. Soc. Am.*, *71*, 1075–1087, 1981.

Spudich, P. A., and J. Orcutt, A new look at the seismic velocity structure of the oceanic crust, *Rev. Geophys.*, *18*, 627–645, 1980.

Stephens, C. D., K. A. Fogleman, J. C. Lahr, and R. A. Page, The Wrangell Benioff zone, southern Alaska, *Geology*, *12*, 373–376, 1984.

Stephens, C. D., R. A. Page, and J. C. Lahr, Evidence for a midcrustal seismic velocity discontinuity beneath the southern Kenia Peninsula Alaska (abstract), *Seismol. Res. Lett.*, *58*, 27, 1987.

Stephens, C. D., R. A. Page, and J. C. Lahr, Reflected and mode-converted seismic waves within the shallow subduction

zone, southern Kenai Peninsula, Alaska, *J. Geophys. Res.*, *95*, 6883–6897, 1990.

Taber, J. J., G. S. Fuis, E. L. Ambos, W. D. Mooney, and R. A. Page, Seismic velocity structure of the Prince William terrane, Alaska (abstract), *Eos Trans. AGU*, *67*, 1196, 1986.

Tatel, H. E., and M. A. Tuve, The Earth's crust; seismic studies, *Year Book Carnegie Inst. Washington*, *55*, 81–85, 1956.

U.S. Geological Survey, Aeromagnetic Map of part of the Valdez quadrangle, Alaska, scale 1:250,000, *U.S. Geol. Surv. Open File Map*, *79-381*, 1979.

von Huene, R., G. G. Shor, Jr., and J. Wageman, Continental margins of the eastern Gulf of Alaska and boundaries of tectonic plates, in Geological and Geophysical Investigations of Continental Margins, edited by J. S. Watkins and L. Montadert, *AAPG Mem.*, *29*, 273–290, 1979.

Wilson, J. M., Supplementary data report (magnetic tape) for Open-File Report 85-531, 1984 TACT seismic-refraction survey, south-central Alaska, *U.S. Geol. Surv. Open File Rep.*, *87-482*, 3 pp., 1 magnetic tape, 1987.

Wilson, J. M., P. Meador, and G. S. Fuis, Data report for the 1985 TACT seismic-refraction survey, south-central Alaska, *U.S. Geol. Surv. Open File Rep.*, *87-440*, 78 pp., 1 magnetic tape, 1987.

Winkler, G. R., and G. Plafker, Geologic map and cross sections of the Cordova and Middleton Island quadrangles, southern Alaska, scale 1:250,000, *U.S. Geol. Surv. Open File Rep.*, *81-1164*, 25 pp., 1 sheet, 1981.

Winkler, G. R., M. L. Silberman, A. Grantz, R. J. Miller, and E. M. MacKevett, Jr., Geologic map and summary geochronology of the Valdez Quadrangle, southern Alaska, scale 1:250,000, *U.S. Geol. Surv. Open File Rep.*, *80-892-A*, 1981.

Wolf, L. W., and A. R. Levander, Upper crustal structure of the accreted Chugach terrane, Alaska, *J. Geophys. Res.*, *94*, 4457–4466, 1989.

Woollard, G. P., N. A. Ostenso, E. Theil, and W. E. Bonini, Gravity anomalies, crustal structure, and geology in Alaska, *J. Geophys. Res.*, *65*, 1021–1037, 1960.

E. L. Ambos, Department of Geological Sciences, California State University, Long Beach, 1250 Bellflower Blvd., Long Beach, CA 90840.

N. I. Christensen, Department of Earth and Atmospheric Sciences, Purdue University, West Lafayette, IN 49707.

G. S. Fuis, E. Geist, and W. D. Mooney, U.S. Geological Survey, MS 977, 345 Middlefield Road, Menlo Park, CA 94025.

(Received October 3, 1988;
revised February 1, 1990;
accepted August 8, 1990.)